Universidad de Valladolid

Escuela de Doctorado Universidad de Valladolid

PROGRAMA DE DOCTORADO

EN INVESTIGACIÓN BIOMÉDICA

TESIS DOCTORAL:

Calcium dynamics in *Caenorhabditis elegans* pharynx

Presentada por **Pilar Álvarez Illera** para optar al grado de
Doctora por la Universidad de Valladolid

Dirigida por:

Dra. Mayte Montero Zoccola
Dr. Javier Álvarez Martín
Dra. Rosalba Inés Fonteriz García

A mi madre y a mi padre

a mis hermanos y sobrinos

a Ana y Laurika

"*Una vez descartado lo imposible,*

lo que queda, por improbable que parezca,

debe ser la verdad"

Arthur Connan Doyle

A part of the results shown in this work have been published in the following scientific journals:

- **Alvarez-Illera P**, García-Casas P, Arias-Del-Val J, Fonteriz RI, Alvarez J, Montero M.*Pharynx mitochondrial [Ca2+] dynamics in live C. elegans worms during aging*.2017. Oncotarget. doi: 10.18632/oncotarget.18600
- **Alvarez-Illera P**, Sanchez-Blanco A, Lopez-Burillo S, Fonteriz RI, Alvarez J, Montero M. *Long-term monitoring of Ca2+ dynamics in C. elegans pharynx: an in vivo energy balance sensor. 2016. Oncotarget.* doi: 10.18632/oncotarget.12177

They have also been presented in the following meetings:

- **EMBO workshop.** *Long-term monitoring of cytosolic and mitochondrial Ca2+ dynamics in C. elegans pharynx.* **Pilar Alvarez-Illera**, Paloma García-Casas, Jessica Arias-del-Val, Adolfo Sanchez-Blanco, Rosalba I Fonteriz, Javier Alvarez and Mayte Montero.Barcelona. 2018 (Accepted) Poster
- **XIV International Meeting of the Calcium European Society**. *Long term monitoring of Ca^{2+} dynamics in C. elegans pharynx: an in vivo energy balance sensor* Pilar alvarez-Illera, Adolfo Sanhez-Blanco, Paloma Garcia-Casas, Silvia Lopez-Burillo, Rosalba I Fonteriz, Javier Alvarez and Mayte Montero. Valladolid. 2016. Poster
- **VI Spanish worm meeting**. Pilar Álvarez Illera; Paloma Garcia-Casas; Jessica Arias-del-Val Rosalba Ines Fonteriz; Javier Alvarez; Mayte Montero. *Long-term monitoring of Ca^{2+} dynamics in C. elegans pharynx: an in vivo energy balance sensor*. Valencia, Comunidad Valenciana, Spain, 2017. Oral communication.

This work was supported by a grant from the spanish Ministerio de Economía y Competitividad [BFU2014-55731-R].

ACKNOWLEDGMENTS

GRACIAS, es la única palabra que se me ocurre para empezar.

Gracias primero a mis tutores de tesis Mayte, Javier y Rosalba por todo su apoyo en esta etapa, por su infinita paciencia y por guiarme en este reto tanto intelectual como personalmente. En especial a Mayte porque fuiste la primera que confió y apostó por mi cuando ni yo misma veía en el horizonte la posibilidad de hacer el doctorado.

Gracias a todas las personas que han pasado por el grupo de Calcio del quinto pino. En mis inicios Sergio, Monty y Laurika, vosotros fuisteis los primeros en aparecer en mi etapa profesional, compartiendo grandes momentos en la penumbra de aequorina, y seguís formando parte importante de mi vida personal. Muchas personas han pasado en estos casi 10 años por el grupo y de cada uno de ellos he aprendido algo, desde doctorandos, alumnos en prácticas o técnicos. Mención especial para Jessi y Paloma, actuales compañeras, que me han apoyado y soportado, principalmente en esta última etapa de escritura.

Gracias a todos los compañeros de la quinta planta de la Facultad de Medicina, desde profesores, doctorandos y técnicos especialmente Josefina, Jesús y Dani. No me olvido de Ana Gordillo, no tengo palabras que expresen todo lo que eres: amiga, compañera, confidente, gran apoyo… todo se queda corto.

Gracias a todos los amig@s fuera del laboratorio difícil nombraros sin olvidarme de alguno, pero a pesar de ser muy castellana, cada uno de vosotros sabéis el lugar que ocupáis.

Gracias a mi familia por apoyarme en cada decisión incondicionalmente. En especial a mis padres, porque a pesar de no saber cómo ayudar en algunas ocasiones, siempre se han desvivido

en dar lo mejor de ellos mismos; sin vosotros esto nunca hubiera sido posible.

Todos y cada uno habéis hecho posible que mis miedos no ocupen el lugar de mi sueño, seguir trabajando en el laboratorio cada día. GRACIAS!!!

INDEX

ABBREVIATION LIST

$[Ca^{2+}]_C$:	Cytosolic Ca^{2+} concentration.
$[Ca^{2+}]_M$:	Mitochondrial Ca^{2+} concentration.
ED:	Energy Depletion
FuDR:	5-fluoro-2'-deoxyuridine
mtROS:	mitochondria Reactive Oxygen Species
NED:	Non energy Depletion
NGM:	Nematode Growth Medium
ROS:	Reactive Oxygen Species
OP50:	*Escherichia coli* strain

SUMMARY

Caenorhabditis elegans se ha convertido en el modelo invertebrado de elección debido a su relativa simplicidad, la riqueza de conocimiento de su biología, la gran cantidad de herramientas genéticas disponibles, transparencia, su corto tiempo de vida y bajo coste de mantenimiento. La principal característica que hace útil este modelo en este trabajo es la capacidad de poder expresar proteínas fluorescentes sensibles a Ca^{2+} y medir las oscilaciones de $[Ca^{2+}]$ que se producen en la faringe, tanto a nivel citosólico ($[Ca^{2+}]_C$ como mitocondrial ($[Ca^{2+}]_M$ en el organismo vivo.

La faringe del *C. elegans* es un órgano neuromuscular que mediante los movimientos peristálticos del itsmo y de bombeo permite introducir y triturar el alimento y llevarlo al intestino. Concretamente en esta tesis hemos medido las oscilaciones de $[Ca^{2+}]_C$ y $[Ca^{2+}]_M$ que se producen en el bulbo posterior de la faringe al estimular la contracción con serotonina.

El objetivo principal del trabajo es conocer los cambios de los patrones de oscilaciones de $[Ca^{2+}]$ y cómo dichos cambios pudieran afectar al envejecimiento. Para ello hemos comparado el gusano con fenotipo silvestre con los mutantes *nuo-6,* que presenta una alteración en una subunidad del complejo I de la cadena mitocondrial y es un modelo de patología mitocondrial; *eat-2* con una mutación en el receptor nicotínico de la faringe que sirve de modelo de restricción calórica y *daf-2* con una mutación en el receptor de insulina/factor de crecimiento I. Todas estas líneas mutantes presentan mayor longevidad que la línea silvestre

Las líneas AQ2038 y AQ3055 tienen el fenotipo silvestre y expresan las proteínas fluorescentes YC2.1 o YC3.60 en citosol o mitocondria respectivamente, dirigidas a la faringe gracias al promotor *p-myo-2*. Para obtener las líneas mutantes que expresen la proteína fluorescente, se cruzan los machos fluorescentes AQ2038 o AQ3055 con los hermafroditas mutantes (*nuo-6, eat-2* o

daf-2). Resultando de este cruce los mutantes que expresan la proteína fluorescente en el citosol: *AQnuo-6*, *AQeat-2* y *AQdaf-2* y en la mitocondria *Mnuo-6* .

Las medidas de calcio se realizan los días 2, 5, 8 y 12 de edad adulta para establecer una evolución de los patrones de calcio a lo largo de la vida del gusano. El tiempo de registro es 30 minutos aproximadamente, con una media de 20 gusanos por condición. Los trazados de Ca^{2+} se analizan con un algoritmo que permite conocer diferentes parámetros como: altura, anchura y frecuencia media.

DINÁMICA DE CALCIO CITOSÓLICO EN *C. ELEGANS*

Observando los patrones citosólicos del gusano silvestre AQ2038 se pueden distinguir dos tipos de picos de Ca^{2+}: **spikes** que corresponden a oscilaciones rápidas y **square-waves** que corresponden con aumentos sostenidos de $[Ca^{2+}]$ durante varios segundos que pueden llegar a minutos. La $[Ca^{2+}]_C$ elevada es generalmente tóxica para las células indicando un mal funcionamiento de las bombas encargadas de bombear el Ca^{2+} del citosol hacia el medio extracelular o hacia los depósitos intracelulares de Ca^{2+}. Los denominados spikes están presentes durante toda la vida del gusano, mientras que los square-waves aparecen principalmente en gusanos jóvenes de día 2 o 5 de edad.

Las líneas mutantes AQ*nuo-6*, AQ*eat-2* y AQ*daf-2* también presentan los dos tipos de picos, los spikes permanecen durante toda la vida del gusano y los square-waves presentes en los primeros días de adulto.

La sarcopenia que es una degeneración de la masa muscular; es una de las principales causas de deterioro funcional en el músculo pero la prevalencia de los spikes en gusanos viejos

indica que aunque las proteínas contráctiles están dañadas, la actividad oscilatoria de $[Ca^{2+}]_C$ en la faringe permanece intacta a lo largo de la vida del gusano.

El Ca^{2+} es un segundo mensajero importante en diversas funciones celulares como la contracción muscular. Para que una célula muscular se contraiga primero se produce un incremento $[Ca^{2+}]_C$ gracias a la entrada de Ca^{2+} del medio extracelular o a su liberación de los depósitos intracelulares de Ca^{2+}; pero rápidamente las bombas de la membrana plasmática o de los depósitos intracelulares se encargan de bajar a niveles basales $[Ca^{2+}]_C$ con el consiguiente gasto de ATP, dejando la célula en condiciones de recibir otro estímulo para la siguiente contracción. Los spikes son cambios de $[Ca^{2+}]_C$ muy rápidos, esto puede desencadenar un agotamiento de ATP que deriva en $[Ca^{2+}]_C$ alta que puede resultar tóxica o nociva si se prolonga en el tiempo.

De esta manera, los patrones de calcio analizados desde el punto de vista energético nos permite dividir los trazados en Depletados-Energéticamente (DE), que son aquellos trazados que tienen varios squares-waves durante 30 minutos o terminan el trazado en alto $[Ca^{2+}]_C$, porque no tiene suficiente ATP pare que funcionen las bombas. Y No-Depletados-Energéticamente (NDE), aquellos trazados que tienen oscilaciones rápidas durante todo el experimento o finaliza el registro con baja $[Ca^{2+}]_C$.

Desde el punto de vista energético hay mayor porcentaje de gusanos DE en los jóvenes que en los viejos aunque mas del 70% corresponde a gusanos NDE, tanto en los gusanos silvestres como en los mutantes. Sin embargo, los mutantes AQ*eat-2* tienen mayor porcentaje en todas las edades estudiadas de gusanos DE, esto hace pensar que la restricción calórica afecta a los patrones de calcio citosólicos.

Para comprobar esta hipótesis, se hizo el estudio de todas las líneas en condiciones de restricción calórica, es decir, desde el día 1 de estadío adulto los gusanos no tienen comida y se realizan las medidas los días 2, 5, 8, 12. El ayuno produce un cambio drástico en el porcentaje de gusanos DE en las líneas AQ2038, AQ*eat-2* y AQ*daf-2* que llega al 80%. Sin embargo, la línea mutante AQ*nuo-6,* aunque aumenta el porcentaje de gusanos DE respecto a la condición normal pero sólo hasta el 50%.

Los mutantes *nuo-6* tienen una producción de ATP baja y un consumo de ATP bajo esto indica que los mutantes AQ*nuo-6* pueden mantener un mejor equilibrio energético al disminuir el consumo de energía. El mayor porcentaje de gusanos DE en los gusanos más jóvenes indica que tienen un desequilibrio entre la producción de ATP y su consumo cuando son sobre estimulados con la serotonina, presente durante todo el registro.

DINÁMICA DE CALCIO MITOCONDRIAL EN *C. ELEGANS*

Hasta ahora no se habían realizado medidas de calcio mitocondrial en la faringe. Nuestros datos en gusanos AQ3055 muestran que las mitocondrias de la faringe son capaces de oscilar a alta frecuencia, reproduciendo los patrones observados en el citosol A2038.

La faringe se ha llegado a comparar con el corazón, debido a que su desarrollo está controlado por genes homólogos similares y también por sus propiedades eléctricas similares. Se han propuesto dos modelos para explicar la señalización mitocondrial cardiaca, uno sugiere que la mitocondria es capaz de reproducir las oscilaciones del citosol, el segundo propone que la $[Ca^{2+}]_M$ refleja una lenta integración de los aumentos $[Ca^{2+}]_C$. Nuestros datos apoyan el primer modelo, es decir: la mitocondria es capaz de reflejar las oscilaciones rápidas de Ca^{2+} que se producen en el citosol.

Los registros observados en la mitocondria muestran también spikes y square-waves como en el citosol. La hipótesis de estos transitorios de square-waves en las mitocondrias de la faringe podría ser la misma que en el citosol, es decir, el balance energético es el que da lugar a los spikes o square-waves, ya que puede atribuirse al agotamiento de la energía, que podría detener las bombas de Ca^{2+} y mantener alta la $[Ca^{2+}]_C$ llevando a una mayor acumulación mitocondrial de Ca^{2+}.

Observando los parámetros anchura y frecuencia de los picos de Ca^{2+} mitocondriales se observa que es menor que en el citosol, esto indica que para que se active la captación de Ca^{2+} mitocondrial se necesita un mínimo $[Ca^{2+}]_C$. Además se mantiene estable a lo largo de toda la vida del gusano la captación de Ca^{2+} mitocondrial.

Hemos estudiado si una mutación en la cadena respiratoria mitocondrial afecta a la captación de calcio, para ello se ha usado el mutante *nuo-6.* Se ha visto que estos gusanos M*nuo-6,* a pesar tener función mitocondrial reducida las mitocondrias, son capaces de mostrar oscilaciones rápidas de Ca^{2+} aunque con una frecuencia y amplitud algo menores que el AQ3055.

Las conclusiones son:

1.- La expresión de la proteína sensible a Ca^{2+} derivada del camaleón YC2.1 y YC3.60 en las células musculares de la faringe del *C. elegans* permite medir la dinámica de calcio de la actividad faringea *in vivo* durante un tiempo prolongado, tanto en el citosol como en la mitocondria.

2.- Las oscilaciones de calcio citosólico en la faringe presentan variabilidad, pero es posible distinguir dos tipos de picos de Ca^{2+} citosólicos:

- ✓ **Square-waves**: elevaciones prolongadas en $[Ca^{2+}]_C$, que duran varios segundos o incluso minutos. En su mayoría están presentes en gusanos jóvenes y desaparecen a medida que el gusano envejece.
- ✓ **Spikes**: picos cortos que tienen una anchura menor a 10s. Se mantienen durante toda la vida del gusano.

3.- La tasa de bombeo sufre una disminución progresiva durante el envejecimiento debido a la sarcopenia. Sin embargo, los picos citosólicos están presentes a lo largo de la vida del gusano. Por lo tanto, hay una disociación entre la señalización de calcio y la contracción muscular que se desarrolla con el envejecimiento.

4.- Los square-waves se deben a la depleción de energía en las células de la faringe, que detiene las bombas de Ca^{2+} e impide la extrusión de Ca^{2+} del citosol. Los gusanos que presentan square-waves de larga duración se clasifican como deficientes de energía (DE)

5.- Los picos square-waves y los gusanos depletados de energía aparecen con mayor frecuencia en los gusanos jóvenes, a pesar de su mayor contenido de energía. Esto puede deberse un alto consumo energético de los gusanos jóvenes sobrepasando la tasa de producción de energía.

6.- La cepa mutante AQ*eat-2*, un modelo de restricción calórica, presenta un mayor porcentaje de gusanos agotados energéticamente a lo largo de toda la vida que los gusanos de tipo silveste. En cambio, las cepas mutantes AQ*nuo-6* (alteración mitocondrial) o AQ*daf-2* (alteración de la señalización de la insulina) presentan un porcentaje menor de gusanos depletados energéticamente que los gusanos de tipo silvestre.

7.- Cuando todos los gusanos tanto las cepas mutantes como el fenotipo silvestre se colocan bajo privación de alimentos, el

porcentaje de gusanos con baja energía aumenta. Sin embargo, el aumento es menor en los mutantes AQ*nuo-6* y AQ*daf-2*.

8.- Las cepas mutantes AQ*nuo-6* y AQ*daf-2* mantienen mejor el balance energético (producción/consumo), incluso bajo privación de alimentos. Esto es probablemente debido a una adaptación metabólica para disminuir el consumo de energía.

9.- Las oscilaciones de calcio mitocondriales en la faríngе experimentan oscilaciones rápidas y persistentes [Ca^{2+}] similares a las oscilaciones citosólicas. Este resultado apoya el modelo latido a latido de la captación mitocondrial de Ca^{2+} en las células del corazón.

1**0.-** La dinámica mitocondrial [Ca^{2+}] también muestra spikes y square-waves de Ca^{2+}. Los picos square-waves $[Ca^{2+}]_M$ también son más frecuentes en los gusanos jóvenes y menos frecuentes en los mutantes M*nuo-6*.

11.- La captación mitocondrial de Ca^{2+} está relativamente bien conservada en mutantes M*nuo-6*, a pesar de la presencia de una mutación del complejo I de la cadena respiratoria que reduce significativamente la función mitocondrial.

INTRODUCTION

1. *C. elegans* organism model

Sydney Brenner, in the 1960s, proposed the nematode *Caenorhabditis elegans* as a model organism to study different areas such as developmental biology, genetics and nervous systems development among many others (Brenner, 1988), and because of this contribution Brenner was awarded the Nobel Prize in 2002.

C. elegans is a tiny non-parasitic nematode, just 1mm long at the adult state. It is transparent and this feature allows the use of fluorescent proteins to study different developmental processes, isolate cells or characterize protein interactions *in vivo* (Chalfie et al., 1994, Boulin et al 2006, Feinberg et al., 2008).

In nature, the worm can be found in the soil with decomposing plant material that stocks the necessary bacterial source for its feeding and development. In the laboratory, the *E. coli* strain so-called OP50 is the source of its nutrients. There is sexual dimorphism, there are hermaphrodites and males (1000:1); but self-fertilization predominates over fertilization by males. The number of somatic cells is constant in adult state, 959 cells. Each one has its fate, and they are distributed in well-defined tissues: epidermis, nervous system, muscle, digestive system and reproductive system.

C. elegans is a model widely used for studying aging because it has a short life cycle (only 3 days from eggs to egg-laying adult and four larval states) and short lifespan, about 25 days. This characteristic allows obtaining fast results (Kenyon, 1995).

Another characteristic that has made *C. elegans* a model widely used in the genetic research area is its easy genetic manipulation. Gene expression can be altered by RNAi just by

immersing the worms in a solution with dsRNA (Tabara et al. 1998) or administering OP50 with RNAdc (Timmons & Fire 1998).

2. Tissues

Despite being a very simple animal, *C. elegans* has well defined tissues. The worm has a cylindrical shape, and the tissues are like a series of concentric tubes: cuticle surrounds the epidermis, inside there are muscular bands and the nerves that innervate the muscles. Then, inside the neuro-muscular region we find the digestive, excretory and reproductive systems (Chalfie et al., 2015).

2.1. Cuticle

C. elegans cuticle is the most external tissue of the worm. It is a flexible exoskeleton that allows locomotion through junctions with muscle cells and protects the worm from the environment. The worm has four larval states, so at the end of each larval state, new cuticle is synthesized by the epidermis before each change.

The cuticle composition (see figure 1) is mainly made of cross-linked collagens, cuticlins (additional insoluble proteins), glycoproteins and associated lipids. The cuticle presents five layers: the surface coat, epicuticle layer and cortical, medial and basal zones (Cox et al., 1981a). There are few differences in cuticle composition between each larval state and adult. With aging adult cuticle thickness increases due to expansion of the basal zone (Herndon et al., 2002).

The cuticle is secreted by epithelial cells that cover the body of the worm (hypodermis and seam cells) and by interfacial cells lining the four major openings towards the outside (anus, excretory pore, vulva and pharynx) (Page, 2007).

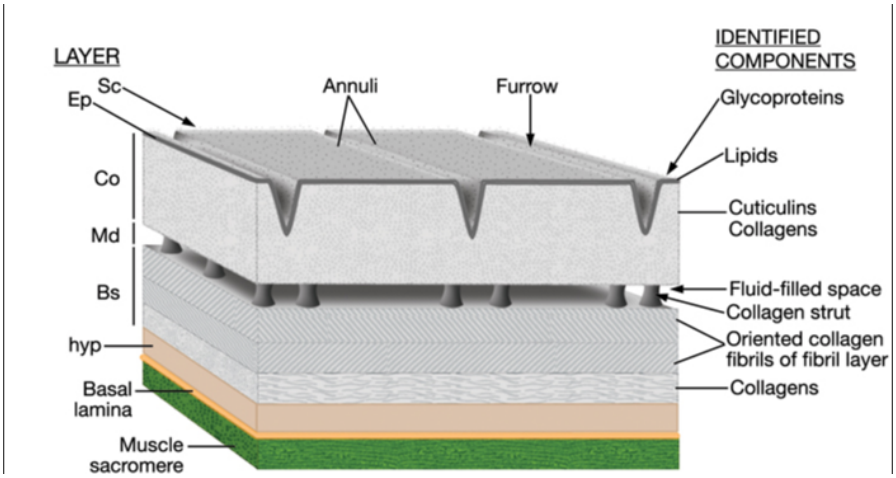

Figure 1: Schematic draw of adult cuticle layers and components (Sc) Surface coat; (Ep) epicuticle; (Co) cortical zone; (Md) medial zone; (Bs) basal zone. (Based on Blaxter and Robertson, 1998). http://www.wormatlas.org/hermaphrodite/cuticle/Images/cutfig3leg.htm.

2.2. Epidermis

The epidermis is a simple epithelium (see figure 2) with an internal basal surface covered by a basal lamina and an apical surface that secretes a flexible collagenous cuticle (Chisholm and Hsiao, 2012).

Morphogenesis of epidermis involves cell-cell interactions with internal tissues, such as the developing nervous system and muscles. Most epidermal cells fuse to generate multinucleate syncytia (Chisholm and Hardin 2005).

The epidermis is made up of a small number of cells. Despite this small number, there are different cells types with their own roles, both in development and in physiology (Chisholm and Hsiao, 2012). The **seminal cells** are one the different cell types;

they are responsible for cuticular specializations, playing roles in epidermal lengthening and molting. Another type of epidermal cells are the **interfacial epithelial cells**, specialized linker cells located at the interface between the hypodermis and the **atypical epithelial cells** located in the cells of the head and tail. These types of epidermal cells have transient epithelial functions in embryonic development (Wormatlas.org).

One of the most important functions of the epidermis is to provide a mechanical connection between body wall muscles and the external cuticle, and also to connect the outside with the nervous system. Other functions are to repair wounds and activate immune responses to skin-penetrating pathogens forming a barrier epithelium. The epidermis is responsible of ionic homeostasis, metabolic storage (mainly fat) and phagocytosis of cellular debris because *C. elegans* lacks phagocytic cells (Chisholm and Xu, 2012).

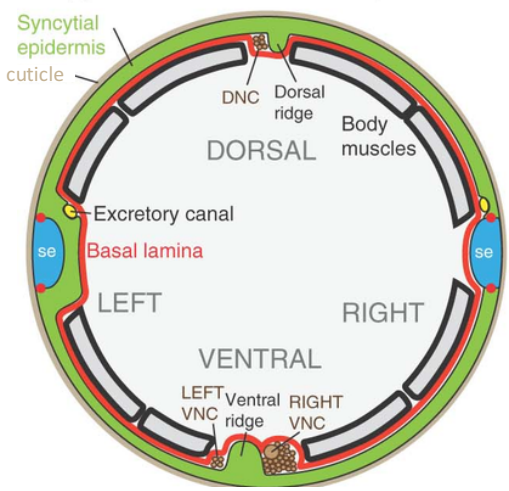

Figure 2. The epidermal basal lamina, and neuronal development. Cross-section of adult body epidermis and adjacent tissues and structures. The external surface is covered by the cuticle (grey); the internal face is covered by basal lamina (BL, red). Neurons (brown) reside on the epidermal side of the BL; (Chisholm and Xu 2012).

2.3. The excretory system

The *C. elegans* excretory system is a very simple tubular organ that consists of three unicellular tubes (canal, duct, and pore in figure 3) connected in tandem to form a continuous lumen. The cell of the excretory canal is the largest and one of the most distinctively shaped mononucleate cells in the worm. It is polarized with distinctive basal and apical surfaces. The cells of the excretory duct and pore connect the canal cell lumen to the exterior to allow fluid excretion and secretion. The duct canal is essential for viability, but mutants without pore cell can survive. The excretory gland is a binucleate cell that connects the canal cell to the canal-duct junction (Nelson et al. 1983).

The main function of the excretory system is osmoregulation. It secretes material to coat the cuticle with physical or osmotic protective material and it maintains the hyperosmotic coelomic fluid keeping the hypodermis rigid for effective muscle attachment and movement (Sundaram and Buechner, 2016).

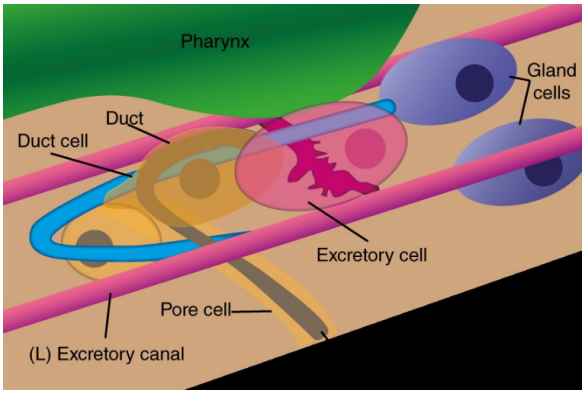

Figure 3: The excretory system consists of the fused pair of gland cells (blue), the excretory canal cell (pink), the duct cell (brown) and the pore cell (yellow). http://www.wormatlas.org/hermaphrodite/excretory/Images/excfig1leg.htm

2.4. The muscle system

There are two main types of muscle in *C. elegans*: striated and non-striated muscle (see figure 4). The striated muscle corresponds to somatic muscles; these have multiple sarcomere and attachment points to the hypodermis and cuticle distributed along their length. The non-striated muscle has a single sarcomere and attachment point to the hypodermis at the end. The non-striated muscle includes 20 pharyngeal muscle cells, 2 stomato-intestinal muscle cells, 1 anal sphincter muscle cell, 1 anal depressor muscle cell, 8 vulvar muscle cells, 8 uterine muscle cells, and a contractile gonadal sheath (Wormatlas.org).

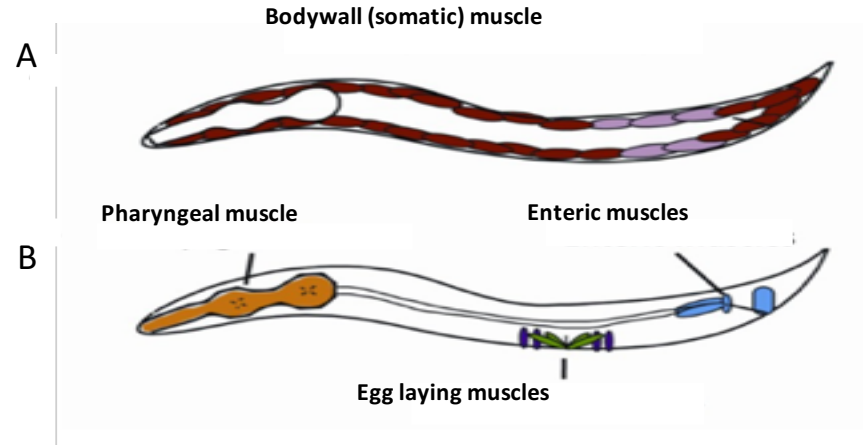

Figure 4. A. Representation of somatic muscle cells. **B**. Representation of some nonstriated muscle cells (Krause, National Institute of Diabetes and Digestive and Kidney Diseases NIDDK).

Three parts of each muscle cell can be distinguished: the **cell body**, containing the nucleus and cytoplasmic organelles; the **arm**, a process extending from the cell body to either the dorsal or ventral nerve cord to receive synaptic input from the motor neurons, (the figure 5 shows a schematic representation); and the region that contains the contractile myofilament lattice itself, bellow and parallel to the hypodermis (Waterson, Wood Ed., 1988).

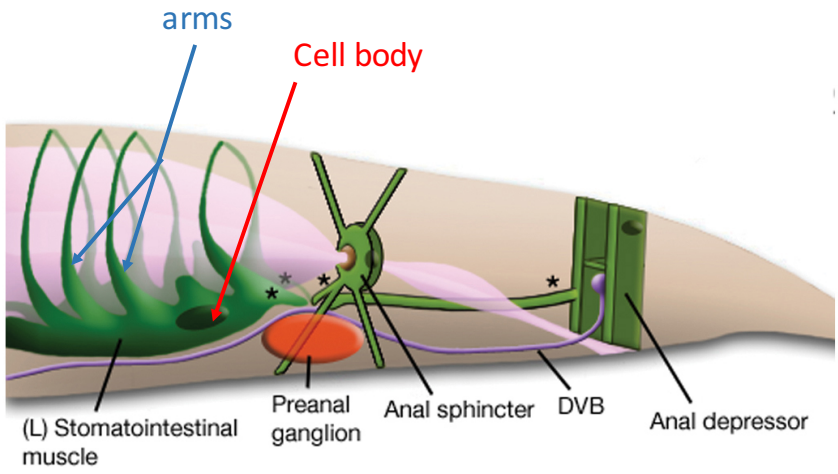

Figure 5: Schematic representation of enteric muscle cells. Muscle arms from enteric muscle synapsing onto DVB neuron.
http://www.wormatlas.org/hermaphrodite/muscleintro/Images/MusFig3.jpg

2.5. The nervous system

The nervous system is the most complex organ in *C. elegans*. Adult hermaphrodites have 302 neurons, and adult males 381; the extra neurons are in the tail, which is necessary for mating. Two different parts of the nervous system can be distinguished, one corresponds only to the pharyngeal system and the other is the somatic nervous system. The main difference between them is that while the somatic neurons share the basal lamina with the hypodermis

isolating the muscle, the pharyngeal neurons are not separated from the muscles by the basal lamina (White et. al, 1986). The pharyngeal and somatic nervous systems are connected by a bilateral pair of gap junctions between the somatic RIP neuron and the pharyngeal I1 neurons (Albertson and Thomson, 1976).

C. elegans has several complex behaviours, including movement and feeding, and also respond to mechanical stimuli or to changes in their environment, osmolarity and temperature (Chalfie and White, Wood Ed. 1988).

C. elegans lacks voltage-gated Na^+ channels, so it can not generate what we know as typical action potentials. It is still debated whether the synapse actually occurs through action potentials or other types of regenerative events, including passive driving or graded regenerative responses (Lockery et al., 2009).

Despite its primitive nervous system, neurotransmitters such as acetylcholine, glutamate, α–aminobutyric acid (GABA), dopamine and serotonin have been identified and receptors have been found for them (Hobert, 2013).

Neurons can be classified in four functional categories depending on their circuitry: motor neurons, which make synapses with muscle cells; sensory neurons, synapsing with sensory specializations that are summarized in figure 6; interneurons, that receive synaptic contacts and also send outgoing synapses to other neurons; polymodal neurons, that act on more than one of these functional modalities. In figure 6 we can see that the pair of ASH neurons located in the head are both chemosensors and nociceptors.

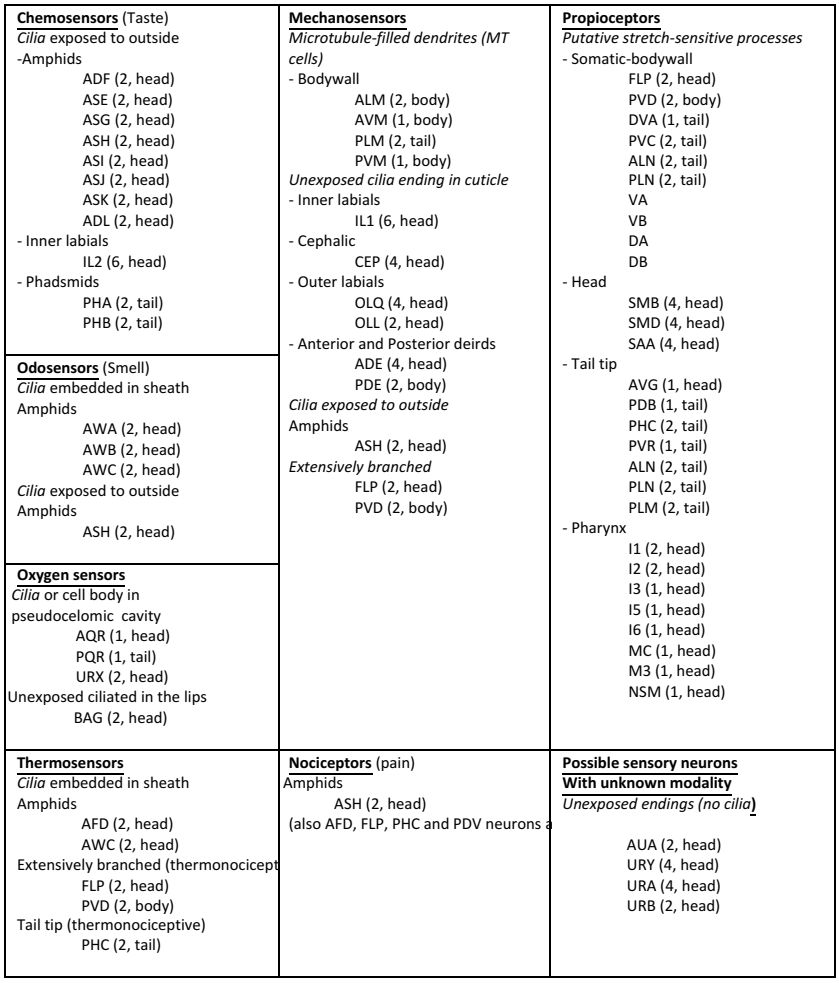

Figure 6: List of hermaphrodite sensory receptor. http://www.wormatlas.org/hermaphrodite/nervous/Images/neurotable1leg.htm

2.6. Reproductive system

C. elegans has two sexual forms, hermaphrodite (XX) and male (X0). In nature, the percentage of males is very low, approximately 0,1%. However, in situations of environmental stress such as an increase in temperature or lack of food, the proportion of males increases by meiotic non-disjunction events (Anderson JL. et al, 2010)

The hermaphrodite keeps inside the gonad both oocytes and spermatheca, and fecundation and development of the eggs takes place along the oviduct. There is also the possibility of being fertilized by males. When hermaphrodites mate, the egg-laying number doubles and the reproduction age increases. The figure 7 shows the difference between self-production and mate production (Herman, 2006).

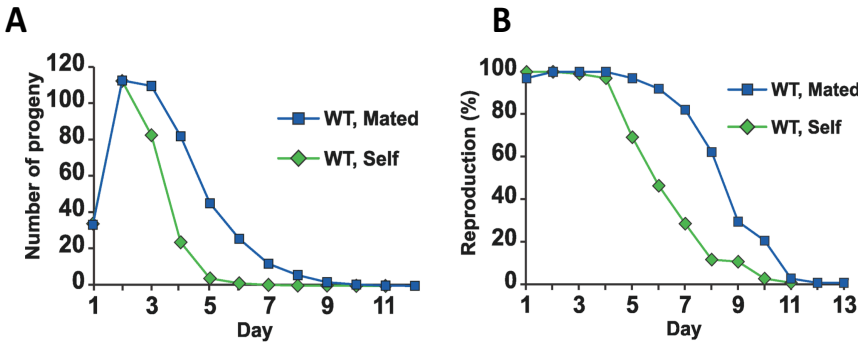

Figure 7: **A**. Average daily progeny production of live hermaphrodites.
B. Percentage of live hermaphrodites producing progeny (Hughes et al., 2007).

Anatomically both sexes are very similar, they only differ in sexual structures, as it can be observed in figure 8. Hermaphrodites have the vulva in the posterior third of the body. This structure allows both egg laying and fecundation by males. Males have a brush-shaped tuft at the end of the tail, which they use to introduce the sperm through the vulva into the hermaphrodite. Males are smaller, thinner and only produce sperm.

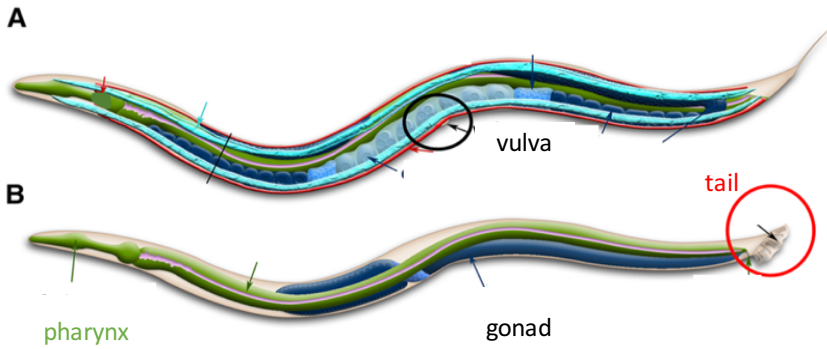

Figure 8: **A**. *C. elegans* hermaphrodite. **B**. *C. elegans* male (Chalfie, 2015)

3. Pharynx

3.1. Pharyngeal anatomy

The pharynx is an epithelial organ with its own muscles, nervous system, gland cells and structural cells. It contains 9 epithelial cells, 20 muscle cells, 20 neurons, 4 gland cells and 9 marginal cells and 6 valves (see figure 9). The pharynx has intrinsic myogenic activity regulated by its nervous system. The pharynx is isolated from the rest of the animal by a specialized basal lamina. The buccal cavity is located in the anterior portion while the intestine is in the posterior position and the pharynx connects both parts (Avery and Thomas, 1997).

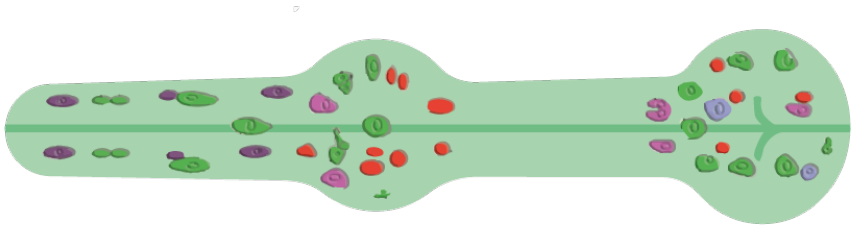

Figure 9: Representation of all some cells that make up the pharynx. (R*ed*) Neuron nuclei; (*green*) pharyngeal muscle nuclei; (*lavender*) gland nuclei; (*fuchsia*) marginal cell nuclei; (*purple*) epithelial nuclei. (Based on drawing by Ron Ellis.)
http://www.wormatlas.org/hermaphrodite/pharynx/Images/phafig1leg.htm

3.1.1. Pharyngeal buccal epithelium.

The interfacial cells join the lips to the buccal cavity and this with the pharynx. A thin cuticle covers the interior surface of the pharyngeal duct from the lips to the pharyngeal-intestinal valve. The cuticle is formed by pharyngeal epithelium and muscle cells. This cuticle has not layers but there is some reinforcement at points of stress, for example at the grinder there is a cuticle specialization made by pm6 and pm7 muscle cells that acts as a valve regulating one-way traffic of food into the intestine (Avery and Thomas, 1997).

3.1.2. Neurons.

The cell bodies of the 20 neurons are located in the anterior or posterior bulb and send the processes forward and/or backward along the three longitudinal pharyngeal nerve cords.

The nervous system is able to integrate its own nutritional status, but also external signals such as the presence or absence of food. Three pharyngeal motor neuron: M3, MC y M4 seem to be enough for normal feeding under laboratory conditions. M3 controls the timing of the pumping (Albertson and Thomson,

1976), MC controls the rate of excitation of pharyngeal muscle (Avery and Horvitz, 1989), and M4 is necessary for posterior isthmus peristalsis.

3.1.3. Muscle cells

Muscles cells contain a single sarcomere and the attachment points are localized at the ends of the cells as half I bands ending in electron-dense attachments connecting the myofilaments to epithelium.

The pharyngeal muscle cells are grouped into eight separate segments (pm1-pm8) and the myofilaments are disposed with threefold radial symmetry. The three muscle cells of each segment are separated from each other by three marginal cells whereas the muscles cells of different segment are linked by gap junctions. Figure 10 represents the disposition of muscle cells and marginal cells in a transversal cut of one segment of the pharynx (Avery and Thomas, 1997).

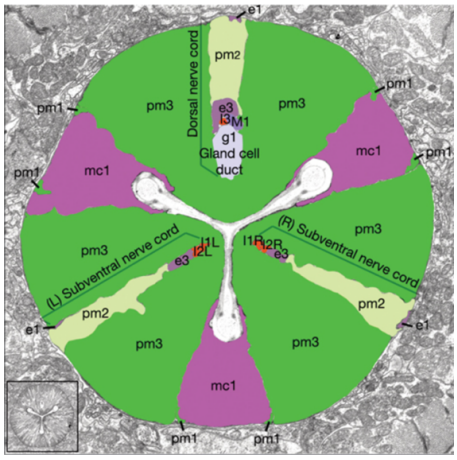

Figure 10: Transversal cut of one segment of the pharynx.
http://www.wormatlas.org/hermaphrodite/pharynx/Images/phafig7Aleg.htm

These muscles can be divided into three functional groups (see figure 11). The **corpus**, pm1-pm4 muscles, constitutes the anterior half of the pharynx, and its function is to take in and trap bacteria. The **isthmus**, pm5 muscle, is the middle part, and it regulates the flow of food from the corpus to the terminal bulb. Finally, the **terminal bulb** is the posterior part of the pharynx, pm6-pm8, where bacteria are grinded (Avery and Thomas, 1997).

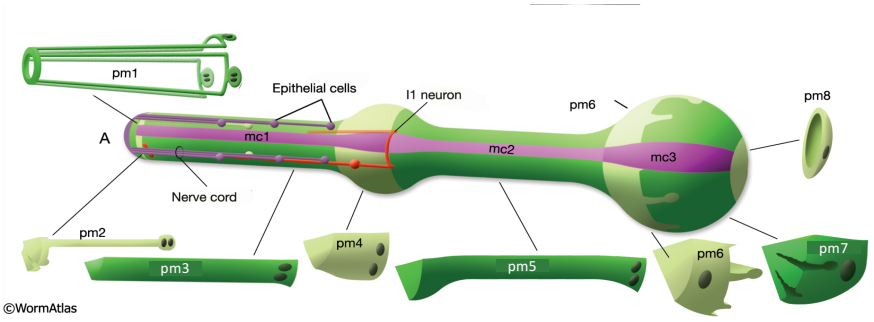

Figure 11: Segment of muscular and marginal cells.
http://www.wormatlas.org/hermaphrodite/pharynx/Images/phafig6leg.htm

3.1.4. Marginal cells.

Marginal cells are coupled by gap junctions to muscle cells with motor function. The gap junction network gives a high connectivity within the pharynx that it is critical for coordinating the waves of muscle contraction and for spreading the neuronal input (Phelan, 2005).

3.1.5. Gland cells

Gland cells located in the second bulb receive motor innervation that stimulates them to secrete digestive enzymes following the rhythm of the pharyngeal pumping activity. Secretion periods associated with moulting have also been seen. (Hall and Hedgecock, 1991).

3.1.6. Valve cells

Valve cells form an epithelium channel lined with the pharyngeal cuticle that links the lumen of the pharynx to the intestinal lumen. These cells do not have muscle elements, so the valve may be a passively open channel with a narrow calibre and the pm8 muscular cell will act alone as a sphincter just before the valve cells (Avery and Thomas, 1997).

3.2. Pharyngeal movement

Normal feeding consists of two motions: pumping and isthmus peristalsis. **Pumping** consists of coordinated cycles of muscle relaxation and contraction. Each cycle of contraction/relaxation corresponds to a round of muscle cells action potential. This action potential occurs through different ion channels explained in detail later (Avery and You, 2012). **Isthmus peristalsis** is less understood. It happens every 3-5 pumps. During this movement the posterior isthmus is opened and closed by a wave that goes in the anterior-posterior direction. Through this wave, bacteria trapped in the isthmus are transported to the posterior bulb where the crusher is located.

The worms ingest bacteria in liquid suspension and the separation between the solid bacteria and water solution is not completely known, but relaxation is an important key in filtering. Motions of the anterior isthmus have a delay with those of the corpus. During a pump there is a perfect synchronization of contraction within corpus or terminal bulb and a delay in the excitation between the isthmus and the corpus of a few milliseconds. The isthmus seems to act as a double valve (see figure 12) that separates the high and low pressure regions of the pharynx. During pumping the mouth until the middle isthmus is at

low pressure while the region between the terminal bulb and the intestine is at high pressure. During an isthmus peristalsis, there is high pressure from isthmus to terminal bulb, (Riddle Cold Spring Harbor Laboratory Press; 1997).

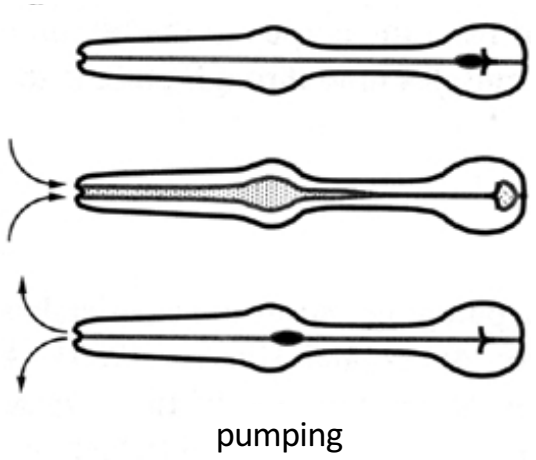

Figure 12: Pharingeal pumping (Avery and Horvitz, 1989)

The pharynx has 20 neurons of 14 different types but only three of them play an important role for normal feeding: M4 neuron is necessary for normal isthmus peristalsis, MC and M3 neurons control the pumping rate. Surprisingly, if all the neurons are removed, the pumping continues, so that synchronization between the corpus and the terminal bulb occurs through muscle gap junctions and do not require the pharyngeal nervous system (Avery and Horvitz, 1989).

3.3. Pharyngeal muscle action potential

The pharynx generates pumping and isthmus peristalsis with precise frequency and with accurate timing. Each contraction/relaxation cycle corresponds to a single pharyngeal muscle action potential. This action potential is due to the sequential action of five ion channels: (1) a nicotinic acetylcholine

muscle action potential. This action potential is due to the sequential action of five ion channels: (1) a nicotinic acetylcholine receptor, (2) a low-threshold voltage-gated calcium channel, (3) a high-threshold voltage-gated calcium channel, (4) a glutamate-gated chloride channel and (5) a voltage-gated potassium channel. Most of the knowledge of the electrical events in the pharynx comes from a simple recording method electropharyngeograms (EPG), which measures electrical currents that flow in and out of the worm mouth (Raizen and Avery, 1994).

3.3.1. Nicotinic acetylcholine receptor: EAT-2

The common pharyngeal action potential starts with the firing of the motoneuron MC. The neurotransmission to the muscle cell goes through neuromuscular junctions whose neurotransmittter is acetylcholine. Acetylcholine acts on the nicotinic receptor (Raizen and Avery, 1994). It is known that the *eat-2* gene encodes a nicotinic receptor subunit in the pharyngeal muscle and is located on the MC neuromuscular junction. Nonetheless, pumping still occurs after mutation of the *eat-2* gene or ablation of the MC motoneuron, although pumping is irregular and slow (McKay et al, 2004). The mechanism of this residual pumping is still unknown. Some authors propose the existence of a hyperpolarization-induced sodium channel, similar to that in vertebrate cardiac muscle (Franks et al., 2002).

3.3.2. T-type calcium channel: CCA-1

CCA-1 is a calcium channel activated in response to excitatory inputs from the MC neuron and accelerates the action potential upstroke. The *cca-1* gene encodes the pore-forming subunit of a T-type Ca^{2+} channel. When it is deficient, the depolarizing phase of the pharyngeal action potential tends to plateau at the voltage that

the CCA-1 channel is likely to be active (Steger et al., 2005; Shtonda and Avery, 2005).

3.3.3. L-type Calcium Channel: EGL-19

The EGL-19 calcium channel is activated at high voltages and inactivates slowly to maintain the plateau phase of the action potential. The *egl*-19 gene encodes the α subunit of a homolog of vertebrate L-type voltage-activated Ca^{2+} channels. *egl-19* has an important role in regulating muscle excitation and contraction, not only in the pharyngeal muscle but also in all *C. elegans* muscles. Several *egl-19* mutants have been isolated and have been classified in three groups: (1) the myotonic group, that corresponds to a semidominant gain of function where the action potentials are lengthened and the relaxation is delayed, (2) the flaccid group, whose partial loss of function triggers slow muscle depolarization and weak contraction and (3) the lethal group, whose severe loss of function eliminates muscle contraction, so this mutation is lethal before hatching (Lee et al., 1997).

3.3.4 Glutamate gated chloride channel: AVR-15

The AVR-15 is a member of the family of ligand-gated chloride channels. It is found in many animal cells, but vertebrates lack them. The timing of pharyngeal muscle relaxation is modulated by the M3 neuron, which generates fast inhibitory postsynaptic potentials in the contracted pharyngeal muscle. Two genes are necessary for the neurotransmission from M3 to muscle: the *eat-4* gene is necessary in the presynaptic glutamatergic neurons and encodes a vesicular glutamate transporter (Raizen and Avery, 1994) and the *avr*-15 gene is required postsynaptically for a functional M3 synapse and for the hyperpolarizing effect of glutamate on the pharyngeal muscle (Dent et al., 1997).

3.3.5 Potassium channel: EXP-2

The EXP-2 is a member of the Kv family of voltage-gated potassium channels. This channel has unusual properties as it allows the muscles to repolarize quickly and with the proper delay (Fleischhauer et al., 2000). It activates slowly, but inactivates very rapidly. Thus, it opens only during repolarization. It remains closed during a typical neuronal action potential but returns efficiently the muscle cells to resting potential when the membrane potential falls below its threshold, for example after the action potentials triggered by M3 neurons. (Shtonda and Avery, 2005).

Based on the properties of these channels, Shtonda and Avery proposed a model for the pharyngeal action potential, (see figure 13). Motor neuron MC excites the pharynx through the nicotinic acetylcholine receptor. The neurotransmission from MC depolarizes the membrane activating CCA-1. CCA-1 gives rise to large fast inactivating inward currents, which drive a quick membrane depolarization activating EGL-19. EGL-19 activation allows calcium entry, triggering muscle contraction and maintaining depolarization during the plateau phase. Then, slow EGL-19 inactivation, probably calcium dependent, starts membrane repolarization, which is accelerated when it achieves the threshold for EXP-2 recovery from inactivation. At the same time, inhibitory neurotransmission from the M3 neuron via the AVR-15 channel also accelerates repolarization. When the threshold is achieved, EXP-2 generates a large outward current causing fast membrane repolarization and termination of the action potential.

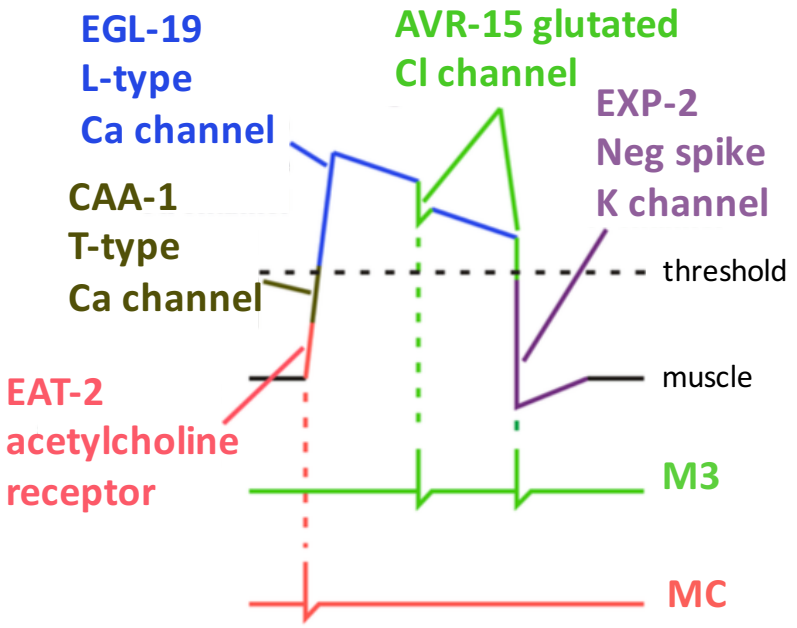

Figure 13: Pharyngeal muscle action potential from terminal bulb muscle (Avery and You, 2012)

3.4. Calcium signalling

Calcium is a broadly signalling ion in all living organisms. Calcium plays important roles in several cellular functions such as cell division and cell death, muscle contraction, gene transcription, or even in the regulation of ATP production. *C. elegans* has many calcium channels, calcium transporters and calcium binding proteins with ortholog human genes. Figure 14 shows different cellular mechanisms involved in calcium homeostasis regulation (Hobert, 2013).

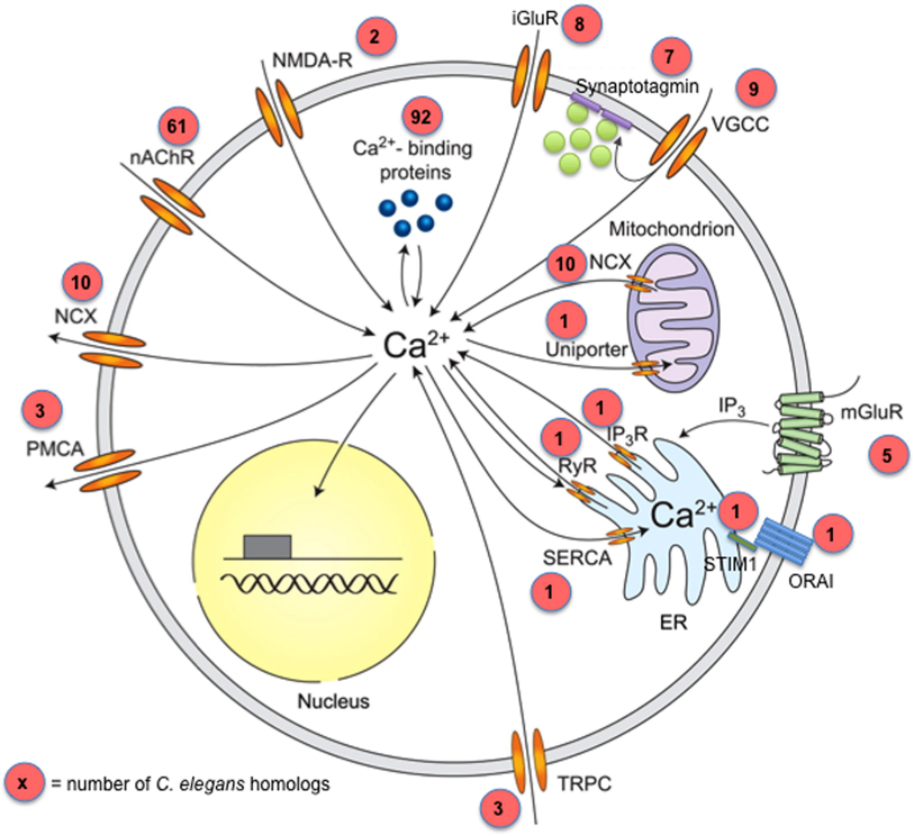

Figure 14: Neuronal calcium signalling. (Hobert, 2013). Red circle represents the number of human homologs.

Under resting conditions, the calcium concentration in the cytosol ($[Ca^{2+}]_C$) is much lower (100nM) than in the extracellular medium (1mM). Regarding intracellular organelles, mitochondria have also a very low resting $[Ca^{2+}]$ (100nM), but others such as endoplasmic reticulum behave as Ca^{2+} stores and have $[Ca^{2+}]$ levels similar to those in the extracellular medium (from 0,5 to 2mM) (de la Fuente et al. 2013).

When the cell is stimulated, calcium signalling occurs and the $[Ca^{2+}]_C$ increases due to the entry of Ca^{2+} from extracellular medium and/or its release from the endoplasmic reticulum, these are called "**ON reactions"**. For the signalling to continue, it is essential to return to the resting state, so there are several mechanisms that extrude calcium out of the cell or sequester it into organelles. These are the "**OFF reactions"** summarized in figure 15 (Berridge MJ, 2012).

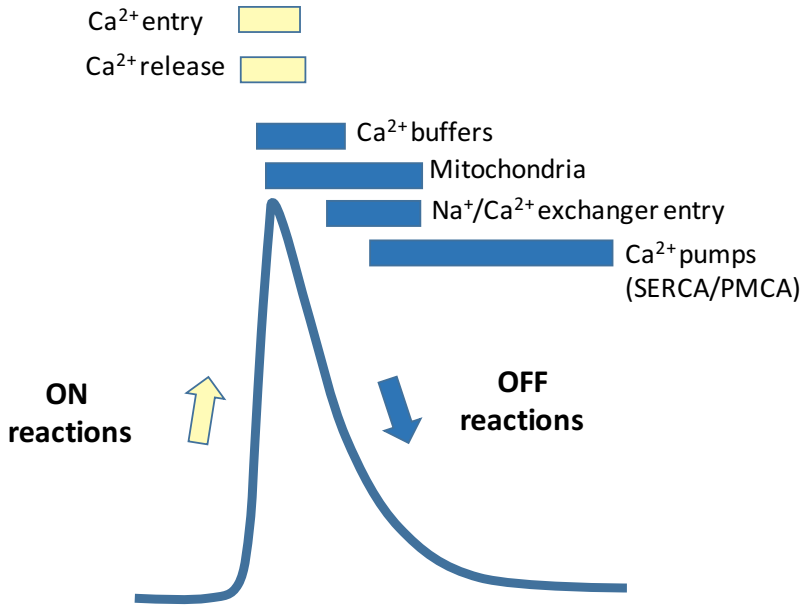

Figure 15: Different mechanisms involved in **on reactions** and **off reactions** (Based on Berridge MJ., 2012)**.**

The neuron releases the neurotransmitter that starts a series of processes that induce muscle contraction. Any mutation on the genes involved in calcium signalling can disturb the regular pumping. For example, the *unc-68* gene encodes the ryanodine receptor and null-mutants of this gene present a weaker

pharyngeal pumping, although electrical activity is normal (Anderson, 1996).

4. Lifespan

The global human lifespan is increasing over the years, therefore the number of people suffering from diseases or disabilities also increasing dramatically. Researchers have a great challenge to explore the way of getting old in a healthy manner. The best way to achieve this goal is to understand health, aging and diseases, their determinants, risk factors and pathways (Luyten et al. 2016). This knowledge will then allow us to develop strategies for prevention, diagnosis and treatment.

Lifespan is the time from birth to death, whereas healthspan is the life period when one is functionally independent and free from severe diseases. In recent years, most of the research has focused on increasing life expectancy taking into account the different genetic and environmental factors of aging. Researchers assumed that lifespan and healthspan were strongly correlated. However, nowadays we know that this is not always the case, and there are interventions that increase healthspan but not lifespan (Garcia-Valles et al., 2013; Bansal et al. 2015).

4.1. Metabolic pathways related to aging

At the beginning of this introduction it was shown that *C. elegans* is a good model for studying lifespan. The worm has a short lifespan, a huge offspring, many homologous genes shared with humans and most importantly: easy genetic manipulation (Kenyon, 1995).

The first discovery showing that it is possible to interfere in the aging process by carefully manipulating genetic targets, was made in the *C. elegans* conserved insulin/IGF-1-like signalling (IIS)

pathway and it was reproducible in mammals (Kenyon et al., 1993; Bartke, 2008).

TOR and AMPK are also evolutionary conserved pathways with a key role in aging, both involved in energy metabolism (Kenyon et al., 2010). Other cellular processes that modulate the rate of ageing are translation rate, autophagy and effects of the antihyperglycemic drug metformin (Hansen et al. 2007; Cabreiro et al. 2013; De Haes et al. 2014).

Dietary restriction is one of the main environmental factors that increases lifespan. There are some mutations targeted to mimic this state and the mutated worms live more than wildtype (Braeckman et al., 1998; Braeckman et al., 2002; Luedtke et al. 2010).

4.2. Age-related changes in *C. elegans*

Along life different age-related changes happen in different tissues. It is interesting to identify these alterations and to be able to measure them in an easy way because they could be markers of aging.

Before defining aging biomarkers, it is important to distinguish between age-related changes that represent development (egg laying) from those that represent senescence (reduced motility). There are diverse useful criteria: point in the life cycle when the change occurs, changes that increase or decrease organization and function and existence of a genetic program that specifies the changes (Collins et al., 2007).

4.2.1. Age-related neuromuscular behaviours

1. Pharyngeal pumping: The rate of pharyngeal pumping reaches a maximum of nearly 300 pumps/min on 2 day-old adults, decreasing progressively with age to about 100 pumps/min by day 8, 10 pumps/min by day 12 and essentially no activity after day 14 (Huang et al., 2004).

2. Body movement: *C. elegans* has a well-coordinated sinusoidal body movement in young hermaphrodite, but becomes progressively slower and less coordinated from day 10 in wildtype worms (Bolanowski et al., 1981; Huang et al 2004, Stamper et al., 2018).

4.2.2. Age-related morphological changes

1. Body size: adults increase in length, width and volume from day 3 to day 14. The change in body size is an example of programmed growth instead of a degenerative change (Bolanowski et al. 1981).

2. Head and pharynx: during aging worms undergo some changes, such as the progressive lack of definition of nuclear boundaries, the appearance of necrotic cavities and curdled texture. These changes have been defined in categories and used as biomarkers (Garigan et al. 2002; Herndon et al., 2002).

3. Bacterial content: *C. elegans* are fed with *E. coli*. Over time, there is a progressive increase in the amount of bacteria in the pharynx and intestine, regardless of the decrease in pharyngeal pumping (Chow et al., 2006; Garigan et al. 2002).

4. Body wall muscles: GFP targeted to the sarcomeres of body wall muscles can be used to visualize muscle structure. Age-related

disorganization of sarcomeres has been studied this way (Glenn et al., 2004; Herdon et al., 2002).

5. Mitochondrial dysfunction: body wall muscle mitochondria undergo progressive fragmentation with aging, together with a decrease in mitochondrial length and area, and increase of mitochondrial circularity (Regmi et al., 2014).

4.2.3. Age-related biochemical changes

1. Accumulation of fluorescent compounds such as lipofuscin during the life of the worm, mainly in the intestine (Garigan et al., 2002).

2. Accumulation of DNA damage, such as increase in single-strand breaks. Decrease in the ability to serve as a transcription template in cell based assays (Klass et al., 1983).

3. Accumulation of protein carbonylation: it is measured from extracts of pooled worms obtained at each age. The level of protein carbonylation per milligram in those extracts increases about 3- fold from 4-8 day to 20 day (Adachi et al. 1998).

4. Accumulation of yolk protein in the body cavity: yolk protein is secreted by the intestine of young worms because it is necessary in late stage oocytes and embryos. Older hermaphrodites accumulate yolk protein in the body cavity (Garigan et al., 2002), because the intestine endures synthesizing and secreting this protein after the oocyte production declines, and it is therefore accumulated in the body cavity (Herndon et al., 2002).

5. Metabolic activity:

- ✓ Carbon dioxide generation declines about 50% from day 6 to day 12 (Van Voorhies and Ward, 1999).
- ✓ Oxygen consumption declines about 60% from adult day 0 to day 12 (Braeckman et al., 2002a).
- ✓ ATP levels decline about 80% from adult day 0 to day 12 (Braeckman et al., 2002a).

6. Enzymatic activities:

- ✓ Protein tyrosine kinase activity decreases 60% from day 5 to day 15 (Vanfleteren et al., 1998).
- ✓ Lysosomal acid hydrolases increase in activity through aging (Bolanowski et al. 1983).

4.3. *C. elegans* mutants with lifespan extension

To study Ca^{2+} homeostasis in the pharynx, we decided to compare wildtype worms with three mutant strains. The mutants present different alterations that induce lifespan extension.

4.3.1 *nuo-6* (*qm200*)

This mutation induces partial loss of function of a subunit of complex I of the mitochondrial respiratory chain (NUDFB4) (figure 16) The phenotype of this worm includes low oxygen consumption, slow growth, slow behaviour and lifespan increase (Yang and Hekimi, 2010a).

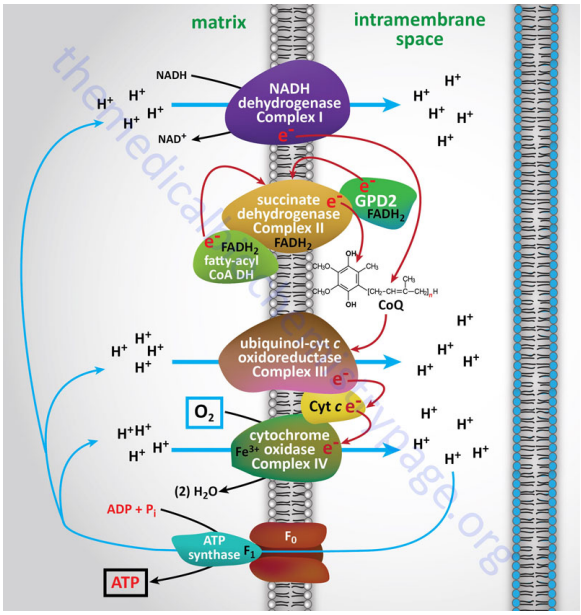

Figure 16: Components of the mitochondria electron transport chain. https://themedicalbiochemistrypage.org/es/oxidative-phosphorylation-sp.php

The mechanism of lifespan extension in this mutant may be in part related to the increased production of reactive oxygen species (ROS). It is known that the mitochondrial respiratory chain is the main source of superoxide anion and other ROS. This mutant has elevated superoxide production in isolated mitochondria, but has no changes in the total level of ROS and or in oxidative stress (Yang W. and Hekimi S., 2010b). The higher mitochondrial ROS (mtROS) levels are essential to increase the lifespan. In vertebrates these mtROS activate the intrinsic apoptosis signalling pathway to protect damaged cells, but in nematodes they stimulate protective mechanisms to preserve the survival of the nematode under stress conditions. (Yee et al., 2014). Figure 17 shows a model.

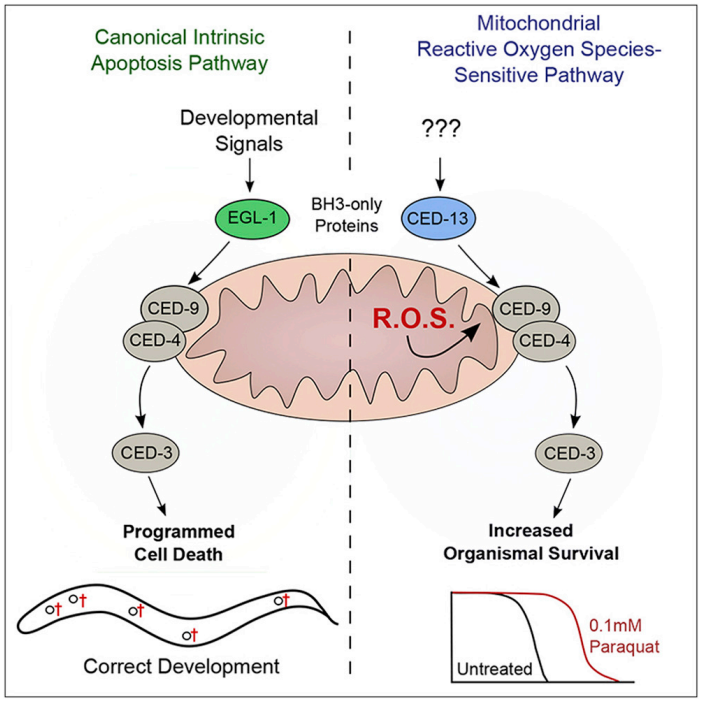

Figure 17: Model for the regulation of the lifespan by mtROS signalling through the intrinsic apoptosis pathway (Yee et al., 2014)

4.3.2 *eat-2* (*ad1113*)

The *eat-2* gene encodes a nicotinic acetylcholine receptor subunit. The protein is present in the pharyngeal muscle localized postsynaptically on the MC neuron synapse (figure 18). Mutations in this gene trigger a defective feeding behaviour: the nematode is unable to pump properly in the presence of food. The reduced food intake is responsible for the increase of lifespan through caloric restriction (McKay et al., 2003).

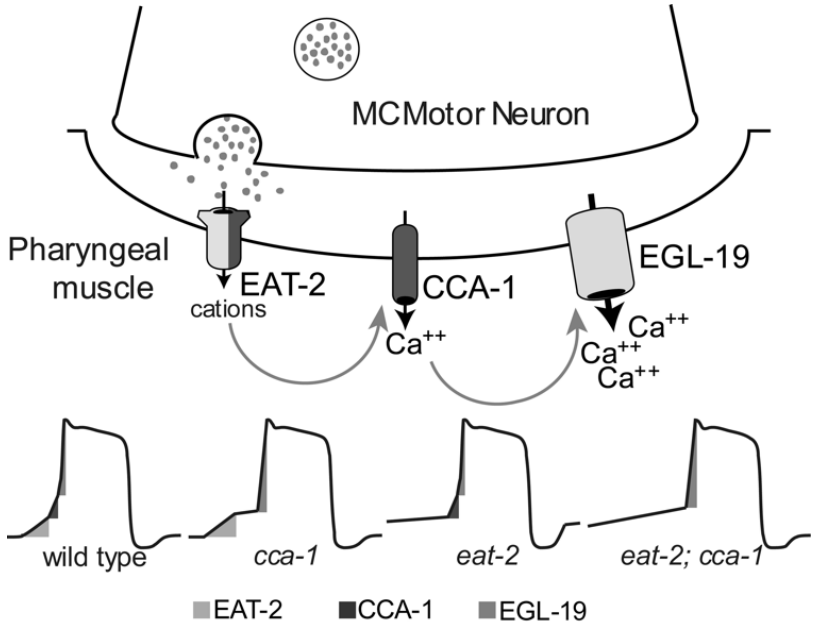

Figure 18: Cooperation of EAT-2, CCA-1 and EGL-19 to produce the upstroke of pharyngeal action potential (Avery and You, 2012).

4.3.3 *daf-2* (*e1370*)

This gene encodes the insulin/IGF-1 like receptor. The first genetic pathway that lengthens lifespan was discovered by mutating this gene and is evolutionarily conserved in several animal models (Kenyon C., 2011). *daf-2* in *C. elegans* plays an important role in dauer formation working together with *daf-16* (cartoon in figure 19). Dauer is the long-term resistance state adopted by the nematode under stress conditions. High reductions in *daf-2* expression using RNAi trigger dauer formation, but low reductions allow growth to adulthood and extend the lifetime. This gene also encodes nutrient sensors and participates in reproductive development, hypoxia or oxidative stress resistance (Kenyon, 2011).

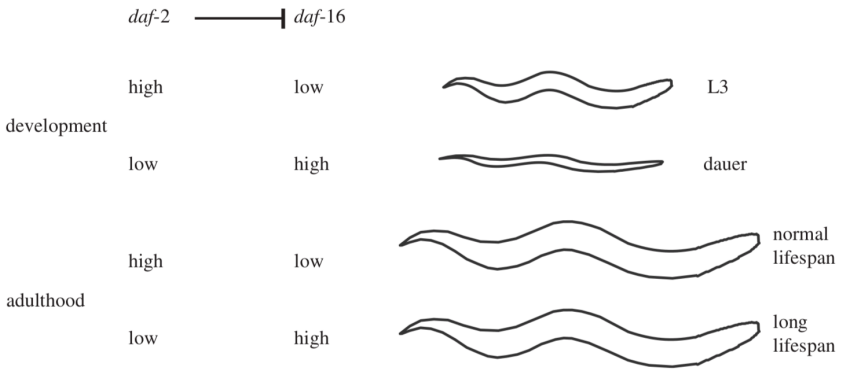

Figure 19: Role of *daf-2* and *daf-16* in regulating development and lifespan (Kenyon, 2011).


AIMS

As described in the Introduction, there are several typical age-related changes in *C. elegans*, and one of the more characteristic ones corresponds to the changes in the neuromuscular system, and specifically the changes in pharyngeal pumping. The pharynx, a neuromuscular organ, undergoes rhythmic contractions to facilitate food ingestion and goes through a progressive decline during aging. Ca^{2+} ions play an essential role in muscle contraction. Therefore, the primary objective of this work was to study the changes in cytosolic and mitochondrial pharynx cells [Ca^{2+}] transients during the worm life.

To achieve this objective, we have undertaken the following specific aims:

1. To perform long-term pharyngeal cytosolic and mitochondrial calcium measurements in wild-type worms.
2. To obtain mutant strains *nuo-6, eat-2* and *daf-2*, expressing the calcium probe YC2.1 in the cytosol and YC3.60 in the mitochondria.
3. To perform long lasting pharyngeal cytosolic and mitochondrial calcium measurements in mutant strains *nuo-6*, e*at-2* and *daf-2*.

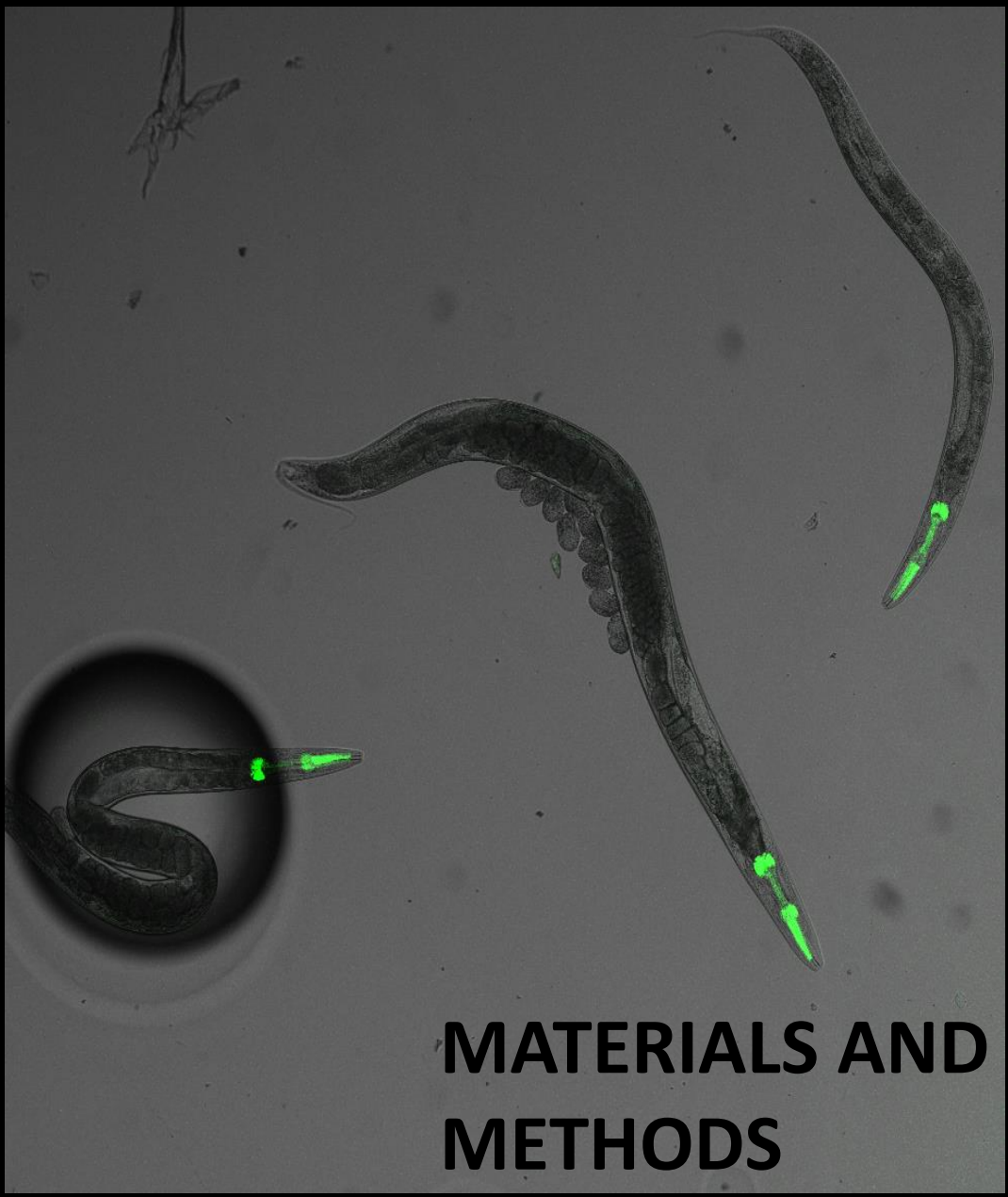

MATERIALS AND METHODS

1.- Worm strains

AQ2038 is an N2 strain which has integrated the sequence *pmyo*_2::YC2.1. These worms express the Ca^{2+} sensor cameleon 2.1 (YC2.1) in pharynx cytosol, controlled by the *pmyo*-2 promoter (Miyawaki et al., 1997; Nagai et al., 2004).

nuo-6(qm200). This strain is defective in a subunit of complex I of the mitochondrial respiratory chain (NUDFB4). These worms have decreased mitochondrial function and as a consequence lower oxygen consumption, slow growth, slow development and decreased ATP levels (Yang and Hekimi, 2010). In spite of this, they have an increased lifespan. This strain is a model to study the pumping affected by low mitochondrial activity and low ATP levels.

eat-2(ad113). The *eat-2* gene encodes a nicotinic acetylcholine receptor subunit located in the pharynx muscle (McKay et al., 2003). The *eat-2* mutation produces slow pharyngeal pumping and mimics caloric restriction (Lakowski and Hekimi, 1998), producing also lifespan extension. This strain is a model of caloric restriction.

daf-2(e1370). The *daf-2* gene encodes insulin/IGF-1 like receptor and this is the first metabolic route known to be involved in the regulation of aging. This receptor also participates in reproductive development, temperature, hypoxia and oxidative stress resistance, as well as bacterium pathogen resistance (Kenyon, 2011). The *daf-2* mutation induces a large increase in *C. elegans* lifespan.

2. Worm maintenance

2.1 NGM plates

Worms are grown at 20°C on Nematode Growth Medium (NGM) agar poured into petri plates. The NGM agar plates were prepared in the lab following this protocol.

NGM (250 ml)	
Agar	4,25g
Peptone	0,625g
NaCl	0,75g

After sterilization, the flask is cooled in a 55°C water bath and then the following compounds are added:

Cholesterol (5mg/ml)	250 µl
$CaCl_2$ 1M	250 µl
$MgSO_4$ 1M	250 µl
KPO_4 buffer (1M) (KH_2PO_4/K_2HPO_4)	4,25ml

When the NGM is ready to aliquot, the medium is distributed in 55mm plates, in sterile conditions. The plates are set aside until they are dry enough for seeding with 250 µl of OP50 (*E. coli* bacteria strain serving as food source for the worms). OP50 is

grown at room temperature in 2xYT medium overnight and it is then seeded in the middle of the NGM agar plates to avoid the worms to go out of the plate (Stiernagle, 2006).

In the case of the plates prepared to make genetic crosses, just 50 μl of OP50 are seeded in the middle of the 55mm plate, to facilitate the encounter between males and hermaphrodites. It is called a drop plate.

2.2. NGM plates with FuDR (15 μM)

FuDR (5-fluoro-2´-deoxyuridine) is an inhibitor of thymidylate synthase, stops the synthesis of DNA and RNA and blocks cell division. In *C. elegans*, cell division occurs only in the germline. Therefore, FuDR stops the development of eggs and larvae, but has no effects in adults (Mitchel, 1979).

The experiments are performed with synchronized day 1 adult worms. Since *C. elegans* are hermaphrodite, FuDR 15μM is added to the NGM plates after autoclaving in order to avoid progeny (which could generate later confusion with the original adults).

The NGM plates with FuDR 15 μM are seeded the next day with 250 μl OP50. Three days later, the seeded FuDR plates are ready to use.

2.3. M9 buffer

M9 buffer is the regular buffer used to work with worms. It is necessary to sterilize it by autoclaving. The M9 buffer composition is as follows:

Compound	**Quantity** for 1l
KH_2PO_4	3g
Na_2HPO_4	6g
NaCl	5g
$MgSO_4$ (1M)	1ml

3. Synchronized worms

To synchronize worms, we used plates with starved adult worms. When the adult worms are starving they keep their eggs inside because it is a stress condition, so they retain the eggs while waiting for better environmental circumstances.

To obtain starved adult worms, fifty adult worms are plated on a fresh new seeded NGM plate, so that two days later the food runs out. This is the right time to collect the worms. Worms are collected with a glass Pasteur pipette in a microtube with 1.5ml of milliQ water. After 2 min spinning at 2000rpm, 1.4ml of the supernatant is removed and the pellet is resuspended with a solution containing 150μl of commercial bleach and NaOH 5mM (2:1) and 250 μl of M9 buffer. The mix must be prepared fresh. This mix kills adult worms, but embryos are protected by the egg shell and survive. The microtube is shaken for 10 seconds every 2 minutes for a total of 10 minutes. This protocol allows breaking the

worms and obtaining intact eggs. Then, the microtube is spun 1 minute at 8000rpm, the supernatant (400 μl) is removed and 1ml of M9 buffer is added to wash the bleach-NaOH mix. This step is repeated twice. Finally, the pellet (~100 μl) is transferred to a seeded plate with a glass Pasteur pipette (c, 2006).

The time required to develop from egg to young adult depends on the *C. elegans* strain used. For example, wild-type worms or AQ2038 need 56h to achieve the stage of young adult (Byerly, 1976). However, mutant *nuo-6*, *eat-2* or *daf-2* strains develop slower and need between 4-5 days to reach the young adult stage.

Once the worms reach the young adult stage, they are transferred to seeded NGM+FuDR 15μM plates, and they are ready to start lifespan or calcium imaging studies.

4. Male stock

A large amount of males are needed in order to perform the calcium experiments and also for crosses. The introduction mentions that the percentage of males is usually very low (0.01-0.1%). Therefore, to make studies with males it is necessary to generate a male stock. The standard method to increase the proportion of males consists in stressing the worms by increasing the temperature of plates containing young adult hermaphrodites. Then, males should be identified among the F1 progeny. We placed five L4 worms in a 55mm NGM plate at 30°C overnight and we verify the presence of male worms among the F1 progeny. We then select the males and put them in a new plate with five L4 hermaphrodites to maintain the male stock because crossing males with hermaphrodites directly, the probability to obtain males in the progeny increase until 50% in the next generation (Fay, 2013).

5. Crosses

The AQ2038 strain has integrated the cDNA for the fluorescent Ca^{2+} sensor protein YC2.1 under the *myo-2* promoter, which is expressed in the cytosol of pharynx cells. The AQ3055 strain contains an extra chromosomal array with the cDNA for the fluorescent Ca^{2+} sensor protein YC3.60 targeted to the mitochondria, also under the *myo-2* promoter. It expresses therefore YC3.60 in pharynx mitochondria. They allow us to study the dynamics of either cytosolic or mitochondrial [Ca^{2+}] during pharyngeal pumping in wild-type worms. In order to monitor [Ca^{2+}] dynamics in mutant strains is necessary to generate crosses between the strains expressing Ca^{2+} sensors (AQ2038 or AQ3055) and the mutant strains.

The mutant strains used in this thesis to make crossings with AQ2038 or AQ3055 are: *nuo-6*, *eat-2*, and *daf-2*. Each cross has to be made separately.

The first step to obtain fluorescent mutant strains is to cross ten AQ2038/AQ3055 males with five mutant strain hermaphrodites, in a drop seeded plate:

Cytosolic [Ca^{2+}] sensor strains	Mitochondrial [Ca^{2+}] sensor strains
10 ♂ AQ2038 x 5 ☿ *daf-2*	10 ♂ AQ3055 x 5 ☿ *nuo-6*
10 ♂ AQ2038 x 5 ☿ *eat-2*	
10 ♂ AQ2038 x 5 ☿ *nuo-6*	

These plates are maintained at 20ºC for four to six days, and plates have to be checked since day three looking for the F1 adult generation; this is called the first cross. Then, the fluorescent males from the F1 progeny are picked and crossed again with

hermaphrodites of the mutant strain. After the fifth cross, we are ready to start checking if the fluorescent hermaphrodites obtained from the cross belong also to the mutant strain. In case they are, they should also be checked to ensure they are able to transfer the fluorescent protein to the offspring. In any case, we should continue repeating the crosses several times and avoid losing any generation (Fay, 2013).

The mutant strains *nuo-6*, *daf-2* and *eat-2* present a longer lifespan and a much slower development than the wild-type strain, so we checked these characteristics in the crossed worms to identify the presence of the mutations.

6. Lifespan

We measured the lifespan in *C. elegans* worms from young adult until death.

After synchronizing the worms, 50 young adult (day 1) worms are plated on NGM+FuDR 15 μM plates. Plates were kept in a temperature-controlled incubator set at 20ºC. Age refers to days following adulthood. The worms are counted every two days until day 12, and thereafter they are counted each day. Dead worms are scored and removed. Plates contaminated with fungi in the first 10 days of the assay were excluded from the study. Worms with extruded gonad, desiccated in the edge of the plate or just missing were also censored. Three different plates are counted for every synchronization and this is repeated at least three times.

7. Confocal imaging

The subcellular localization of the fluorescent Ca^{2+} probes, either cytosolic in the case of AQ2038 and its mutant strains expressing YC2.1 in the cytosol, or mitochondrial in the case of AQ3055 and its mutant strains expressing YC3.60 in mitochondria, were studied by confocal microscopy in synchronized young adult worms.

To confirm the mitochondrial localization of YC3.60, we studied the colocalization of the fluorescences of the YC3.60 Ca^{2+} probe and the mitochondrial indicator MitoTracker Deep Red. A solution was prepared with Mitotracker Deep Red 15μM in M9 buffer; we place the worms in 500μl of this solution and we wait 2-4 hours for them to be loaded with the probe.

We then added a drop of tetramisole 10mM in a 2% agarose pad and using an eyelash pick we transferred 10-15 worms into the drop. Then we placed a coverslip over the drop and we mounted it in the stage of a Leica SP5 confocal microscope to take the fluorescence images. The excitation/emission windows used were: for YC2.1 and YC3.60, 488nm excitation and 500-554nm emission; for MitoTracker Deep Red, 644nm excitation and 657-765 emission.

8. Calcium imaging

The Ca^{2+} measurements are performed at days 2, 5, 8 and 12 of adult state. To stimulate pharynx pumping, the worms are starved for 4-6 hours and during the experiment serotonin 5mg/ml solution in M9 buffer is present (Horvitz, 1982).

Each worm is transferred to a 2% agarose pad made in a 22x40 mm coverslip, (see the figure 20A) and glued there carefully with Dermabond from tail to pharynx without reaching the mouth, as show in figure 20B. Then 300μl of serotonine 5mg/ml is added to the pad, which is mounted in a chamber (Warner Instrument RC-25) and placed in the stage of a Zeiss Axiovert 200 inverted microscope.

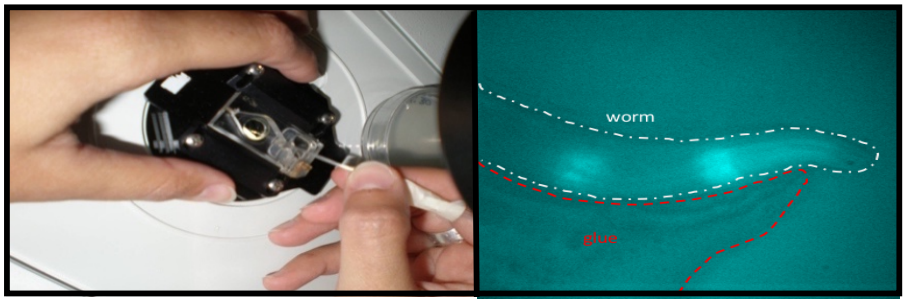

Figure 20: **A**. Worm gluing process. **B**. Worm stuck to the pad. The glue (red line) is not fluorescent so there is no interference with the fluorescent calcium probes.

Fluorescent proteins YC2.1 and YC3.60 show spectral changes upon calcium binding that allow us to perform ratiometric measurements of cytosolic and mitochondrial calcium concentrations. These ratio changes are due to variations in $[Ca^{2+}]$ pharynx cells, which are responsible of muscle contraction. Both probes were excited at 430 nm using a Cairn monochromator (10nm bandwidth, continuous excitation) and images of the

emitted fluorescence obtained with a Zeiss C-apochromat 40x1,2 W objective were passed through a 450nm long pass dichroic mirror. Cairn Optosplit II emission image splitter separates then the 480nm and 535nm emission images (Figure 21A). The splitter has emission filters DC/ET480/40m and DC/ ET535/30m, and the dichroic mirror FF509-FDi01-25x36 (all from Chroma Technology). Simultaneous 200ms images at the two emission wavelengths were recorded continuously (2.5Hz image rate) by a Hamamatsu ORCA-ER camera, and the ratio image was obtained by dividing the image obtained at 535nm emission by the one obtained at 480nm emission. Data obtained at both wavelengths were checked to assure that ratio peaks corresponded to inverted changes in the individual fluorescences (see figure 21B). Experiments were performed at 20ºC and carried on during 30 minutes of continuous recording.

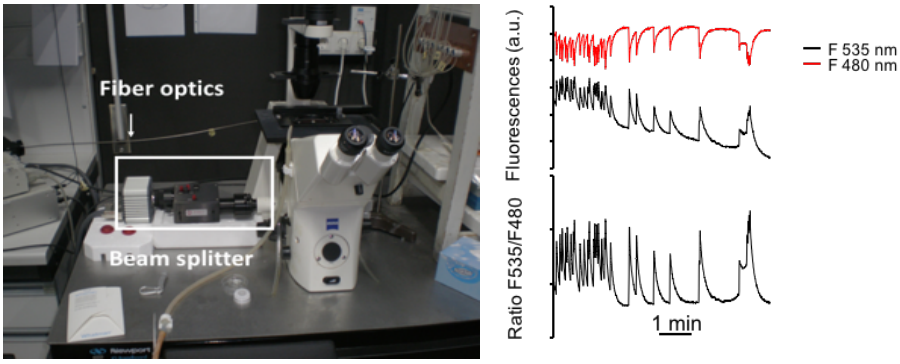

Figure 21: **A**. Image of the inverted microscope Zeiss Axiovert 200 with the beam spliter and The optic fibre. **B**. Traces of the fluorescences emitted at 535nm and 480nm wavelengths, and the F535/F480 ratio.

9. Data analysis

The fluorescence images of the Ca^{2+} sensors are recorded and analyzed using the MetaFluor program (Universal Imaging). The traces shown are 535nm/480nm fluorescence emission ratio values of a region of interest enclosing the pharynx terminal bulb. The ratio of both wavelengths is only considered acceptable when inverted changes at both wavelengths were clearly observed. Fluorescence intensities and ratio changes are then analyzed with a specific algorithm designed to calculate off-line the width at mid-height expressed in seconds, the height obtained as percent of ratio change and the frequency of all the Ca^{2+} peaks in each experiment. The frequency is measured at each peak as 9 divided by the distance among the peak 4 positions before and the peak 4 positions after. The mean frequency is calculated as the mean of all the individual frequencies higher than 5 peaks/ min obtained in worms of a given age and condition.

Materials

Agar	Calbiochem	12177-1Kg
Agarose High gelling (imagen)	Fisher	BP164-100
Bacteriological Peptone	PRONADISA	1616.00
Calcium chloride	MERCK	A935182914
Cholesterol	Sigma-Aldrich	C8503-25G
Dermabond Topical Skin Adhesive	Johnson & Johnson	
Dipotassium hydrogen phosphate	MERCK	A0026704927
FuDR 5'-fluoro-2'-deoxiuridina	Alfa-Aesar	L16497
2xYT (LB broth)	FisherBrand	BP2467-500
Magnesium sulphate	Sigma-Aldrich	M2643-500G
MitoTracker Deep Red	Thermofisher	M22426
Pasteur Pipete 230-250	FisherBrand	1156-6963
Plates 55mm	Deltalab	200201
Potassium dihydrogen phosphate	MERCK	A999073905
Serotonin hydrochloride	Alfa-Aesar	B21263
Sodium chloride	EMSURE	K46991504540
Sodium phosphate dibasic	Sigma-Aldrich	S0876-1KG
Tetramisol hydrochloride	Sigma-Aldrich	L9756-


RESULTS

1. Cytosolic pharyngeal Ca^{2+} measurement

There are many studies about pharyngeal pumping in *C. elegans* (Kerr et al., 2000; Shizomono et al., 2004) but none of them has studied pharyngeal pumping activity for more than two minutes. This work shows pharyngeal calcium dynamics for long periods of time, about 30 minutes, and the different patterns of activity observed along the worm lifecycle.

1.1. Cytosolic pharyngeal Ca^{2+} measurement in AQ2038

To study pharyngeal Ca^{2+} variations we used the AQ2038 strain, which is an integrated transgenic strain that expresses the Ca^{2+} probe (YC2.1) in the cytosol of pharynx cells driven by the *myo-2* gene promoter (Miyawaki A. et al., 1999; Miyawaki A. et al., 1997; Nagai T. et al., 2004).

In order to know if the expression of the YC2.1 sensor affected somehow worm survival, the lifespan of the strains AQ2038 and N2 (wildtype strain) were compared. Figure 22 shows that both strains have similar lifespans, so the expression of YC2.1 does not affect the survival of the worms.

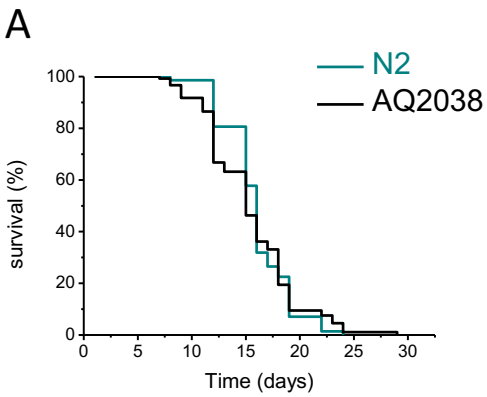

Figure 22: Lifespan of N2 and AQ2038

1.1.1. Experimental traces

Figure 23 shows the traces of three different Ca^{2+} experiments made in three different worms at day 2 of adult life. We can see that it is possible to monitor Ca^{2+} dynamics in the pharynx during at least 30 minutes with live worms.

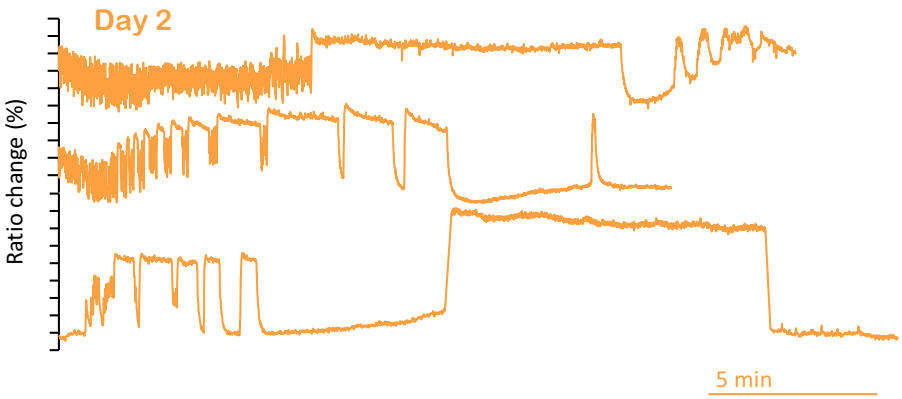

Figure 23: Three AQ2038 pharynx $[Ca^{2+}]_C$ traces, that are representative of 24 similar experiments made in 2-day-old worms (Alvarez-Illera P. et al., 2016)

In order to study if the pattern of pharynx Ca^{2+} transients changes during aging, pharynx $[Ca^{2+}]_C$ dynamics was studied not only on day 2 of adult life (figure 23) but also on day 5, day 8 and day 12 of adult life. Representative traces of the Ca^{2+} patterns observed are depicted in figure 24.

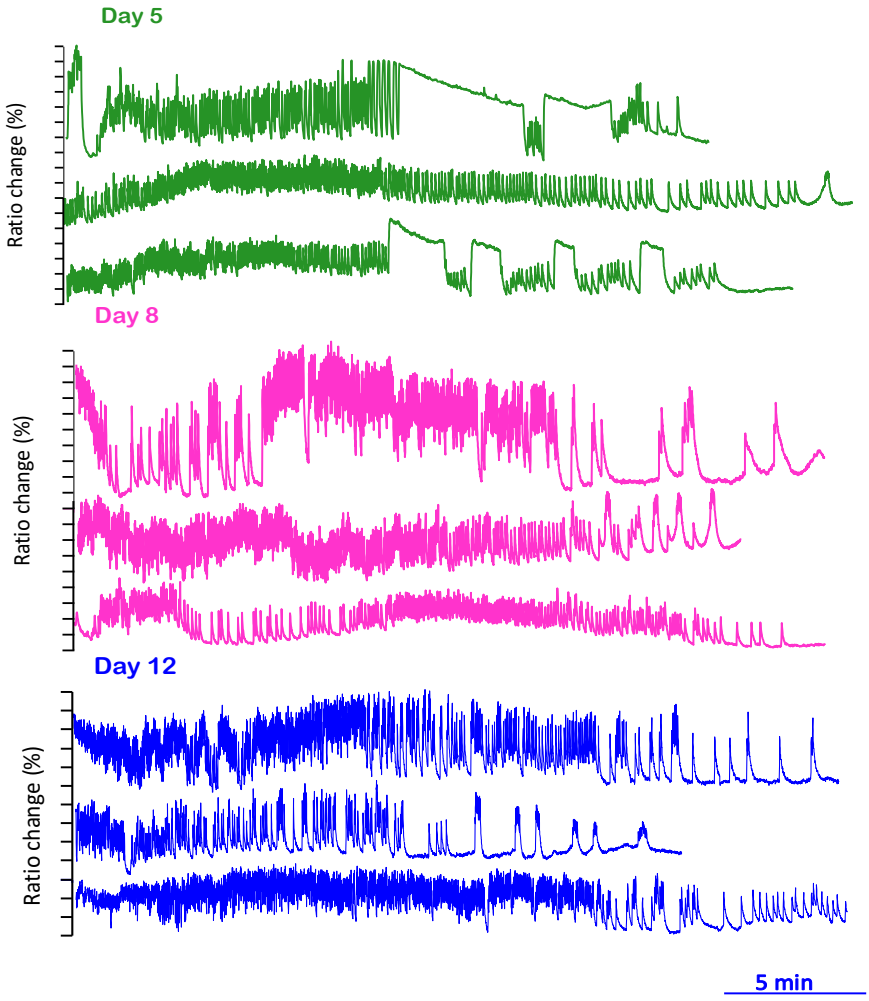

Figure 24: Three representative $[Ca^{2+}]_C$ experiments obtained at day 5 (n= 28) (green), at day 8 (n= 28) (pink) and at day 12 (n=25) (blue) in AQ2038 worms (Alvarez-Illera et al. 2016).

The Ca^{2+} traces obtained at each age showed a high variability between worms of the same day of adult life. Among the Ca^{2+} patterns, two different kinds of peaks can be distinguished (figure 25), one corresponding to fast calcium oscillations, that we call ***spikes***, and the other corresponding to prolonged peaks that

keep a high level of calcium for a long time, even for several minutes. We call them ***square-wave*** Ca^{2+} transients.

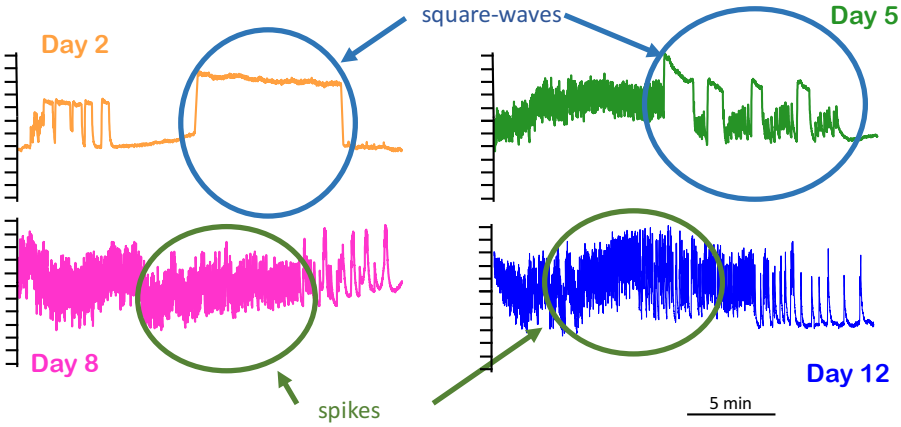

Figure 25: Representation of Ca^{2+} *square-waves* and *spikes* at different days.

The origin of what we call "square-wave" Ca^{2+} transients is not well-known. The pharynx is an organ responsible for pumping in and grinding bacteria due to persistent contraction (Avery L. and Shtonda, 2003). A persistent increase in cytosolic calcium concentration is not useful for that, and it is also generally considered deleterious for cells, leading to mitochondrial Ca^{2+} overload and the activation of different hydrolytic enzymes, oxidative stress and cell death, as observed during ischemia/reperfusion in the myocardium (Mozaffari MS. Et al. 2013). When muscles are activated for contraction, $[Ca^{2+}]_C$ increases from the resting level following a transient activation of plasma membrane channels, which allows entry of Ca^{2+} from the extracellular medium and release of Ca^{2+} from the intracellular stores. Then, in order to return to the resting conditions, ATP-dependent Ca^{2+} pumps in the plasma membrane and in the endoplasmic/sarcoplasmic reticulum pump Ca^{2+} out of the cytosol. When the pharynx is continuously contracting (see figure 15), the

continuous pumping of Ca^{2+} consumes a huge amount of energy. This occurs during the spikes (fast oscillations). A possible explanation for the square-wave Ca^{2+} transients (variable plateau phase of high cytosolic Ca^{2+} concentration) is that the lack of energy prevents extrusion of Ca^{2+} from the cytosol. ATP depletion would make contractions stop and would also lead to a prolonged high cytosolic Ca^{2+} concentration due to the arrest of the Ca^{2+} pumps.

1.1.2. Data analysis

We have obtained a large number of $[Ca^{2+}]_C$ recordings acquired for many worms at different days of adult life, in particular day 2, day 5, day 8 and day 12. In order to optimize the complete analysis of all the $[Ca^{2+}]_{cyt}$ transients in each record, a specific algorithm was developed that allows obtaining the following parameters from each experimental trace: time, height and width of each peak, and the peak frequency during the experiment. *Height* is the change in the ratio between the basal level and the peak level of calcium; *width* is the peak width in seconds at half-height; and *frequency* represents the number of peaks of each trace per minute, and is calculated at each peak taking into account the distance between the 4^{th} peak before it and the 4^{th} peak after it. The mean frequency is the mean of all the frequencies obtained, excluding those smaller than 5 peaks/min.

In order to detect the presence of the square-wave peaks we studied the distribution of the $[Ca^{2+}]_C$ peak widths obtained from experiments performed with multiple individual worms at different ages. The figure 26 shows the distribution of the widths of the peaks expressed as the percentage of peaks having increasing widths (at 0,5s intervals).

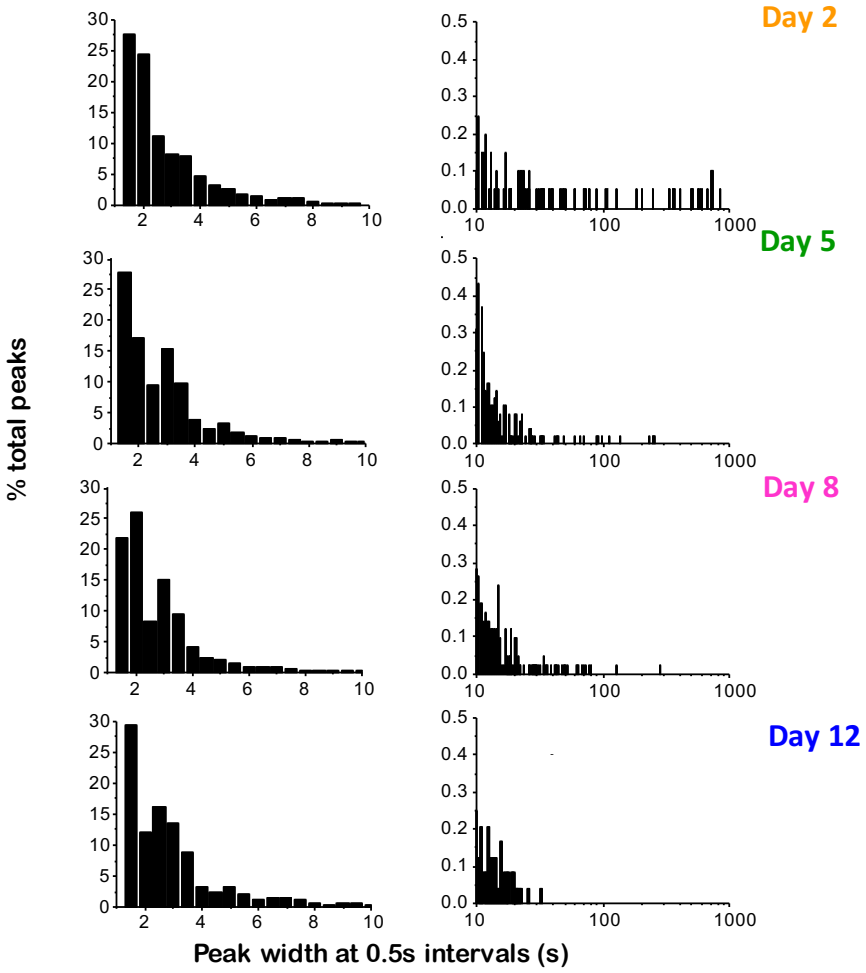

Figure 26. Distribution diagrams of the peak width in *C. elegans* worms of 2, 5, 8, and 12 days old. The left panel shows the percentage of peaks having widths smaller than 10s, at 0,5s intervals. The right panel show the percentage of peaks with widths between 10 and 1000s with 0,5s intervals (Alvarez-Illera et al. 2016).

The left panel of the figure 26 shows that 50% of the $[Ca^{2+}]_c$ peaks at each age correspond to rapid spiking, have a narrow width (between 1-2s) and there is no difference between ages. The right panel of the figure 26 shows peaks with widths between 10s and 1000s, which correspond to those called square-wave $[Ca^{2+}]_c$ transients, that are mainly present in young worms and progressively decline with aging.

In figure 27 each point represents a single Ca^{2+} peak, and each plot includes all the peaks from all the experiments performed with worms of a given age, either 2, 5, 8 or 12 days of adult life. As it was the case of figure 26, there is a progressive reduction of the square-wave $[Ca^{2+}]_C$ transients during aging (figure 27). Most of the peaks displayed widths smaller than 10s, and square-wave peaks can be easily distinguished than those peaks with a larger width. We can clearly see in these plots that square-wave peaks are present mainly in the first days of life and disappear progressively as the worms become older.

Both, figure 26 and 27 gave similar information, so the rest of the results shown in this work are represented as height *vs.* width plots because we think it is a more visual representation.

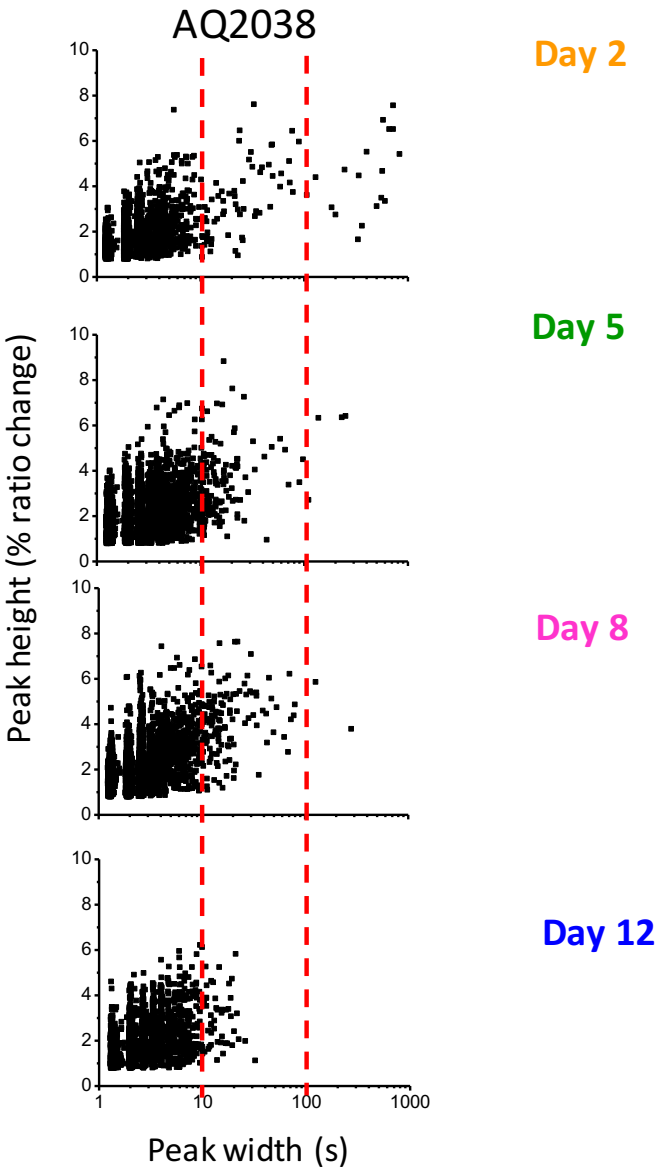

Figure 27: Plots of peak height *versus* peak width for all the peaks analysed in worms of Day 2 (2017 peaks from 24 worms studied), Day 5 (4854 peaks from 28 worms studied), Day 8 (4211 peaks from 28 worms studied) and Day 12 (2412 peaks from 25 worms studied). The peak width is represented in logarithmic scale (Alvarez-Illera et al. 2016).

Figure 25 shows that it is possible to return to fast Ca^{2+} oscillations after a period of square-wave Ca^{2+} transients. This suggests that the misbalance in ATP production/consumption ratio can be in some cases reversible. However, in many cases the square-wave transients persist and $[Ca^{2+}]_c$ keeps high until the end of the experiment. If the presence of "square-wave" peaks is due to the lack of energy to reduce $[Ca^{2+}]_c$, the worms could be classified in two categories according to energy availability:

- If the Ca^{2+} activity includes square-wave $[Ca^{2+}]$ transients lasting for at least 1 min, the worm is classified as "energy depleted" (ED). This worm has no energy (ATP) to reduce cytosolic Ca^{2+} concentration.
- If the spike activity continues along 30 minutes or ends earlier, but in narrow spikes way, the worm is classified as "Non Energy Depleted" (NED). The worm has enough energy to reduce cytosolic Ca^{2+} concentration to resting levels.

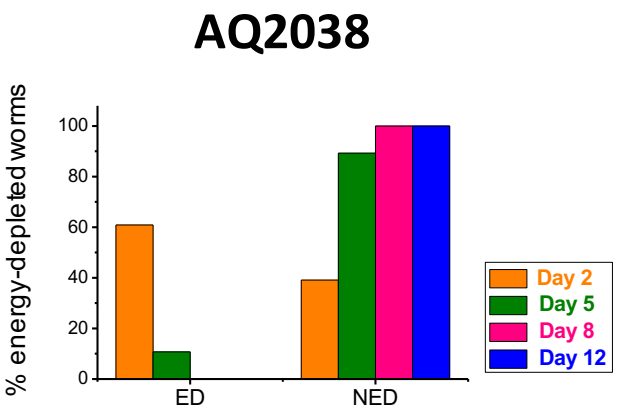

Figure 28: Percentage of worms classified as "Energy Depleted" (ED) or "Non Energy Depleted (NED) at every day of the worm life (Alvarez-Illera P. et al., 2016).

The classification (figure 28) of the worm in ED or NED surprisingly shows that young worms become more frequently ED than older worms. This may be due to a misbalance in the ATP production/consumption ratio. Young worms are more active at day 2 and may use energy faster than they are able to produce. Instead, older worms would keep a better balance between ATP production/ATP consumption.

The rest of the parameters calculated are represented in figure 29, which shows the variations of height, width and frequency studied at day 2, 5, 8 and 12 on AQ2038. We can see that the *height* of the peaks changes little throughout the life of the worm. The most significant finding is the decrease in the width of the total peaks with age, which is due to the decrease in the number of the square-wave Ca^{2+} peaks. In fact, the *width* of the total peaks has a high error bar at day 2 because there is a mixture of spikes and square-wave peaks. If we analyze only those peaks corresponding to **spikes** (peaks <10s), the error bar is much smaller. The number of square-wave peaks considerably decreases at day 5 and afterwards, and so decreases also the total width and the error. Regarding the *frequency*, mean values around 15 peaks/min are observed, and it shows a small decrease from day 2 to days 8-12.

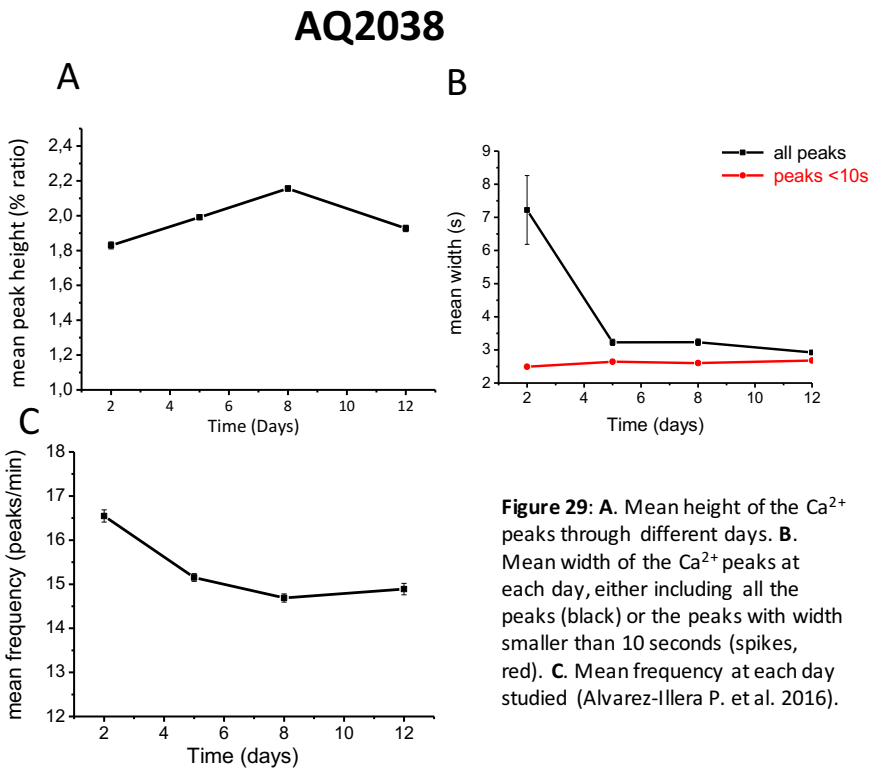

Figure 29: **A**. Mean height of the Ca^{2+} peaks through different days. **B**. Mean width of the Ca^{2+} peaks at each day, either including all the peaks (black) or the peaks with width smaller than 10 seconds (spikes, red). **C**. Mean frequency at each day studied (Alvarez-Illera P. et al. 2016).

1.2. AQ*nuo-6*

The mutant strain *nuo-6* (*qm200*) has a mutation in a subunit of complex I of the mitochondrial respiratory chain. These worms have reduced mitochondrial function and display lower oxygen consumption, slow growth, slow movement, decreased ATP levels and significant lifespan extension (Yang and Hekimi, 2010; Yee and Hekimi, 2014).

1.2.1. *nuo-6(qm200)* expressing YC2.1

The probe YC2.1 was introduced into the mutant worms by crosses (see Methods 5). *nuo-6* mutants present increased lifespan, and in fact, AQ*nuo-6* showed also a lifespan increase with respect to AQ2038 (figure 30B). It was also necessary to confirm that the probe is expressed in the cytosol, so we obtained confocal microscope images showing a cytosolic pattern of the fluorescence of the Ca^{2+} sensor (figure 30A).

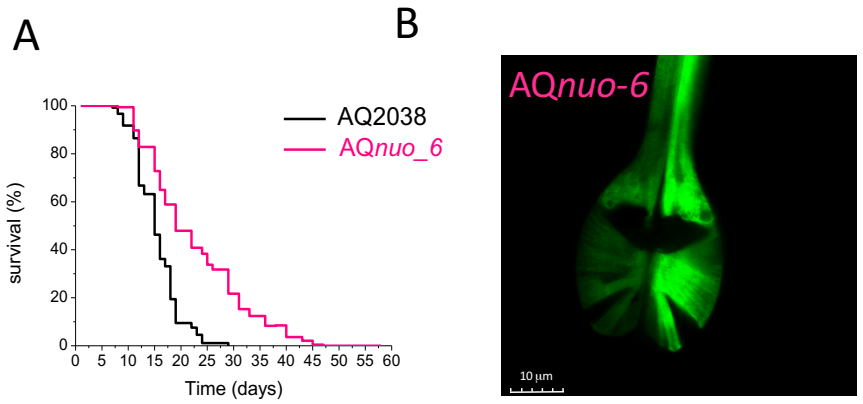

Figure 30: **A**. Lifespan assays of AQ2038 and AQ*nuo-6*. **B**. confocal microscopy image of AQ*nuo-6*.

The confocal microscopy image (figure 30B) shows the protein YC2.1 expressed in the cytosol in a typical diffuse cytosolic pattern. Figure 30A shows the lifespan experiment comparing the lifespan of AQ2038 *versus* that of AQ*nuo-6.* The mutant AQ*nuo-6* strain has a longer lifespan than the AQ2038 control, as previously reported (Yang W. & Hekimi S., 2010).

1.2.2. Experimental traces

Figure 31 shows calcium traces of AQ*nuo-6* worms at four different days of adult life.

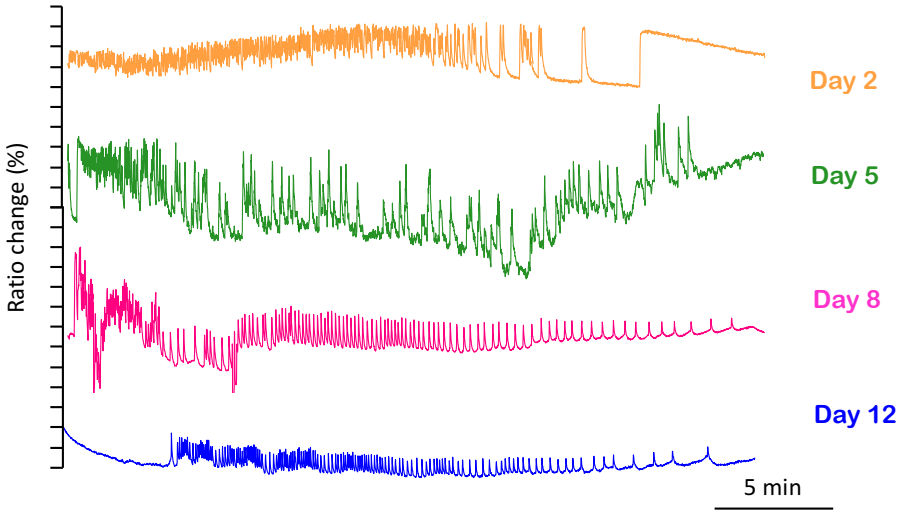

Figure 31: Representative traces at four different experimental days: Day 2 (n=43) (orange); at Day 5 (n=19) (green); at Day 8 (n=41) (pink) and at Day 12 (n=23) (blue).

As in the experiments with AQ2038, we measured $[Ca^{2+}]_C$ in AQ*nuo-6* worms for 30 minutes and we also found two types of Ca^{2+} peaks, fast spikes present all the days studied, and square wave peaks, present only in the first days of life.

1.2.3. Data analysis

Following the same data analysis performed in control AQ2038 worms (figure 27), in figure 32 we represent the height *versus* mean width plots obtained with the AQ*nuo-6* worms. Each point represents one $[Ca^{2+}]_C$ peak, and each plot includes all the $[Ca^{2+}]_C$ peaks analysed in experiments performed at each day of adult life.

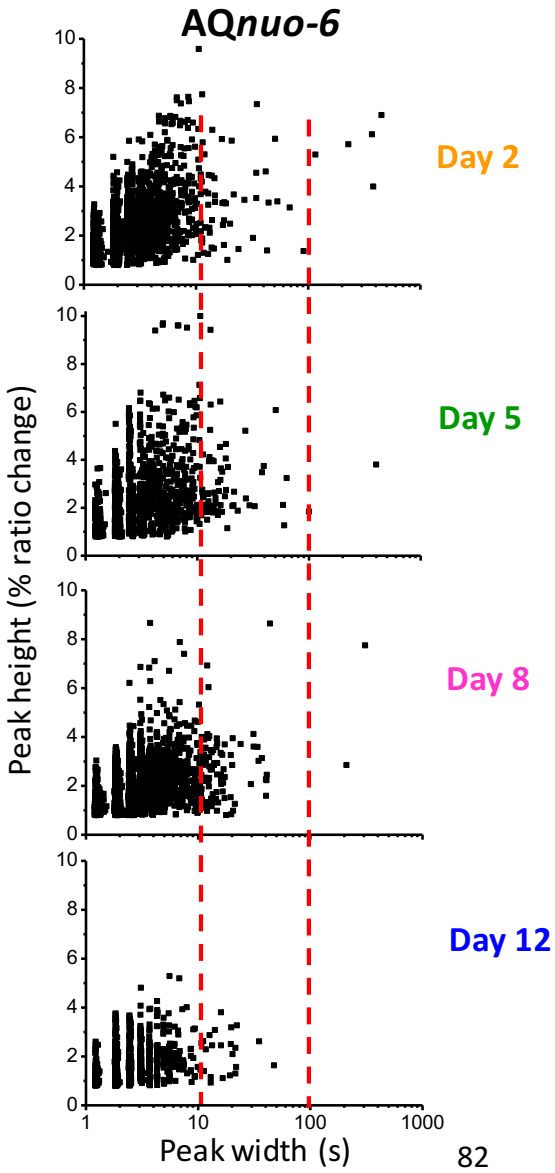

Figure 32: Plots of peak height *versus* peak width for all the peaks analysed in worms of Day 2 (2561 peaks from 43 worms studied), Day 5 (1409 peaks from 19 worms studied), Day 8 (2873 peaks from 41 worms studied) and Day 12 (1241 peaks from 23 worms studied). The peak width is represented in logarithmic scale (Alvarez-Illera et al. 2016).

In figure 32, we can see that AQ*nuo-6* worms also have more square-wave peaks on day 2 than in older worms, whereas peaks with a width smaller than 10s remain present throughout the life of the worm.

Figure 33 shows worms classified by energy status, as described above for wild type worms (figure 28). Represented in figure 33 is the percentage of worms that correspond to the ED group and those that correspond to the NED group.

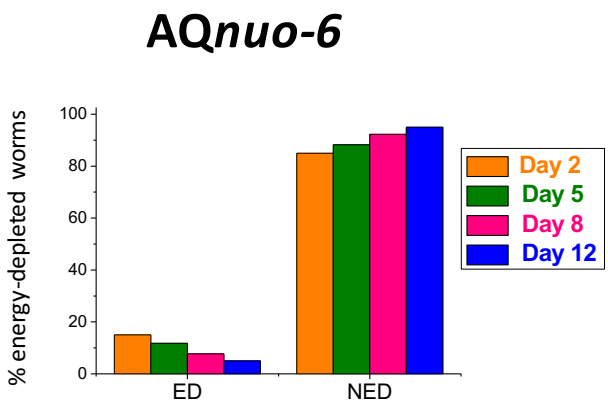

Figure 33: Percentage of worms classified as "Energy Depleted" (ED) or "Non Energy Depleted (NED) at different days of AQ*nuo-6* life (Alvarez-Illera et al., 2016).

Surprisingly, most of the AQ*nuo-6* worms are in the non-energy-depleted group. In particular, the percentage of ED worms at day 2 is much lower than in wild type AQ2038 worms (see figure 28).

All the traces were analysed with an algorithm that allows obtaining the following parameters: mean height, mean width and mean frequency at each day. Data corresponding to these parameters are represented in figure 34A-C. We can see that all of them decrease along the AQ*nuo-6* lifetime.

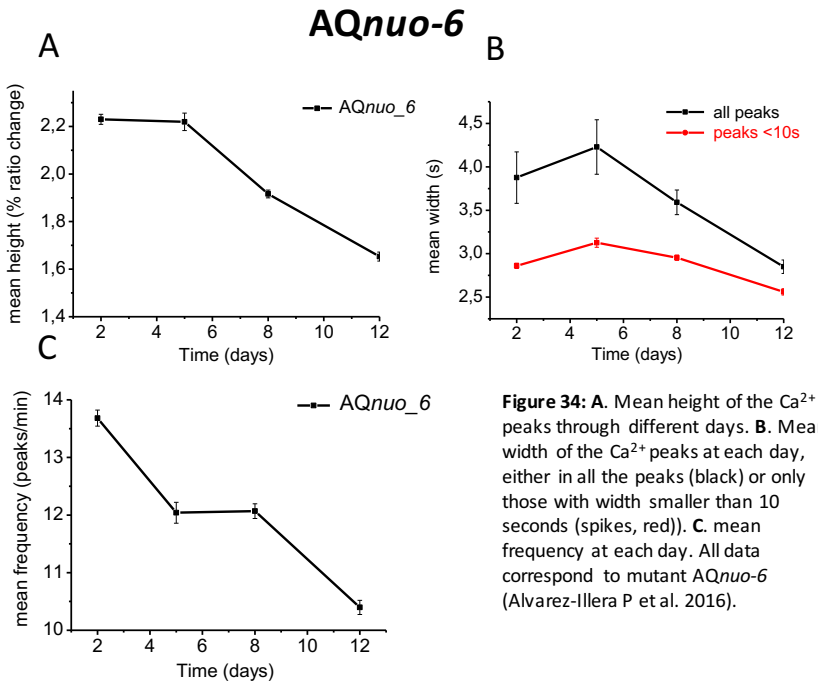

Figure 34: A. Mean height of the Ca^{2+} peaks through different days. **B**. Mean width of the Ca^{2+} peaks at each day, either in all the peaks (black) or only those with width smaller than 10 seconds (spikes, red)). **C**. mean frequency at each day. All data correspond to mutant AQ*nuo-6* (Alvarez-Illera P et al. 2016).

1.3. AQ*eat-2* (ad1113)

The gene *eat-2* encodes a non-α-nicotinic receptor expressed in the pharynx. *C. elegans* with the *eat-2(ad1113)* mutation are defective in pumping rate although display longer lifespan than wild type worms. The reason for the lifespan extension is that this mutation mimics caloric restriction (Lakoswki and Hekimi, 1998; McKay et al., 2003).

1.3.1. *eat-2* expressing YC2.1

Mutant AQ*eat-2* worms were obtained by crossing males AQ2038 with hermaphrodite *eat-2(ad1113)* (see Methods 5). After several crosses, *eat-2* mutants expressing YC2.1 are obtained. Then we have to demonstrate that these worms are *eat-2* mutants expressing the probe. For that, the pharynx fluorescence of AQ*eat-2* was studied by confocal microscopy to confirm it has a cytosolic

pattern, and the lifespan of AQ*eat-2* was also studied and compared with that of AQ2038 (wild type strain) (see figure 35A and B).

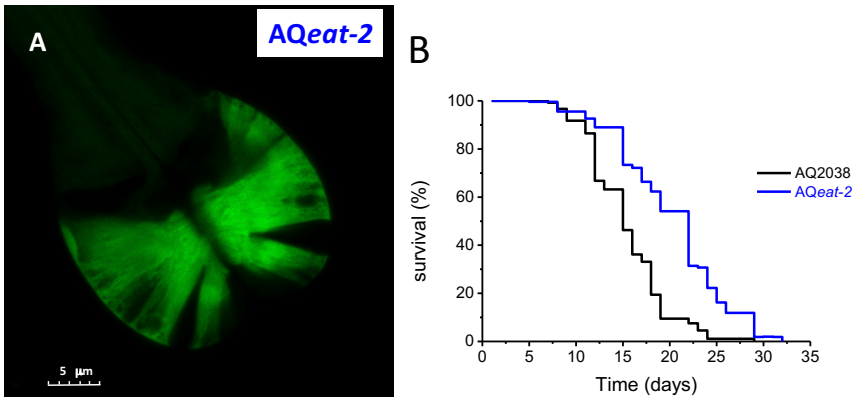

Figure 35: A. Confocal imaging of AQ*eat-2*. **B**. Lifespan of AQ*eat-2* and AQ2038.

Confocal microscopy imaging shows a cytosolic distribution of the Ca^{2+} probe YC2.1 (figure 35A). Lifespan measurement shows that AQ*eat-2* mutant lives longer than wild type AQ2038, and the lifespan obtained is consistent with survival studies of the *eat-2* mutant (Lakowski and Hekimi, 1998).

1.3.2. Experimental traces

Figure 36 shows typical traces of AQ*eat-2* of four different worms at different days of adult life.

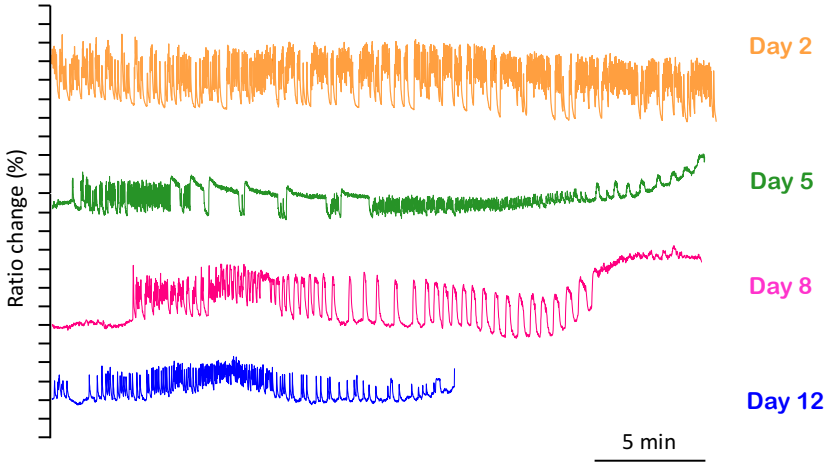

Figure 36: Representative traces of four AQeat-2 worms with different age: day 2 (n=29) (orange); at Day 5 (n=23) (green); at Day 8 (n=18) (pink) and at Day 12 (n=26) (blue).

1.4.2. Data analysis

All the experimental records of $[Ca^{2+}]$ dynamics of the mutant AQ*eat-2* were analyzed with the same algorithm as in Figure 37 shows the results obtained by plotting the height against the width for each $[Ca^{2+}]$ peak obtained in worms of a given age. The plots show patterns similar to those found in the other strains. In young worms (day 2) there are more peaks with a long width (*square-wave*) and they then disappear in older worms. The fast transients, called spikes, are present through the AQ*eat-2* worm life.

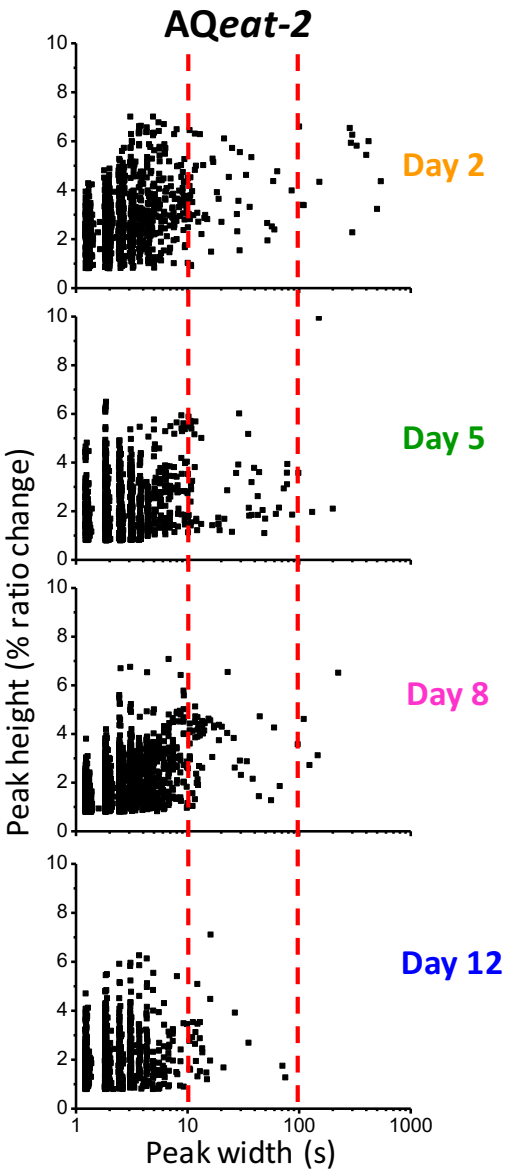

Figure 37: Plots of peak height *versus* peak width for all the peaks analysed at Day 2 (3756 peaks from 29 worms studied), Day 5 (1559 peaks from 23 worms studied), Day 8 (2186 peaks from 18 worms studied) and Day 12 (1659 peaks from 12 worms studied in **AQ*eat-2*.** The peak width is represented in logarithmic scale

The worms were also studied from the energy point of view and classified in two groups, as described before: those that have long square-waves or end up with high Ca^{2+} levels correspond to the Energy-Depleted group (ED) and those worms whose records have fast transients continuously or stop oscillating correspond to the Non-Energy-Depleted (NED) group (figure 38).

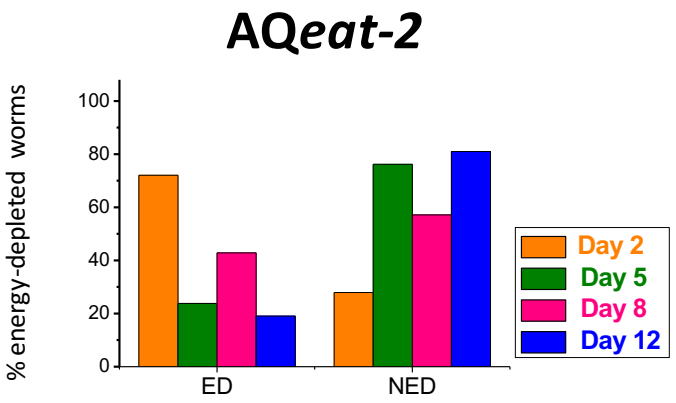

Figure 38. Percentage of worms classified as "Energy Depleted" (ED) or "Non Energy Depleted" (NED) in AQeat-2 worms of different ages.

Figure 38 shows a higher percentage of AQ*eat-2* worms corresponding to the ED group compared with the AQ2038 controls. We found AQ*eat-2* ED worms at all ages, even in old worms, although the percentage was higher at day 2. This behaviour is probably a consequence of the mutation in the *eat-2(ad1113)* gene. This strain has a low pumping rate, which triggers caloric restriction. As a consequence, these worms have less energy, and this may facilitate energy depletion.

The behaviour of the parameters mean height, width and frequency in the AQ*eat-2* strain are represented in the figure 39A-C.

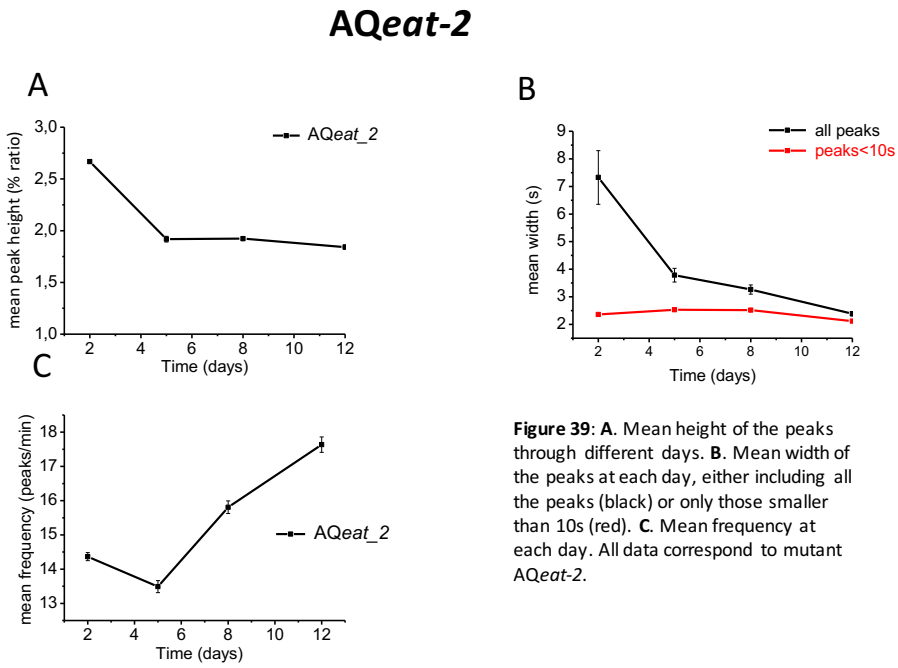

Figure 39: **A**. Mean height of the peaks through different days. **B**. Mean width of the peaks at each day, either including all the peaks (black) or only those smaller than 10s (red). **C**. Mean frequency at each day. All data correspond to mutant AQ*eat-2*.

In figure 39A the mean height decreased during the life of the worm. The parameter width (figure 39B) decreases as worms become older when all peaks where analyzed together because of the decrease in the frequency of the square-wave peaks with age. However, the width of the peaks shorter than 10s (spikes) changed little with the age whereas the frequency increased with the age of the worms (figure 39C).

1.4. AQ*daf-2*

The *daf-2* gene encodes the Insulin-like Growth Factor 1 Receptor (IGFR1). The worms with mutation in this gene show a lifespan longer than wildtype. *daf-2* plays a role in different pathways such as a dauer state formation, sensing of nutrient availability and even oxidative stress resistance (Kenyon C., 2011).

1.4.1. *daf-2 (e1370)* expressing YC2.1

daf-2(e1370) hermaphrodites were crossed with AQ2038 males (see methods 5). To verify that worms expressing YC2.1 have the *daf-2(e1370)* mutation, the confocal microscopy image (see Methods 7) and the lifespan of the cross product were studied (see Methods 6), as shown in the figure 40A-B.

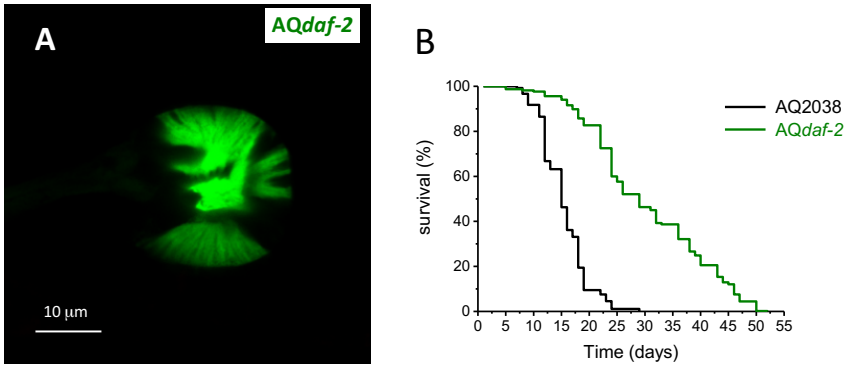

Figure 40: **A**. Confocal image of AQ*daf-2*. **B**. Lifespan measurement of AQ2038 and AQ*daf-2.*

The terminal bulb expresses the probe YC2.1 with a typical diffuse cytosolic pattern (figure 40A). The lifespan of AQ*daf-2* is longer than that of the AQ2038 control (figure 40B) and similar to that reported in the literature (Dorman et al., 1995).

1.4.2. Experimental traces

Once verified that the strain AQ*daf-2* expresses the YC2.1 probe in the cytosol, the behaviour of the calcium dynamics was studied (see Methods 8). Figure 41 shows typical experimental records corresponding to each day of adult life.

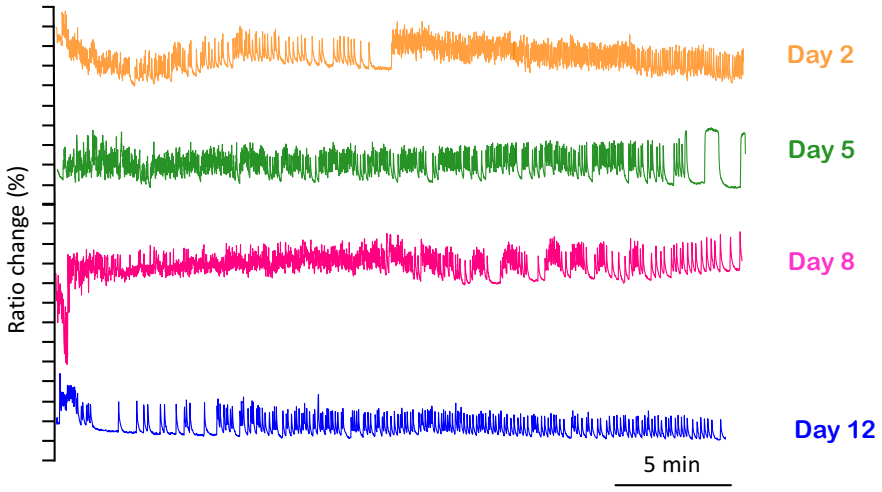

Figure 41: Representative traces at four different experimental days of adult life: Day 2 (n=19) (orange); Day 5 (n=11) (green); Day 8 (n=17) (pink) and Day 12 (n=14) (blue).

1.4.3. Data analysis

The traces were analysed with the algorithm and figure 42 shows the relationship between height and width of all the $[Ca^{2+}]$ peaks analysed in each of the studied days of life, in order to know the distribution of heights and widths of the $[Ca^{2+}]_C$ peaks in these worms.

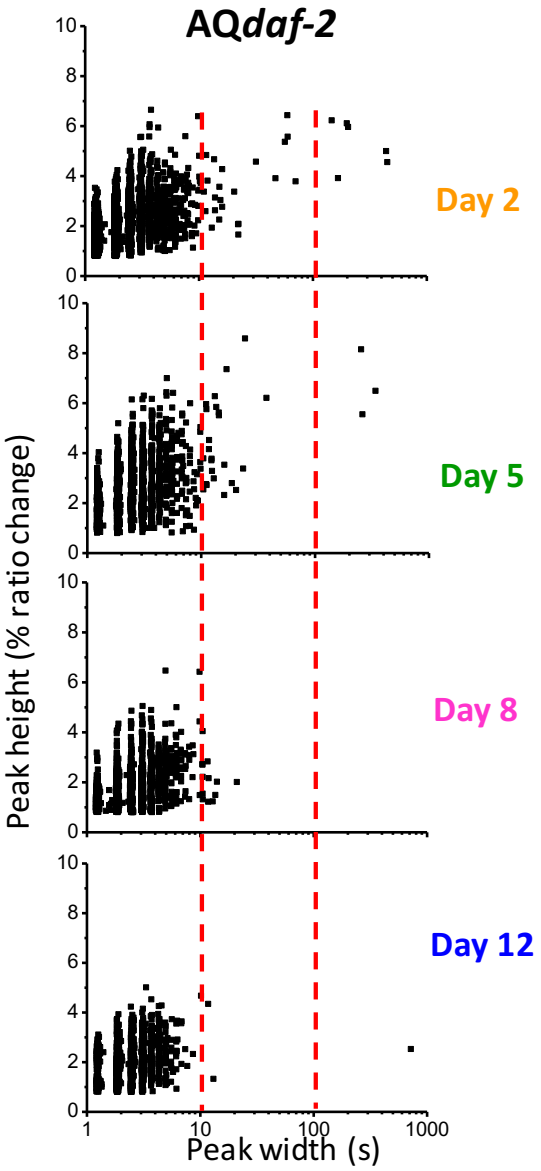

Figure 42: Plots of peak height *versus* peak width for all the peaks analysed in worms at Day 2 (7710 peaks from 19 worms studied), Day 5 (2607 peaks from 11 worms studied), Day 8 (1794 peaks from 17 worms studied) and Day 12 (1513 peaks from 14 worms studied) in **AQ*daf-2*.** The peak width is represented in logarithmic scale

At day 2 there are long square-wave peaks in the AQ2038, AQ*nuo-6*, AQ*eat-2* and also in AQ*daf-2*. These square-wave peaks disappear progressively as worms get older. Instead, the peaks with a width smaller than 10s (spikes) are present throughout the entire life of the worms.

If the worms are studied from the energy point of view, as the other strains studied before, the graph in figure 43 shows that the percentage of ED worms decreases with age. However, most of AQ*daf-2* worms correspond to the non-energy-depleted group, even when worms are still young.

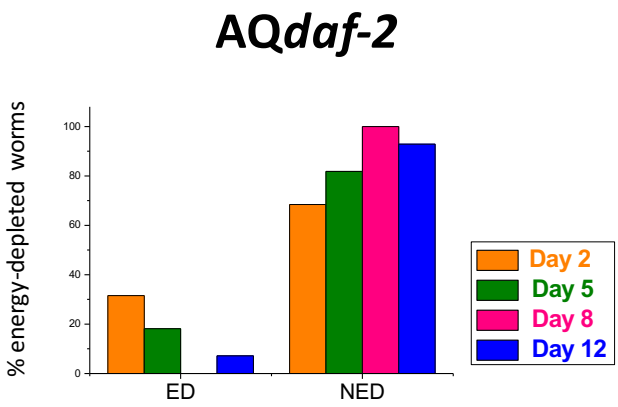

Figure 43: Percentage of worms classified as "Energy Depleted" (ED) or "Non Energy Depleted (NED) in the different days of worm life studied.

The others parameters obtained with the algorithm, mean height, mean width and mean frequency at different days of life are represented in figure 44A-C.

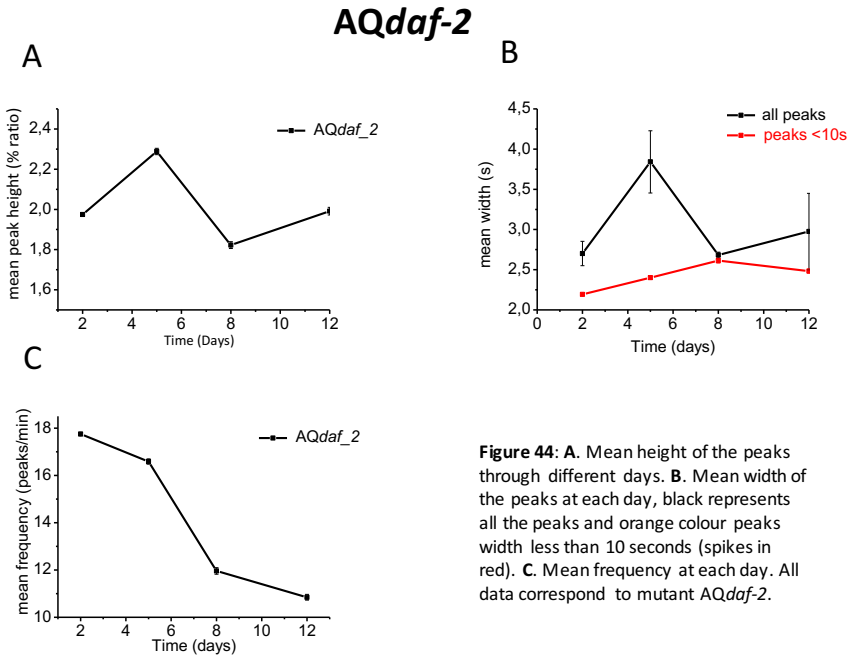

Figure 44: **A**. Mean height of the peaks through different days. **B**. Mean width of the peaks at each day, black represents all the peaks and orange colour peaks width less than 10 seconds (spikes in red). **C**. Mean frequency at each day. All data correspond to mutant AQ*daf-2*.

The mean height changed little along the worm lifespan. The mean width or peaks of less than 10 seconds increased along the lifespan, but the long square-wave peaks were more frequent at day 5 and decreased afterwards. The frequency showed a significant decrease during the worm life.

1.5. AQ2038 males

C. elegans has hermaphroditic and male sexual dimorphism. Although the proportion of males is very low (1000:1) in the laboratory (see Methods 5) it is possible to obtain enough males to carry out experiments to see if there are any differences in the calcium dynamic patterns between the hermaphrodites and the males.

1.5.1. Experimental traces

Figure 45 shows characteristic traces of each day of adult life on AQ2038 males. A great variability was also observed here in worms of the same age, as occurs in AQ2038 hermaphrodites.

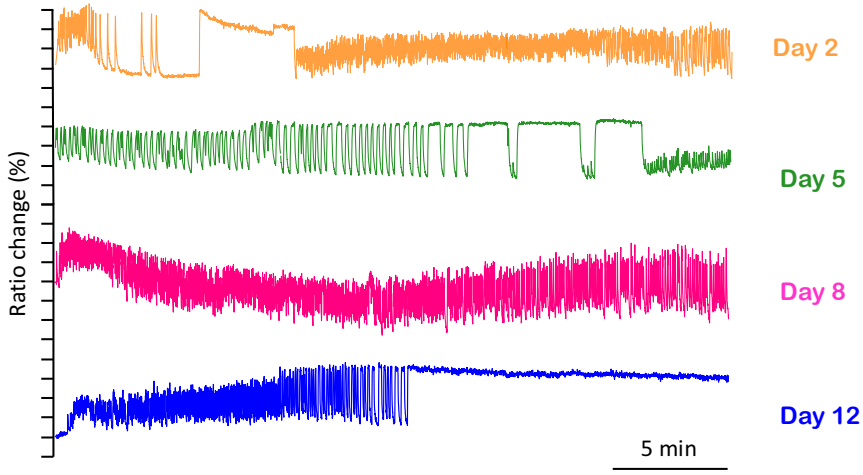

Figure 45: Representative traces at four different days of adult life: at Day 2 (n=19) (orange); at Day 5 (n=15) (green); 41 at Day 8 (n=14) (pink) and at day 12 (n=20) (blue).

1.5.2. Data analysis

The traces corresponding to each day were analyzed with the same algorithm we used in the previous analyses, and we obtained the plots of height versus width shown in Figure 46.

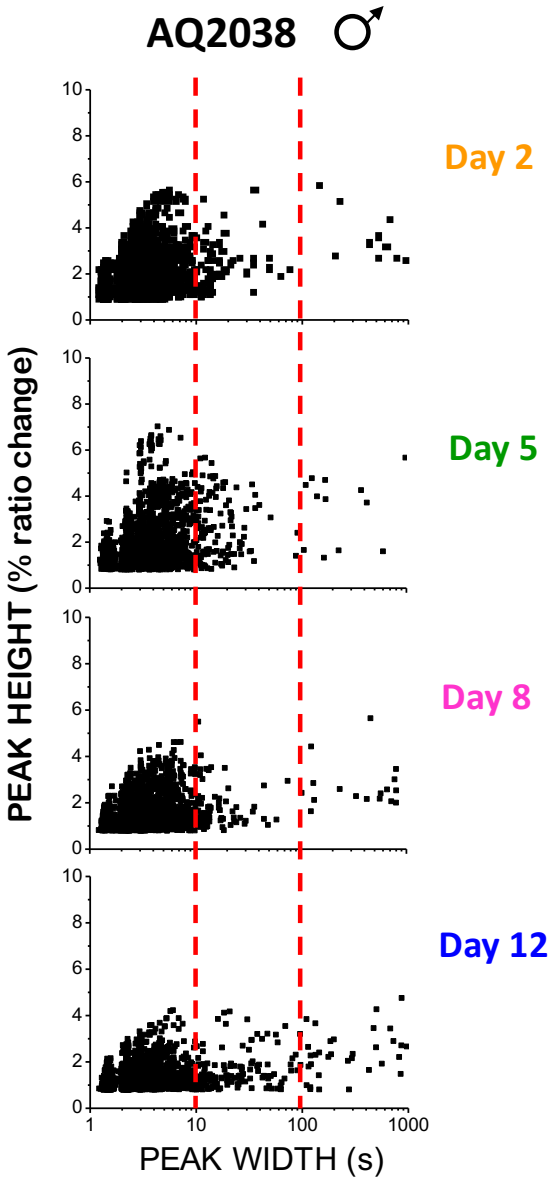

Figure 46: Plots of peak height *versus* peak width for all the peaks analysed in worms at Day 2 (1912 peaks from 19 worms studied), Day 5 (2142 peaks from 15 worms studied), Day 8 (3150 peaks from 14 worms studied) and Day 12 (2544 peaks from 20 worms studied) in **males AQ2018** The peak width is represented in logarithmic scale

Figure 46 shows a high percentage of peaks longer than 100s at every age studied. This is higher than that observed in hermaphrodite worms.

We calculated the mean height, mean width and mean frequency at each day studied, and the results are represented in figure 47A-C. The more significant finding is the large increase in the width of all the peaks at every age, even at day 12th, due to the increase in the number of square-wave peaks. There were instead little changes in the mean width of the spikes <10s along aging, although it was larger than in the hermaphrodites. Regarding height and frequency, the height decreases with the age more than in the hermaphrodites AQ2038 (figure 29A), and the frequency instead increases in males AQ2038 when they get older, in contrast to the results of hermaphrodites (see figure 29C).

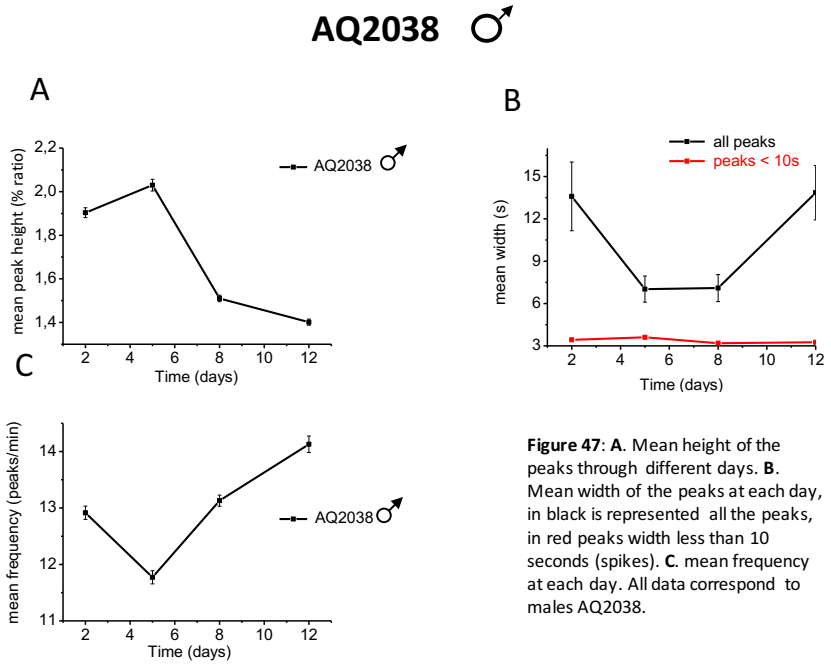

Figure 47: **A**. Mean height of the peaks through different days. **B**. Mean width of the peaks at each day, in black is represented all the peaks, in red peaks width less than 10 seconds (spikes). **C**. mean frequency at each day. All data correspond to males AQ2038.

Figure 48 shows the result of the analysis of the experiments to classify them in either ED or NED.

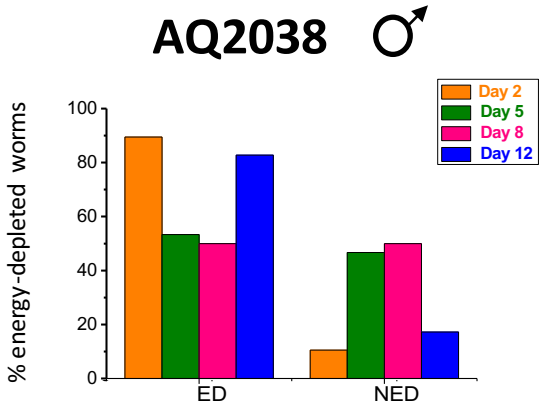

Figure 48. Percentage of worms classified as "Energy Depleted" (ED) or "Non Energy Depleted (NED) at different days of life of the AQ2038 male worms.

The division in both groups shows that in the males there is a large number of worms at all ages in the Energy-Depleted group. In fact, the percentages of ED are much higher than those obtained in mutant AQ*eat-2* hermaphrodites, which has reduced food intake and higher percentages of ED worms than wild type or other mutants.

1.6. Fasting

A possible explanation for the presence of square-wave peaks, keeping high $[Ca^{2+}]_C$ levels for long periods, was the lack of ATP. In the mutant AQ*eat-2* the number of worms corresponding to the Energy-Depleted group is higher than in other lines. Figure 49 shows a summary of the different strains studied.

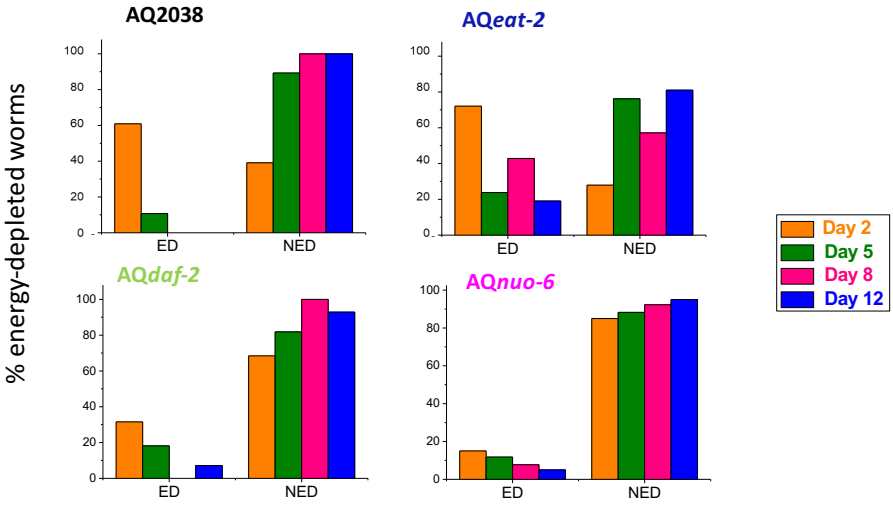

Figure 49: Summary of percentage of ED and NED worms of each strain under feeding conditions.

Mutant AQ*eat-2* had less pumping rate and less food intake than AQ2038, AQ*nuo-6* and AQ*daf-2.* To investigate whether low food intake evokes a higher percentage of Energy-Depleted worms, the subsequent experiments were done under fasting conditions. The protocol for fasting conditions was: when the worms reached the adult state they were transferred to a FuDR plate as in previous experiments, but the plates were not seeded with OP50 or any other type of food. In this situation, the worms were completely under fasting conditions from day one until the day of experiment.

1.6.1. Fasting AQ2038

Figure 50 shows a typical experimental trace corresponding to different days of adult life in AQ2038 grown under fasting conditions.

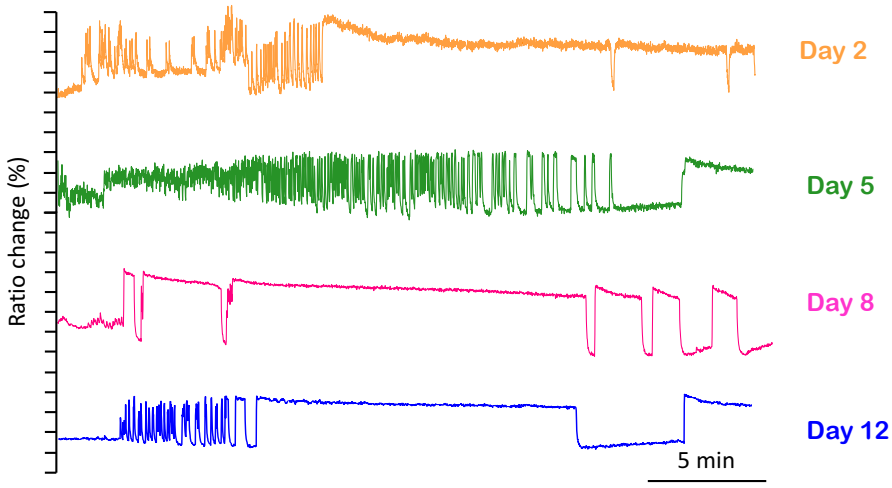

Figure 50: Representative traces at four different days of adult life: Day 2 (n=19) (orange); at Day 5 (n=35) (green); at Day 8 (n=14) (pink) and at Day 12 (n=14) (blue) (Alvarez-Illera P. et al., 2016).

The traces of each day were analysed individually to classify them as ED/NED. Figure 51 shows that fasting AQ2038 show a pattern of ED/NED which is quite different from that found under control conditions (see figure 27). In this case, most worms were Energy-Depleted at all days studied.

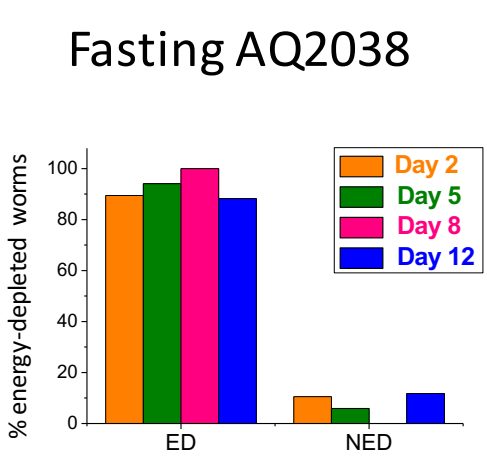

Figure 51. Percentage of fasting AQ2038 worms classified as "Energy Depleted" (ED) or "Non Energy Depleted (NED) at different days of adult life (Alvarez-Illera P. et al., 2016).

The experimental traces of each day were analysed, and the mean height, mean width and mean frequency corresponding to each day were represented (figure 52A-C).

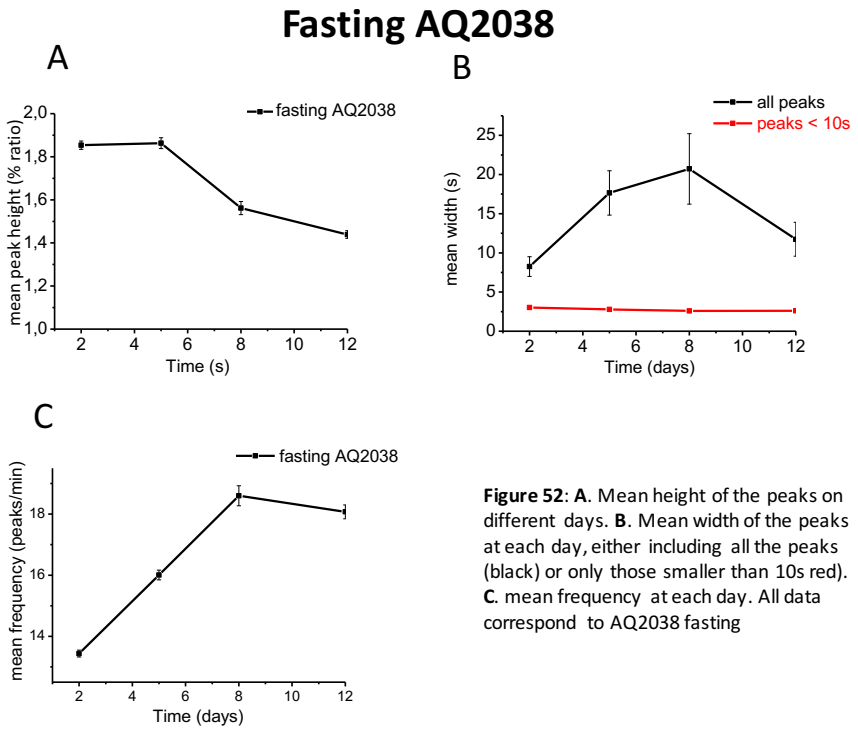

Figure 52: **A**. Mean height of the peaks on different days. **B**. Mean width of the peaks at each day, either including all the peaks (black) or only those smaller than 10s red). **C**. mean frequency at each day. All data correspond to AQ2038 fasting

The height of the peaks decreases with aging. The width of the peaks shorter than 10s did not change throughout the lifespan in fasting worms, but there is a large increase in the mean width calculated including all the peaks, indicating that there is an increase in the percentage of long square-wave peaks throughout the life of the worms (see figure 29B). The frequency under fasting conditions increases with the age. This behaviour is opposite to what happens under non-fasting conditions, but is the same found in AQ*eat-2* mutants that mimic caloric restriction

1.6.2. Fasting AQ*nuo-6*

Figure 53 shows a representative trace obtained at different days of adult life on fasting AQ*nuo-6.*

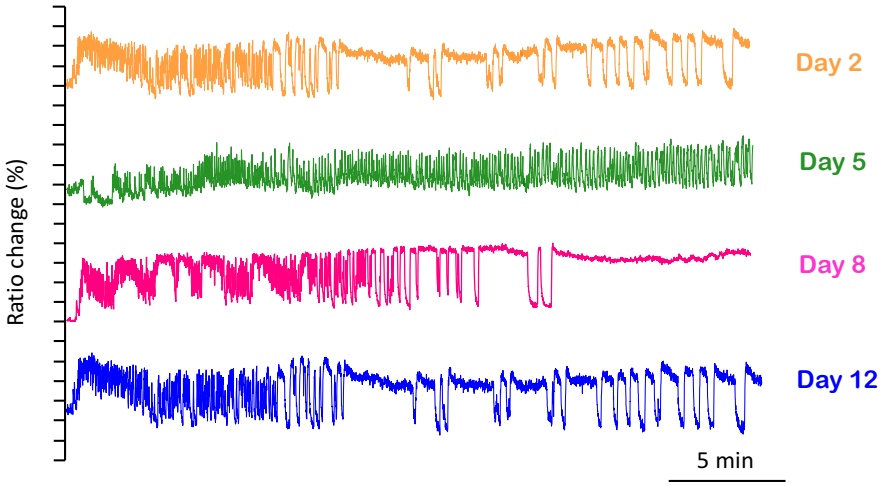

Figure 53: Representative traces at four different days of adult life in fasting AQnuo-6 worms: day 2 (n=18) (orange); at day 5 (n=12) (green); at day 8 (n=15) (pink) and at day 12 (n=12) (blue).

The parameters obtained from all the traces of each day are represented in the figure 54A-C.

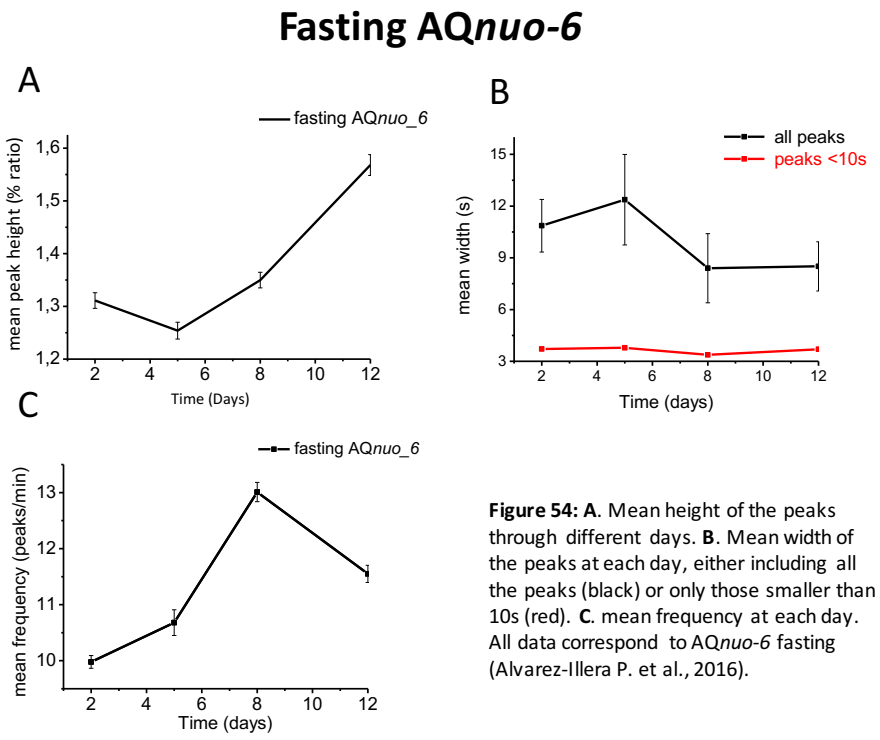

Figure 54: A. Mean height of the peaks through different days. **B**. Mean width of the peaks at each day, either including all the peaks (black) or only those smaller than 10s (red). **C**. mean frequency at each day. All data correspond to AQ*nuo-6* fasting (Alvarez-Illera P. et al., 2016).

The mean height in the presence of food decreases during aging, (see figure 34A-C), while the opposite happens under fasting conditions (figure 54A-C). Regarding the width, we also find here a large increase in the total width, which keeps high even at day 12. The increase in the percentage of the square-wave peaks suggest energy depletion. Finally, the mean frequency in the presence of food decreases with age, but under fasting conditions it has an increasing trend during aging.

Figure 55 shows the percentage of individual worms that correspond to the Energy-Depleted or Non-Energy-Depleted group. The percentage of energy-depleted worms is higher than that obtained in the AQ*nuo-6* fed worms (see Figure 33), but is much lower than that obtained in the fasting AQ2038 controls (see figure 51).

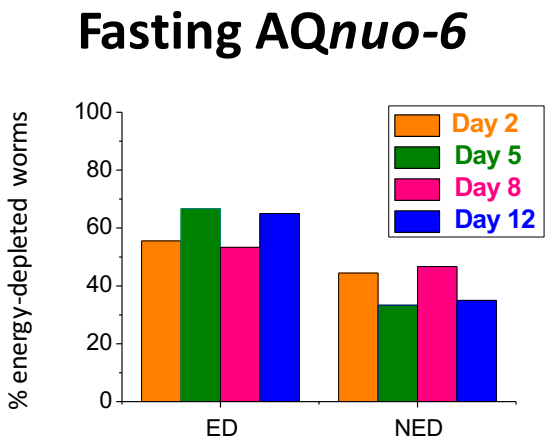

Figure 55: Percentage of fasting AQnuo-6 worms classified as "Energy Depleted" (ED) or "Non Energy Depleted (NED) at every day of the worm life (Alvarez-Illera P. et al., 2016).

1.6.3. Fasting AQ*eat-2*

Figure 56 shows typical traces of Ca^{2+} dynamics obtained at each day of adult life in fasting AQ*eat-2.*

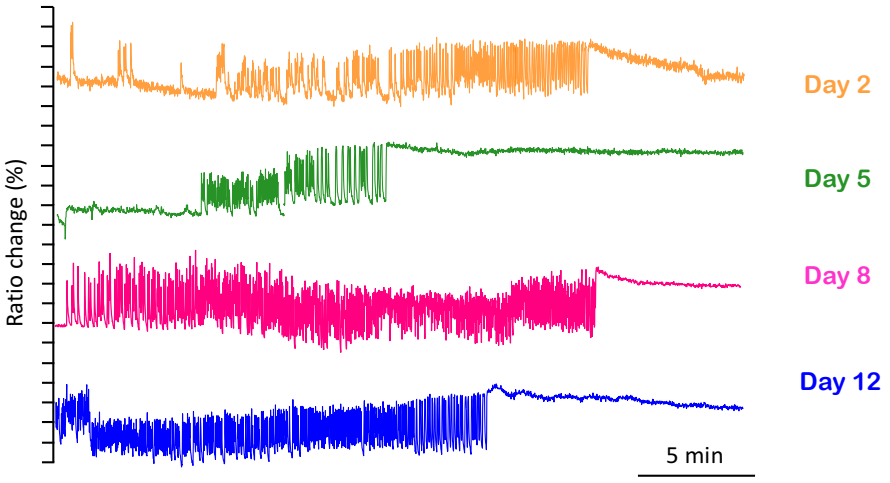

Figure 56: Representative traces of Ca^{2+} dynamics obtained at four different days of adult life in fasting AQeat-2 worms: day 2 (n=23) (orange); at day 5 (n=18) (green); at day 8 (n=20) (pink) and at day 12 (n=22) (blue).

The mean height, mean width and mean frequency obtained each day are represented in figure 57A-C. The height and the frequency behaved similarly both in food deprivation and in the presence of food (see figures 39A and C 57 A and C). Regarding the width, that corresponding to the peaks smaller than 10s was also similar at all ages, but the width including all the peaks increased in the fasting AQ*eat-2* worms because of the much higher percentage of square-wave peaks, even in older worms (see figures 39B and 57B).

Fasting AQ*eat-2*

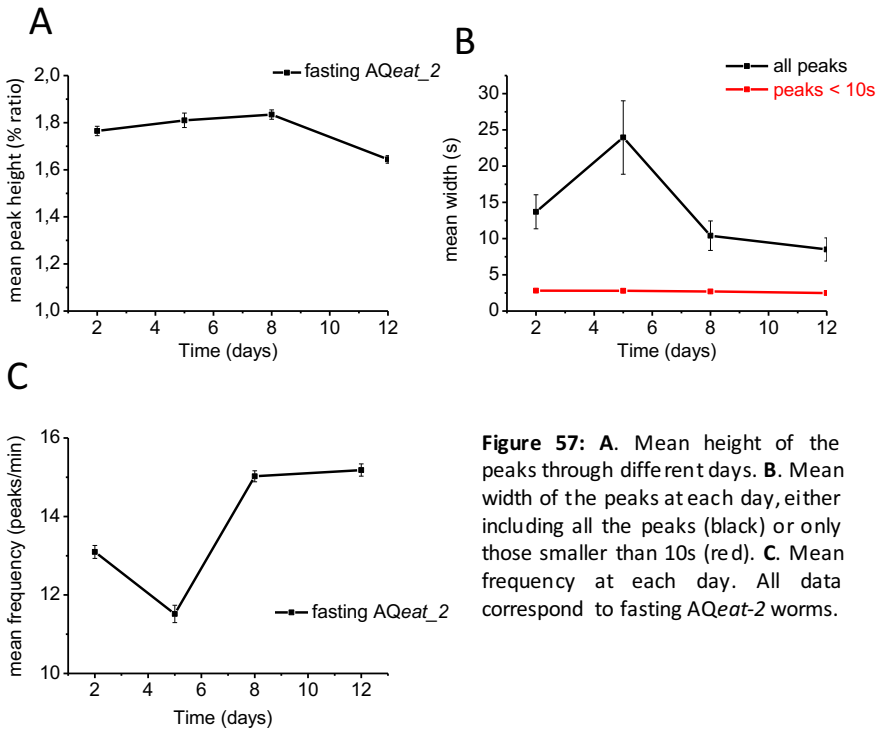

Figure 57: A. Mean height of the peaks through different days. **B**. Mean width of the peaks at each day, either including all the peaks (black) or only those smaller than 10s (red). **C**. Mean frequency at each day. All data correspond to fasting AQ*eat-2* worms.

When we analyse the worm traces individually to classify them as ED or NED, we can see that the percentage of worms corresponding to the group with energy depletion was much greater in fasting AQ*eat-2* (see figure 58) than in the feeding condition (see figure 38), and similar to that obtained in fasting AQ2038 worms (see figure 51).

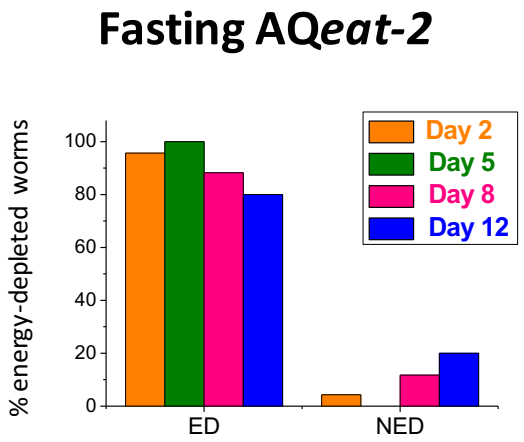

Figure 58: Percent of fasting AQ*eat-2* worms classified as "Energy Depleted" (ED) or "Non Energy Depleted (NED) at every day of adult life.

1.6.4. fasting AQ*daf-2*

The behaviour of AQ*daf-2* worms under fasting conditions was also studied in this work. Figure 59 shows typical traces of Ca^{2+} dynamics in the pharynx of these worms obtained at different days of adult life.

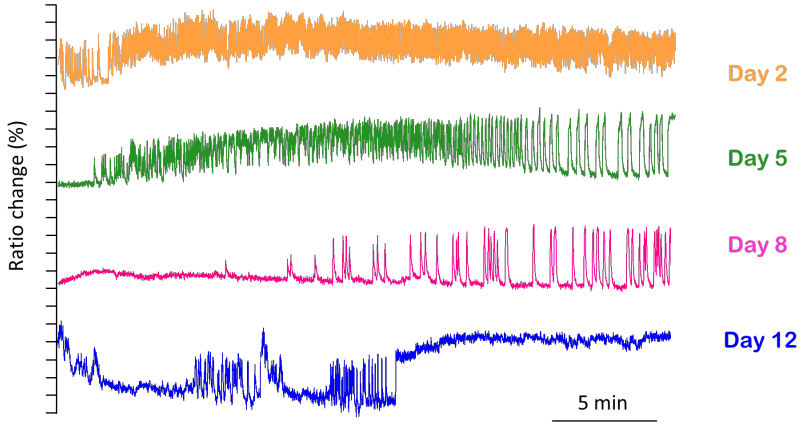

Figure 59: Representative traces at four different days of adult life in fasting AQdaf-2 worms: day 2 (n=24) (orange); at day 5 (n=22) (green); at day 8 (n=15) (pink) and at day 12 (n=15) (blue).

The values obtained when we calculate the mean height, width and frequency of Ca^{2+} oscillations in fasting AQ*daf-2* worms are represented in figure 60A-C.

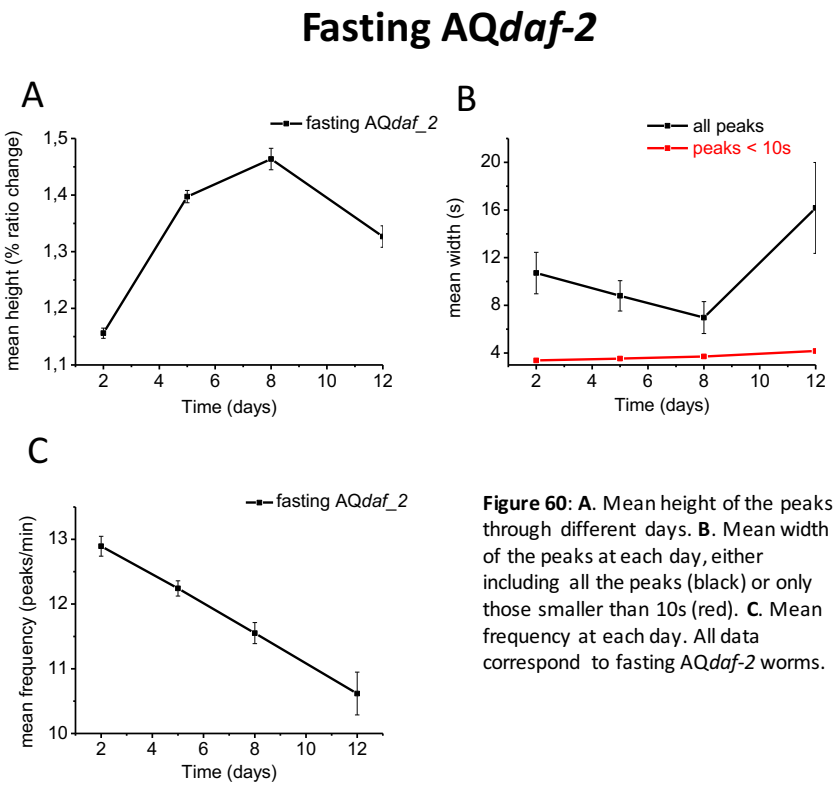

Figure 60: **A**. Mean height of the peaks through different days. **B**. Mean width of the peaks at each day, either including all the peaks (black) or only those smaller than 10s (red). **C**. Mean frequency at each day. All data correspond to fasting AQ*daf-2* worms.

The mean height is lower under fasting conditions than in normal fed-conditions (see figure 44A). The mean width of peaks shorter than 10s showed the same pattern than in fed worms, but the values were higher in fasting conditions (see figure 44B). The width including all the peaks was much higher because of the increase in the square-wave peaks. The mean frequency shows the same tendency in the presence or absence of food, although the absolute values under food deprivation were lower (see figure 44C).

The division in ED and NED groups in this case is represented in the figure 61. We can see that there is an increase in the percentages of ED worms at every age with respect to the fed AQ*daf-2* worms, but the increase is smaller than that found in the fasting AQ2038 wild type worms.

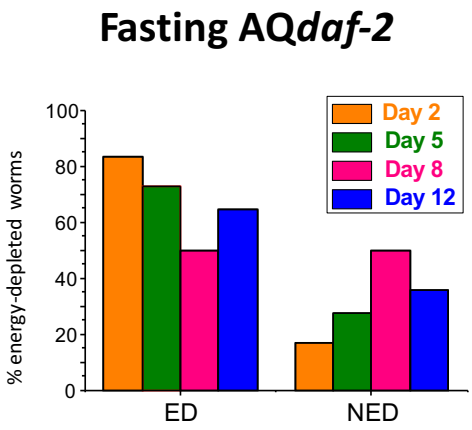

Figure 61: Percent of fasting AQ*daf-2* worms classified as "Energy Depleted" (ED) or "Non Energy Depleted (NED) at every day of adult life.

2. Mitochondrial pharyngeal Ca^{2+} measurements.

The mitochondria is an intracellular organelle that plays an important role in cellular energetics and ATP production. The level of [Ca^{2+}] inside mitochondria is one of the main modulators of these pathways. Mitochondria can capture Ca^{2+} through the mitochondrial Ca^{2+} uniporter (MCU) when this ion increases in the cytosol after cell activation. The return to resting Ca^{2+} levels is mediated by mitochondrial Na^{+}/Ca^{2+} or H^{+}/Ca^{2+} exchangers (Palty R. et al., 2010; Nagai T. et al., 2004). This transient mitochondrial Ca^{2+} uptake is driven by the mitochondrial membrane potential (-150/-180mV), which is created by the respiratory chain and which in some way reflects the functional state of the mitochondria.

Mitochondrial dysfunction is one of the most distinctive features of aging in all living organisms (Picard M. et al., 2010; Siegel MP. et al., 2013; Morsci NS. et al., 2016). In *C. elegans* mitochondria of body wall muscle cells undergo progressive fragmentation with aging (Regmi SG. et al., 2014). But the mechanisms and functional significance of this progressive mitochondrial alteration is still unknown, mainly because a series of *C. elegans* mutants with mild mitochondrial alterations have an extended lifespan (Munkácsy E. et al., 2014).

2.1. Mitochondrial pharyngeal Ca^{2+} measurement in AQ3055

Strain AQ3055 is the control strain that expresses the yellow cameleon 3.60 (YC3.60) (Miyawaki A. et al., 2004) targeted to the pharyngeal mitochondria. The promoter used to target YC3.60 to the pharyngeal mitochondria is *pmyo-2*, and mitochondrial targeting is achieved by including at the beginning of the DNA of the sensor a signal peptide containing the first 36 amino-acids of subunit VIII of human COX, inserted in duplicate (*pmyo-2*::2mt8::YC.3.60). The probe is not integrated, and is expressed as extrachromosomal array with more than 95 percent transfer to the next generation. The worms selected for the experiments were always the brightest in terms of green pharyngeal fluorescence.

To check if the Ca^{2+} probe was expressed in pharynx mitochondria, it was necessary to perform a confocal microscopy image colocalization study with Mitotracker Deep Red (see Methods 7), a selective dye for mitochondria. We have to take into account that Mitotracker Deep Red stains mitochondria in all the worm cells, whereas YC3.60 is only expressed in pharyngeal cells mitochondria. When we merged the green image of mitochondrial YC3.60 (figure 62A) with the red image of Mitotracker Deep Red (figure 62B), we obtained figure 62C, where the yellow image represents the colocalization of the two probes in pharynx mitochondria. Therefore, this provides good evidence for the correct mitochondrial localization of the YC3.60 probe.

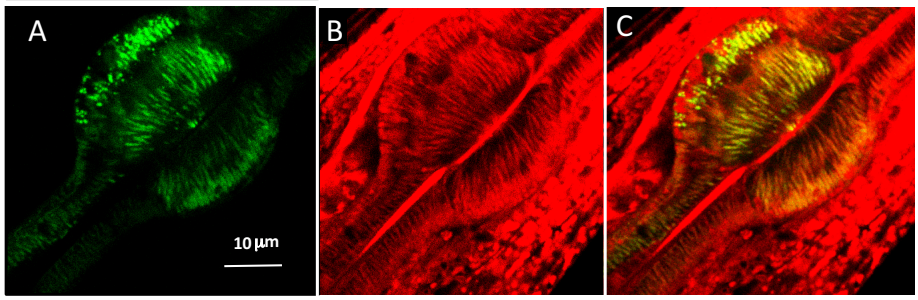

Figure 62: confocal images of the terminal bulb of AQ3055 loaded with MitoTracker Deep Red. **A**. YC.3.60 fluorescence. **B**. Mitotracker Deep Red fluorescence. **C**. merge of panel A and B (Álvarez-Illera et al., 2017).

2.1.1. Experimental traces

Figure 63 shows typical traces of mitochondrial Ca^{2+} dynamics in worms at different days of adult life.

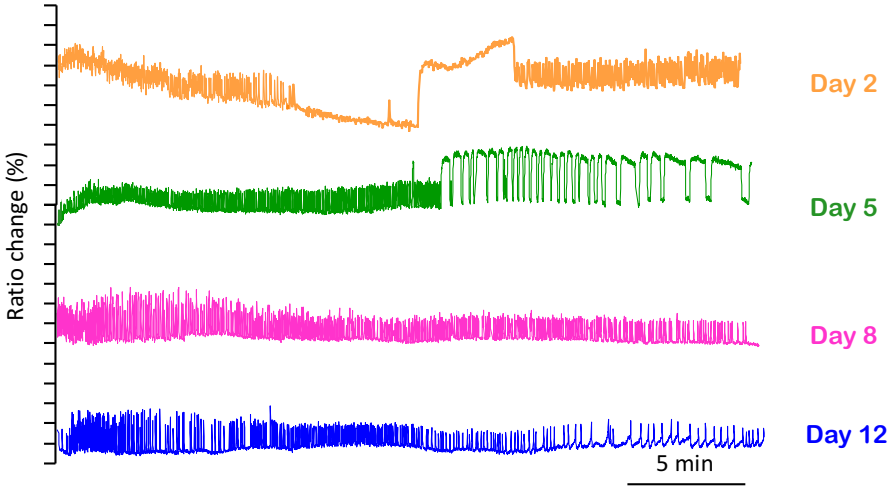

Figure 63: Representative traces at four different experimental days in AQ3055 worms: day 2 (n=38) (orange); at day 5 (n=29) (green); at day 8 (n=29) (pink) and at day 12 (n=35) (blue) (Álvarez-Illera et al., 2017).

The calcium dynamics pattern observed in pharyngeal mitochondria was quite similar to that of the cytosol. There were fast peaks, named *spikes* and others that correspond to *square-wave* transients, which showed prolonged high Ca^{2+} levels for many seconds or minutes.

2.1.2. Data analysis

Experiments of pharynx mitochondrial [Ca^{2+}] were analyzed with the algorithm as described above, obtaining values for the mean height, mean width and mean frequency at every age. We therefore followed the same process as we did with the measurements of cytosolic [Ca^{2+}]. First, figure 64 represents plots of peak height *versus* peak width in order to know the distribution of peaks with different heights and widths. The figure shows results similar to those previously obtained in cytosol (figure 27). The proportion of long square wave peaks is higher in young worms and progressively declines as worms get older.

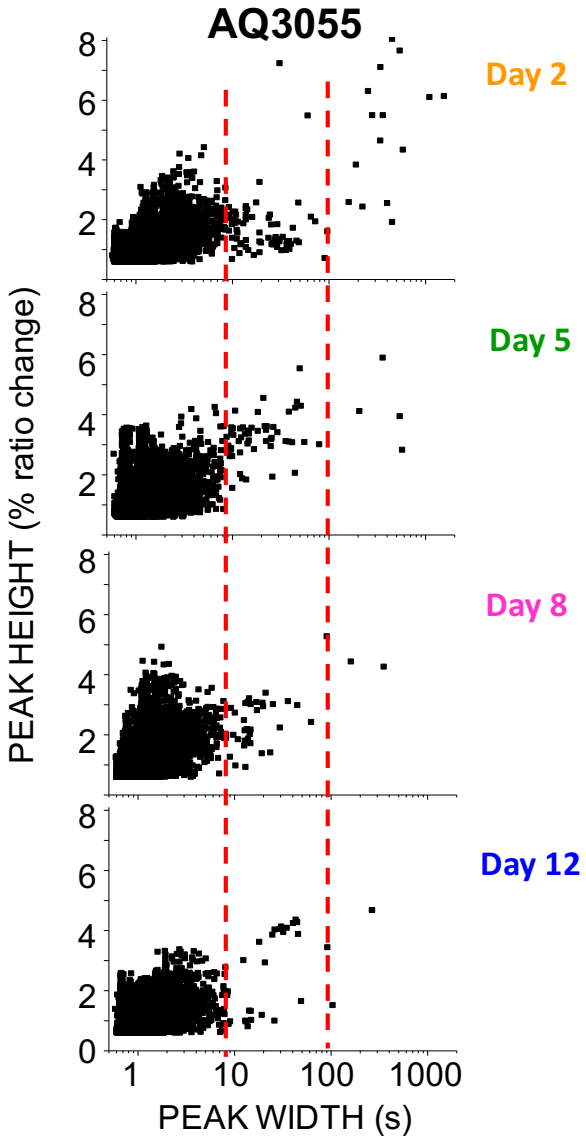

Figure 64: Plots of peak height *versus* peak width for all the peaks analysed in worms of Day 2 (8414 peaks from 38 worms studied), Day 5 (9365 peaks from 29 worms studied), Day 8 (10802 peaks from 29 worms studied) and Day 12 (11232 peaks from 35 worms studied). The peak width is represented in logarithmic scale (Alvarez-Illera P. et al. 2017).

The parameters mean height, mean width and mean frequency were analysed comparing AQ2038 and AQ3055, that correspond to wild-type worms expressing either the cytosolic or the mitochondrial Ca^{2+} sensor, respectively.

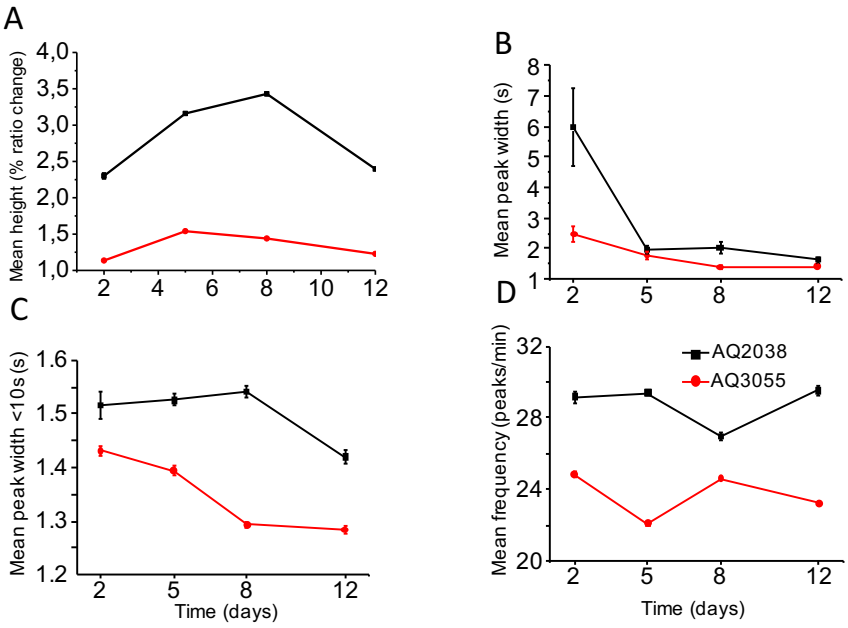

Figure 65: A. Mean height of the peaks at different days. **B**. Mean width of the peaks at each day, C. Mean width of the peaks only those smaller than 10s. **D**. Mean frequency at every day. All data correspond to AQ3055 (Álvarez-Illera et al., 2017).

The mean height of the Ca^{2+} peaks and the mean width of the Ca^{2+} peaks show a similar progression with age in both cytosol and mitochondria (see figure 65A and B). The magnitude of the changes in height cannot be compared because the Ca^{2+} sensors are different, YC2.1 in AQ2038 and YC3.60 in AQ3055. This does not affect measurements of width and frequency, but may modify the ratio changes. Regarding the width, there are few differences. Both $[Ca^{2+}]_C$ and $[Ca^{2+}]_M$ measurements show that younger worms

have a total mean width higher because of the presence of the square-wave peaks. The peaks smaller than 10s show also a decreasing trend with aging in both compartments. The mean frequency, on the other hand, is smaller in the $[Ca^{2+}]_M$ measurements and changes little during aging.

In cytosol we hypothesized that the presence of square-wave peaks is due to energy depletion of the pharyngeal cells, so we analysed also the experimental Ca^{2+} traces in mitochondria from the energy point of view. Worms were divided into two groups: ED or NED, as described above. The results are in figure 66. The graph is similar to that obtained in AQ2038 worms. The percentage of worms corresponding to the ED group is higher in young worms and decreases as the worms become older.

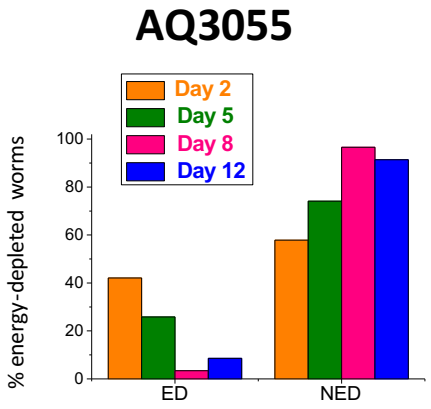

Figure 66: Percentage of worms classified as "Energy Depleted" (ED) or "Non Energy Depleted (NED) at every day of the worm adult life in AQ3055 worms.

If we compare the worms that correspond to the Energy-Depleted group both in cytosolic $[Ca^{2+}]$ studies (AQ2038 strain) and in mitochondrial $[Ca^{2+}]$ studies (AQ3055 strain), we can see that both present more energy depleted worms in young worms (figure 67). Attention to the scale.

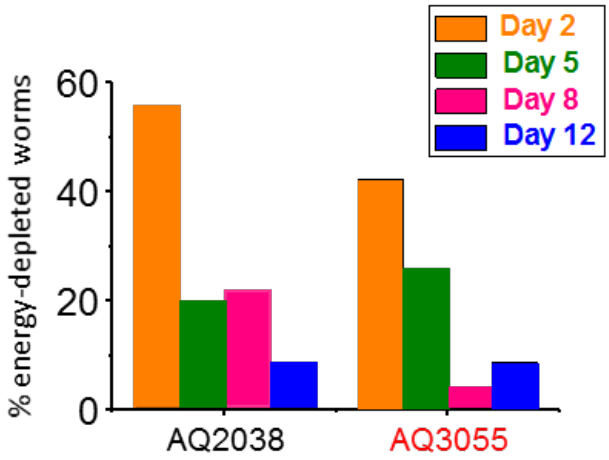

Figure 67: Percentage of worms considered as Energy-Depleted. (Álvarez-Illera et al., 2017).

2.2. M*nuo-6*

The M*nuo-6* strain was obtained by crossing AQ3055 males with hermaphrodite mutants *nuo-6(qm200)* (see Methods 5). The worms of this cross were *nuo-6* mutants and expressed the fluorescence protein YC3.60 targeted to pharyngeal mitochondria.

To demonstrate the proper localization of the probe YC3.60 in the mitochondria (figure 68A-C), a confocal microscopy study with Mitotracker Deep Red was performed, in the same way as we did in the AQ3055 strain. The mitochondrial YC3.60 expressing *nuo-6* strain (Mnuo-6) has a longer lifespan than wild-type worms (Yang W. & Hekimi S., 2010). Figure 69D plots the lifespan study comparing M*nuo-6* and AQ3055 and shows that M*nuo-6* has a longer life expectancy than AQ3055 control worms.

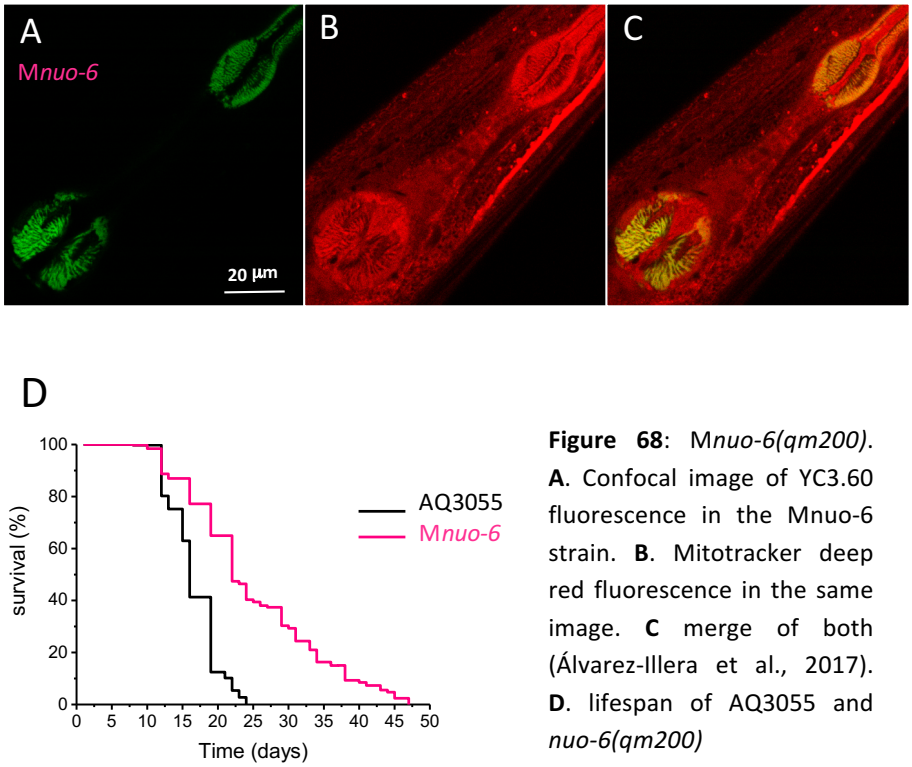

Figure 68: M*nuo-6(qm200)*. **A**. Confocal image of YC3.60 fluorescence in the Mnuo-6 strain. **B**. Mitotracker deep red fluorescence in the same image. **C** merge of both (Álvarez-Illera et al., 2017). **D**. lifespan of AQ3055 and *nuo-6(qm200)*

Figure 68A shows the mitochondrial YC3.60 image of the pharyngeal terminal bulb. The figure 68B corresponds to the image of mitochondria loaded with Mitotracker Deep Red and the figure 68C shows the merge between figures 68A and B. The yellow image corresponds to the colocalization of both fluorescences. Figure 68D shows that the lifespan of the M*nuo-6* strain is longer than that of AQ3055, but similar to that of AQ*nuo-6* (see figure 29).

2.2.1. Experimental traces

Figure 69 shows Ca^{2+} traces representative of those obtained in worms of different days of adult life in the M*nuo-6* strain. The calcium patterns are similar to those obtained in the mitochondrial-YC3.60 expressing AQ3055 control strain (figure 63) and in the cytosolic mutant AQ*nuo-6*. (figure 30). In the M*nuo-6* strain we could not obtain traces at day 2 because the fluorescence level was too weak and thus the Ca^{2+} measurements were very noisy.

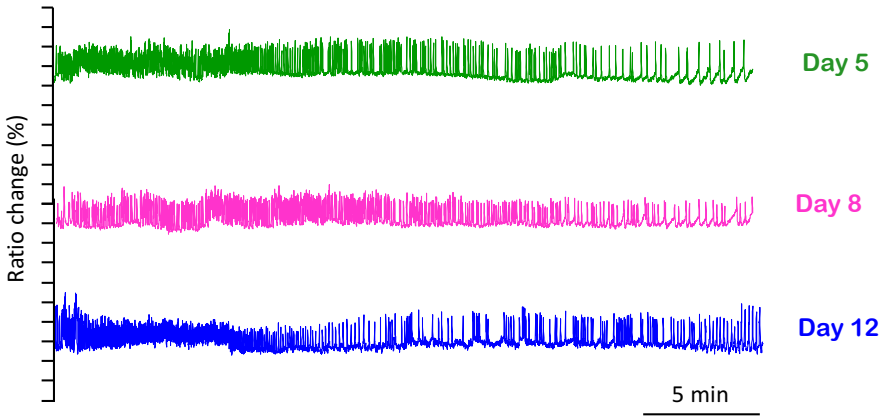

Figure 69: Representative traces at three different experimental days in Mnuo-6 worms: at day 5 (n=36) (green); at day 8 (n=28) (pink) and at day 12 (n=23) (blue) (Álvarez-Illera et al., 2017).

2.2.2. Data analysis

The parameters mean height, mean width and mean frequency were obtained with the algorithm for M*nuo-6* worms of every day of adult life. The traces shown in figure 69 do not present square wave peaks but figure 70, which includes all the peaks measured at each day of study shows that square wave peaks are also present and mainly in young worms.

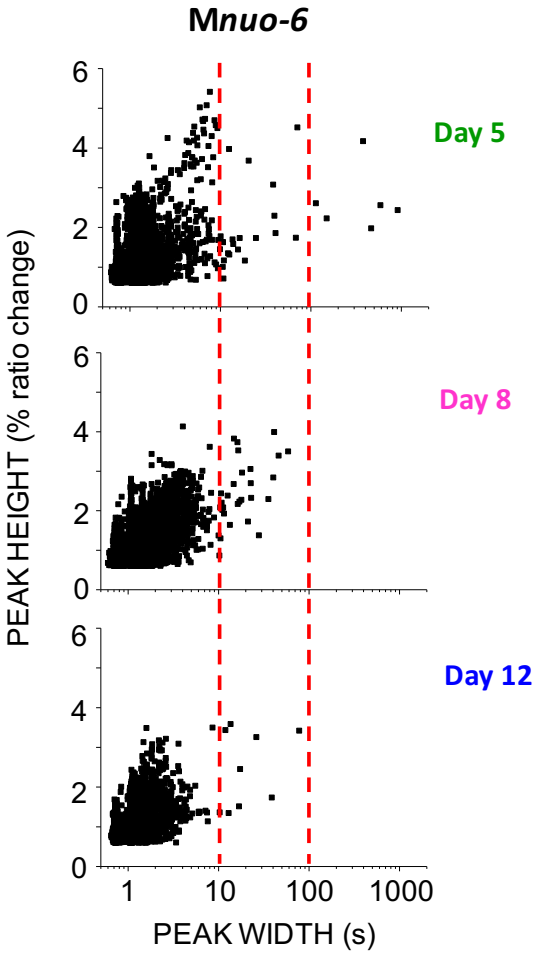

Figure 70: Plots of peak height *versus* peak width for all the peaks analysed in worms on Day 5 (4016 peaks from 36 worms studied), Day 8 (5512 peaks from 28 worms studied) and Day 12 (4430 peaks from 23 worms studied). The peak width is represented in logarithmic scale (Alvarez-Illera P. et al. 2017).

Figure 70 shows that the patterns were similar to those of AQ2038 and AQ*nuo-6*. The presence of long square-wave peaks was greater in young M*nuo-6* worms but progressively disappear when worms age.

From an energy point of view, the AQ*nuo-6* mutants (figure 71) correspond mainly to the non-energy-depleted group. Figure 71 shows that the percentage of worms that correspond to the group ED is lower in M*nuo-6* than in AQ3055, and is instead more similar to that of the AQ*nuo-6* worms (see figure 33). Both have a low percentage of energy depleted worms. Therefore, this phenomenon could be due to the *nuo-6* mutation, which may somehow protect worms from energy depletion.

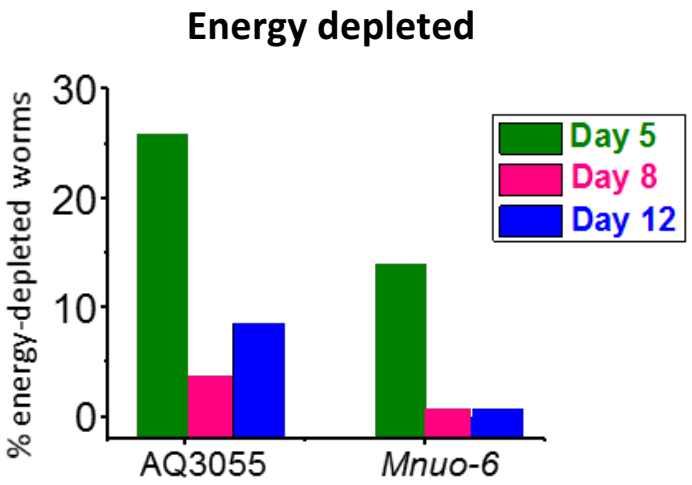

Figure 71: Percentage of worms classified as "Energy Depleted" (ED) of AQ3055 and M*nuo-6* at every studied day of the worm adult life (Álvarez-Illera et al., 2017)

The mean height, mean width and mean frequency are represented in figure 72. In this case we compared both mitochondrial YC3.60 expressing strains, AQ3055 and M*nuo-6.*

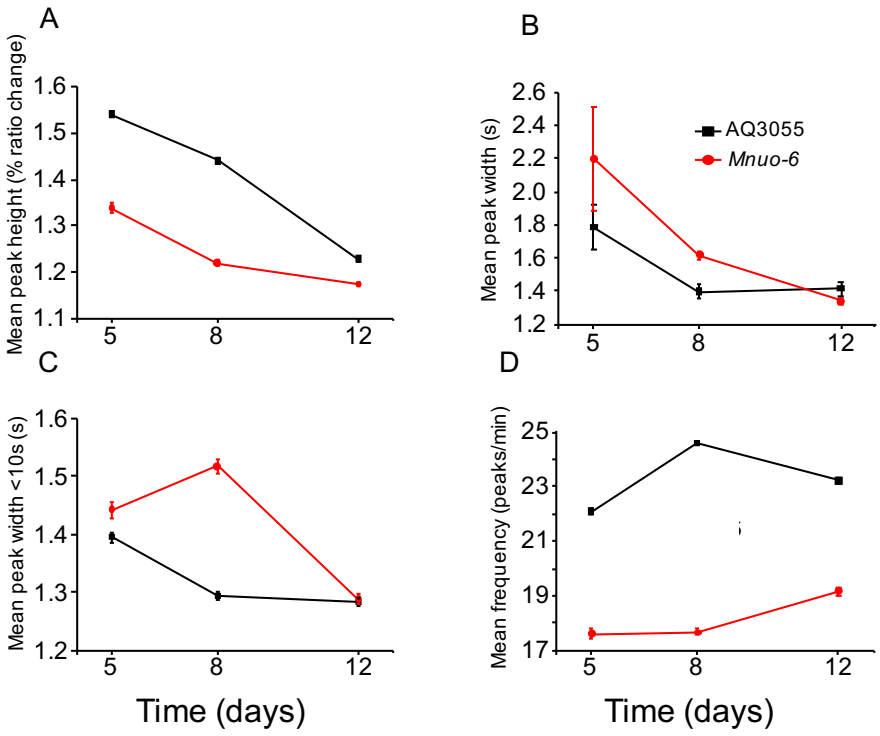

Figure 72: A. Mean height of the peaks through different days. B. Mean width of the peaks at each day, either including all the peaks (black) or only those smaller than 10s (light blue). C. Mean frequency at each day. All data correspond to AQ3055 (Álvarez-Illera et al., 2017).

The mean height of the mitochondrial [Ca^{2+}] peaks was smaller in *nuo-6* mutant worms than in the controls at every age that we tested (Figure 72A). The mean peak width of the [Ca^{2+}] peaks was larger in the M*nuo-6* worms than in the controls at days 5 and 8, and similar at day 12. The same happened with the mean peak width calculated excluding the [Ca^{2+}] peaks longer than 10s (Figure 72B and C), and these data follow exactly the same pattern we previously found for the cytosolic [Ca^{2+}] peaks in the *nuo-6* mutant strain compared with the control (Figure 29B and 34B). Therefore, *nuo-6* worms have wider cytosolic and mitochondrial [Ca^{2+}] peaks than controls at days 5 and 8 of adult life, and return to the control values at day 12. There were also significant

differences in the frequency of the mitochondrial [Ca^{2+}] peaks, which was much smaller in *nuo-6* mutant worms than in the controls at every age, as it also occurred with the frequency of the cytosolic [Ca^{2+}] peaks (Figure 72D, 29C and 34C).

DISCUSSION

The *C. elegans* pharynx is a neuromuscular organ that undergoes rhythmic contractions in order to allow food ingestion. The maximum rate of pharyngeal pumping is obtained at day 2 of adult life and reaches values of up to 300 pumps per minute. Then, the pharyngeal pumping rate undergoes a progressive decline and usually ceases around day 12 (Huang et al., 2004; Miyawaki et al., 1997). In addition, this decline in pumping rate correlates with the lifespan, because it is significantly delayed in several long-lived mutants and occurs earlier in short-lived ones (Huang et al., 2004). For these reasons, we thought that the study of Ca^{2+} dynamics in the pharynx during aging could provide clues and new functional parameters related to the aging process. The results showed that there were in fact changes in the pattern of Ca^{2+} dynamics during aging and revealed also several unexpected findings.

1. Cytosolic calcium measurement in the pharynx

Many studies have been published about the changes in the pumping rate during aging, and it has always been shown to decrease as the worms become older (Hosono et al., 1980; Huang et al., 2004; Chow et al., 2006). However, only the muscle contraction has been monitored. Changes in Ca^{2+} activity have only been monitored for short periods of time (no more than 2 minutes). Figures 23 and 24 show that it is possible to make Ca^{2+} measurements in the pharynx of the worm for much longer periods of time.

The oscillatory Ca^{2+} activity in the pharynx did not undergo a progressive decline with age as shown previously for pharyngeal pumping (see figure 25). When the transients of $[Ca^{2+}]_C$ were analyzed together, the width and the height of the Ca^{2+} spikes changed little from day 2 to day 12, and just a 10% decrease in the

mean frequency of the peaks was observed in figures 29A-C. This suggests that aging affects much more to muscle contraction, the physical binding of myosin and actin to develop force, than to the development of the $[Ca^{2+}]_C$ signal required to induce contraction. In old animals, the $[Ca^{2+}]_C$ signal in the pharynx cells remains essentially intact, but the contraction nearly disappears. This is consistent with previous data indicating that muscle sarcopenia or loss of muscle mass and strength is the major cause of aging-related functional decline, and that contraction-related injury may significantly promote the progression of sarcopenia in the pharynx (Herndo et al., 2002). In contrast, the nervous system appears to be much better preserved with age (Olson, 2006). Therefore, it seems that the machinery required to generate oscillatory $[Ca^{2+}]_c$ activity in the pharynx is preserved in old adults, even though the contractile proteins cannot longer be functional.

Another important result regards to the meaning of the long "square-wave" $[Ca^{2+}]_C$ transients (see figure 25). Such prolonged elevations of Ca^{2+} are ineffective for food ingestion because they would just induce a persistent contraction. In addition, prolonged elevations of $[Ca^{2+}]_C$ are generally detrimental to cells and imply poor functioning of the mechanisms responsible for pumping calcium either out of the cells or into the sarcoplasmic reticulum. In normal functioning cells, the global $[Ca^{2+}]_C$ elevations are always transient, because the mechanisms that remove calcium from the cytosol (pumps, exchangers) are always active, while the mechanisms that introduce Ca^{2+} in the cytosol (channels) are activated in a transient form. Therefore, the long "square-wave" $[Ca^{2+}]_C$ transients, where $[Ca^{2+}]_C$ is kept high for minutes, are most likely attributed to the blocking of the Ca^{2+} pumps responsible for clearing $[Ca^{2+}]_C$, and the most probable reason for this is the lack of ATP energy. According to this hypothesis, we classified the worms in two groups:

- ✓ **Energetically Depleted** (ED), the traces present several square-wave Ca^{2+} peaks during the experiments, or when the experiment ends with a prolonged high cytosolic Ca^{2+} level.
- ✓ **Non- Energetically-Depleted** (NED), the traces show fast Ca^{2+} transients during the whole experiment, or when the worm stops making Ca^{2+} transients before the end of the 30 minutes but with a low resting $[Ca^{2+}]_C$ level.

To obtain more evidence for the hypothesis of ATP depletion in the origin of the "square-wave" $[Ca^{2+}]_C$ transients, we decided to study worms subjected to starvation by complete elimination of food during adulthood. It has been described that complete removal of food actually extends lifespan in *C. elegans* and can be considered an extreme type of dietary restriction (Song and Avery, 2012; Kaeberlein, 2006). These worms under conditions of total diet deprivation have in fact an increased pumping rate and average locomotion than those fed *ad libitum* (Van Raamsdonk et al., 2010). It has also been shown that the metabolic rate is not reduced in food restricted worms (Houthoofd et al., 2002).

However, this condition should significantly limit the total amount of energy available. Therefore, the combination of increased pumping and locomotion activity as well as the sustained metabolic rate should lead to earlier energy depletion in pharynx muscle. Accordingly, the number of "square-wave" $[Ca^{2+}]_C$ transients and the percentage of worms that correspond to the ED group were largely increased by this treatment not only in young adults but also in all the ages we tested (see figure 51, 54, 58, 60). Therefore, this represents further evidence that lack of energy may be a key determinant for the occurrence of "square-wave" $[Ca^{2+}]_C$ transients.

The main paradox in these results was that the higher number of "square-wave" $[Ca^{2+}]_C$ transients in control fed worms was obtained in young worms, when we should not expect ATP depletion or cell deterioration. Instead, the number of "square-wave" $[Ca^{2+}]_C$ transients was largely decreased by day 12. The ATP content in wild-type *C. elegans* worms is maximum at days 2-4 and then decreases progressively until day 12-14, reaching values close to 10% of the original (Braeckman B.P. et al., 1999; Collins JJ. et al., 2007; Horvitz H.R. et al., 1982). The total amount of ATP is thus much higher in young nematodes. So, if energy depletion is the reason for the development of "square-wave" $[Ca^{2+}]_C$ transients, it seems contradictory that they appear only in young wild-type adults and then progressively disappear as they get older.

The way we interpreted this phenomenon is based in the concept of **energy balance**. In the case of young adults, energy depletion would come from a very high rate of use of energy, which would exceed the higher availability of energy at that stage. When the worms were stimulated with serotonin, the calcium oscillatory activity in the pharynx is rapidly induced. In young worms, this leads to a very fast pumping rate because the contractile machinery is still intact. Repetitive contraction uses large amounts of ATP and in many worms this leads to depletion of the energy reserves during the 30-min time of the experiment. As the worms increase age, the Ca^{2+} oscillatory activity remains, but the pumping rate decreases and also the amount of energy dedicated to the contraction. Worms at day 12 of adulthood showed little contraction, despite the Ca^{2+} oscillatory activity remained nearly intact. The lack of contraction reduces substantially the amount of energy used and this may allow the worm to maintain Ca^{2+} oscillations.

Further evidence for this energy balance hypothesis comes from the data obtained in several long-lived mutants:

- ✓ AQ*eat-2*, with mutation in a nicotinic receptor in the pharynx and YC2.1expression (see figure 36).
- ✓ AQ*nuo-6*, with mutation in a subunit complex I of the mitochondria respiratory chain and expression of YC2.1 (see figure 30).
- ✓ AQ*daf-2*, with mutation in Insulin/Growth Factor-1 and expression of YC2.1 (see figure 41).

The *eat-2* mutant has a lower pumping rate, which mimics caloric restriction. As a consequence, these worms have less energy, and this may facilitate energy depletion (Lakowski and Hekimi, 1998). In fact this was the case. In this mutant we found a higher percentage of ED worms at all ages, even in old worms, although the percentage kept higher at day 2. In addition, when *eat-2* worms underwent food deprivation, the percent of ED worms increased to the same levels as those found in food-deprived AQ2038 controls. The percent of ED worms thus correlates with the degree of caloric restriction.

nuo-6 mutant worms have a lower ATP content than wild type worms (Mozaffari et al., 2013). However, *nuo-6* mutant worms showed very few "square-wave" $[Ca^{2+}]_C$ transients at any age (see figure 32). It has been shown that the pumping rate of this mutant is much smaller than that of wild-type worms (Avery L. and Shtonda B.B., 2003), and these mutants also show low oxygen consumption, slow growth, slow behavior, and increased lifespan. If the proposed hypothesis is correct, the smaller rate of energy use in this mutant would allow maintaining the balance among energy production and consumption, despite the lower rate of energy production (see figure 33). Therefore, the balance between energy production and consumption becomes essential to avoid the total energy depletion of pharynx muscle cells, and the deleterious effects of the persistent increase in $[Ca^{2+}]_C$. Of course, if

they are maintained under conditions of food deprivation, the lack of energy production rapidly leads to ATP depletion even in the mutants (see figure 54).

The lower degree of energy use in the *nuo-6* mutants may also be the reason for the increase in the width of the fast spikes in the mutants (the mean peak width <10s), which depends mainly on the rate of Ca^{2+} pumping out of the cytosol, either outside the cell or into the sarcoplasmic reticulum (see figure 34A-C). Therefore, the ATP concentration is lower in the *nuo-6* mutants, as previously reported (Mozaffari M.S. et al., 2013), but they are able to maintain those reduced levels during activity thanks to the smaller rate of consumption. Uncoupling of energy production and consumption through decreased energy utilization has been proposed before to be at the origin of the extended lifespan of some *C. elegans* mutants (Braeckman B.P. et al., 1999; Nagai T. et al., 2004).

The *daf-2* mutant is also a long-lived mutant with an alteration in the insulin/IGF-1 signaling. Interestingly, the degree of energy depletion of *daf-2* worms is quite similar to that of *nuo-6* mutants in both, under fed as well as with food-deprivation conditions. There was a smaller number of young ED worms when under fed conditions were used, and the percentage increased less under food deprivation conditions. Therefore, it seems that these two long-lived mutants activate a survival mechanism that allows them to improve the balance between energy production and energy consumption.

Finally, we have also made the same measurements in males, in order to know if there could be any differences because of the sexual dimorphism (see figure 47A-C). We found a decrease in the mean height and mean frequency of the Ca^{2+} oscillations, but the main difference was the large increase in the number of

square-wave peaks and in the percentage of ED worms, which was larger than the difference we observed for the *eat-2* mutants. A possible explanation for this is that males mainly appear under stress conditions (high temperature, starvation, etc) in order to improve reproduction, and their only mission is to search for hermaphrodites without worrying about energy consumption. This would explain why they enter easily into energy depletion conditions.

2. Mitochondria calcium measurement in the pharynx

We show here the first dynamic measurements of mitochondrial Ca^{2+} transients in the pharynx in live *C. elegans*. Figure 62A-C shows that the protein YC3.60 has a typical mitochondrial distribution and its fluorescence colocalized with that of Mitotracker Deep Red, indicating a mitochondrial localization of the Ca^{2+} sensor. Our data show the behavior of $[Ca^{2+}]_M$ dynamics in the pharynx of *C. elegans* for long periods of time, and how it changes as worms age and in *nuo-6* mutants, which have a defect in the respiratory chain complex I.

The data showed that mitochondrial $[Ca^{2+}]$ oscillates at high frequency, reproducing cytosolic $[Ca^{2+}]_C$ oscillations (see figures 23, 24, 63). The recorded frequencies of $[Ca^{2+}]_M$ oscillation were up to 1Hz. This point is important because the pharynx of *C. elegans* is a neuromuscular organ that has been compared to the heart because it has similar electrical properties and its development is controlled by similar genes (Olson et al., 2006). Mitochondrial $[Ca^{2+}]$ signaling in the heart is controversial because there are two different models to explain how the $[Ca^{2+}]_C$ oscillations are translated to mitochondria. One of the models suggests that mitochondria rapidly follow the oscillations in $[Ca^{2+}]_C$ “beat-to-

beat", while the other model proposes that $[Ca^{2+}]_M$ only reflects a slow integration of the $[Ca^{2+}]_C$ transients (Dedkova & Blatter, 2013). The two models predict very different $[Ca^{2+}]_M$ kinetics in response to the repetitive cytosolic $[Ca^{2+}]$ spikes, either repetitive $[Ca^{2+}]_M$ spikes in the first model or a slow progressive increase in the second. Our data showed that *C. elegans* pharynx mitochondria behave in a "beat-to-beat" mode, indicating that Ca^{2+} uptake and release from the mitochondria are fast enough to recover resting levels after each Ca^{2+} spike. The "beat-to-beat" model has several physiological implications. Energy consumption is higher with this model because both, Ca^{2+} uptake and release by mitochondria consume mitochondrial membrane potential and larger amounts of Ca^{2+} are taken up by mitochondria during each $[Ca^{2+}]_C$ spike, so that mitochondrial Ca^{2+} buffering may potentially become an important regulator of $[Ca^{2+}]_C$ and therefore, of contraction.

When we examined in detail the parameters of the $[Ca^{2+}]_M$ peaks (see figure 65A-C), we found a 10-20% smaller width and frequency with respect to the $[Ca^{2+}]_C$ peaks. This may be due to the low Ca^{2+}-affinity of the mitochondrial Ca^{2+} uniporter (Bernardi, 1999; Montero et al., 2000), which may open only when $[Ca^{2+}]_C$ is near the peak levels, thus reducing the time mitochondrial Ca^{2+} uptake is active. The decrease in frequency could also be attributed to the presence of $[Ca^{2+}]_C$ peaks, which would be too small to evoke any mitochondrial Ca^{2+} uptake. It was surprising to find that $[Ca^{2+}]_M$ dynamics changes little during aging. The frequency values was stable and there was only a small progressive reduction in the width and amplitude of the $[Ca^{2+}]_M$ peaks with age. The data indicate that mitochondrial Ca^{2+} fluxes in *C. elegans* pharynx, both Ca^{2+} uptake and Ca^{2+} release, are relatively well preserved during aging, but there is a progressive decrease in their magnitude during aging.

Mitochondria showed rapid $[Ca^{2+}]_M$ oscillations and also prolonged elevations of $[Ca^{2+}]_M$ similar to those of "square-wave" $[Ca^{2+}]_C$ increases. Many of them also lasted several minutes and sometimes $[Ca^{2+}]_M$ stayed high for the rest of the experiment. The proportion of worms undergoing "square-wave" $[Ca^{2+}]_C$ or $[Ca^{2+}]_M$ increases decayed in parallel during aging, suggesting that they are both directly linked (figures 27 and 64). In cytosol our hypothesis was that these long $[Ca^{2+}]$ transients could be attributed to energy depletion, which would arrest the Ca^{2+} pumps and thus keep $[Ca^{2+}]_C$ high, leading to mitochondrial Ca^{2+} accumulation. If energy depletion is transient, cells can recover and restart spiking, but if it is persistent, the increased $[Ca^{2+}]_M$ may induce cellular damage by triggering ROS production or by activating apoptotic pathways. Energy depletion would be a consequence of the increased energy consumption during the experiment due to the accelerated pharyngeal pumping induced by serotonin (figure 65 and 66). The significance of these "square-wave" $[Ca^{2+}]_C$ or $[Ca^{2+}]_M$ increases would therefore be that in these worms the energy production is unable to cope with the increased energy consumption at some point during the 30 minutes duration of the experiment.

nuo-6 worms have a mutation in complex I of the respiratory chain that produces a reduced mitochondrial function, lower oxygen consumption, slow growth, slow movement (Yang & Hekimi, 2010a) and decreased ATP levels (Yee et al., 2014). Despite these functional defects, *nuo-6* mitochondria were able to display beat-to-beat $[Ca^{2+}]_M$ (figure 69) oscillations coupled to the $[Ca^{2+}]_C$ dynamics. $[Ca^{2+}]_M$ oscillations in *nuo-6* mutant worms were slightly wider and had smaller amplitude and frequency than in the controls (figure 72), suggesting reduced Ca^{2+} fluxes in and out of the mitochondria. Similar results were obtained by comparing the $[Ca^{2+}]_C$ oscillations of the *nuo-6* mutant worms with respect to the controls, and therefore the differences in $[Ca^{2+}]_M$ dynamics could

be secondary to the changes in $[Ca^{2+}]_C$ dynamics in these worms. *nuo-6* worms also had a reduced number of "square-wave" $[Ca^{2+}]_C$ and $[Ca^{2+}]_M$ increases at every age. This phenomenon could be due to the smaller rate of energy consumption in these mutants, which may balance the decreased rate of energy production (figure 71).

CONCLUSIONS

1.- The expression of the Ca^{2+} sensors cameleon YC2.1 and YC3.60 in *C. elegans* pharynx muscle cells allow measurement of calcium dynamics in these cells in vivo during long periods of pharyngeal activity, both in cytosol and mitochondria.

2.- Pharyngeal cytosolic calcium oscillations present variability, but it is possible to distinguish two types of cytosolic Ca^{2+} peaks:

- ✓ **Square-wave peaks:** prolonged elevations in [Ca^{2+}], lasting for many seconds or even minutes. They are mostly present in young worms and disappear as the worm ages.

- ✓ **Spikes:** short peaks having widths smaller than 10s. They are maintained throughout the life of the worm.

3.- The pumping rate undergoes a progressive decline during aging due to sarcopenia. However, cytosolic spikes are present throughout the life of the worm. Therefore, there is a dissociation between calcium signalling and muscle contraction that develops with aging.

4.- The square-wave peaks are due to energy depletion in the pharynx cells. This energy depletion arrests Ca^{2+} pumps and precludes Ca^{2+} extrusion from the cytosol. Worms undergoing long square-wave peaks are therefore classified as energy-depleted.

5.- Square-wave peaks and energy-depleted worms appear more frequently in young worms, despite their larger energy content. This may be due to the very high energy use rate in young worms, which would overwhelm the energy production rate.

6.- The mutant strain AQ*eat-2*, a model of dietary restriction, presents a higher percentage of energy-depleted worms at every age than wild type worms. Instead, the mutant strains AQ*nuo-6* (mitochondrial alteration) or AQ*daf-2* (insulin signalling alteration) present a lower percentage of energy-depleted worms than wild type worms.

7.- When all worms, mutant or wild type, are placed under food deprivation, the percentage of energy-depleted worms increases. However, the increase is smaller in *AQnuo-6* and *AQdaf-2* mutants.

8.- The mutant strains AQ*nuo-6* and AQ*daf-2* maintain a better energy balance (production minus consumption), even under food deprivation. This is probably due to a metabolic adaptation that decreases energy consumption.

9.- Pharyngeal mitochondrial calcium oscillations undergo rapid and persistent [Ca^{2+}] oscillations similar to the cytosolic ones. This result favours the "beat-to-beat" model of mitochondrial Ca^{2+} uptake in heart cells.

10.- Mitochondrial [Ca^{2+}] dynamics also show both square-wave Ca^{2+} peaks and spikes. The square-wave $[Ca^{2+}]_M$ peaks are also more frequent in young worms and less frequent in *Mnuo-6* mutants.

11.- Mitochondrial Ca^{2+} uptake is relatively well preserved in *Mnuo-6* mutants, despite the presence of a respiratory chain complex I mutation that significantly reduces mitochondrial function.

BIBLIOGRAPHY

Adachi H, Fujiwara Y and Ishii N (1998). *Effects of oxygen on protein carbonyl and aging in Caenorhabditis elegans mutants with long (age-1) and short (mev-1) life spans*. J. Gerontol. A Biol. Sci. Med. Sci. *53*, B240–B244.

Albertson DG and Thomson JN. (1976) *The pharynx of Caenorhabditis elegans.* Philos. Trans. R. Soc. Lond. B Biol. Sci. *275*, 299-325

Alvarez-Illera P, García-Casas P, Arias-Del-Val J, Fonteriz RI, Alvarez J and Montero M. (2017) *Pharynx mitochondrial [Ca^{2+}] dynamics in live C. elegans worms during aging*. Oncotarget. Jun 22;8(34):55889-55900

Alvarez-Illera P, Sanchez-Blanco A, Lopez-Burillo S, Fonteriz RI, Alvarez J and Montero M. (2016) *Long-term monitoring of Ca2+ dynamics in C. elegans pharynx: an in vivo energy balance sensor*. Oncotarget. 7:67732–67747.

Anderson JL, Morran LT and Phillips PC. (2010) *Outcrossing and maintenanceof males within C. elegans populations*. J. Hered 101:S62-S74

Avery L and Horvitz HR. (1989) *Pharyngeal pumping continues after laser killing of the pharyngeal nervous system of C. elegans*. Neuron; 3:473–485.

Avery L and You YJ. (2012). *C. elegans feeding.* WormBook. ed. The C. elegans Research Community, WormBook, doi/10.1895/wormbook.1.150.1, http://www.wormbook.org.

BIBLIOGRAPHY

Avery L and Thomas JH (1997) *Feeding and defecation. In C. elegans II*, eds. Riddle, D. L. Blumenthal T., Meyer B. J., Preiss, and J. R. (Cold Spring Harbor Press, New York) pp. 679-716

Bansal A, Zhu LJ, Yen K and Tissenbaum HA (2015) *Uncoupling lifespan and healthspan in Caenorhabditis elegans longevity mutants*. Proc Natl Acad Sci USA 12(3):E277–E286

Berridge MJ, (2012) *Cell Signalling Biology*; doi:10.1042/csb0001002.

Bartke A (2008) *Impact of reduced insulin-like growth factor-1/ insulin signalling on aging in mammals: novel findings*. Aging Cell 7:285–290.

Bernardi P (1999) *Mitochondrial transport of cations: channels, exchangers, and permeability transition.* Physiol. Rev. 79, 1127-1155.

Braeckman BP, Houthoofd K, De Vreese A and Vanfleteren JR. (1999) *Apparent uncoupling of energy production and consumption in long-lived Clk mutants of Caenorhabditis elegans.* Curr Biol.; 9:493-496.

Bolanowski MA, Russell RL and Jacobson LA. (1981). *Quantitative measures of aging in the nematode Caenorhabditis elegans. I. Population and longitudinal studies of two behavioral parameters.* Mech. Ageing Dev. 15, 279–295.

Boulin T, Etchberger JF and Hobert O. (2006) *Reporter gene fusions,* ed. The C. elegans Research Community, WormBook doi/10.1895/wormbook.1.106.1; http://www.wormbook.org.

Braeckman BP, Houthoofd, K, Brys, K, Lenaerts, I, De Vreese, A, Van Eygen, S, Raes, H, and Vanfleteren, JR. (2002a). *No reduction of energy metabolism in Clk mutants.* Mech. Ageing Dev. 123, 1447–1456.

Brenner, S. (1988) *The Nematode Caenorhabditis elegans,*. W. B. Wood, Cold Spring Harbor Laboratory Press, Cold Spring Harbor,New York Foreword

Byerly L, Cassada RC and Russell RL. (1976) *The life cycle of the nematode Caenorhabditis elegans. I.* Wild-type growth and reproduction.DevBiol.51:23-33.

Cabreiro F, Au C, Leung K-Y, Vergara-Irigaray N, Cochemé HM, Noori T and Gems D. (2013) *Metformin retards aging in C. elegans by altering microbial folate and methionine metabolism.* Cell 153(1):228–239

Chalfie M and White J. (1988). *The nervous system. In The nematode C. elegans*, Cold Spring Harbor Laboratory Press, (Cold Spring Harbor, New York) pp. 337–391

Chalfie M, Tu Y, Euskirchen G, Ward WW, and Prasher DC. (1994) *Green fluorescent protein as a marker for gene expression.* Science 263: 802-805

Chisholm AD and Xu S. (2012) *The C. elegans epidermis as a model skin. II: differentiation and physiological roles*. Wiley Interdiscip Rev Dev Biol. November 1; 1(6): 879–902

Chisholm AD and Hsiao TI. (2012) *The C. elegans epidermis as a model skin. I: development, patterning, and growth.* Wiley Interdiscip Rev Dev Biol. November 1; 1(6): 861–878.

BIBLIOGRAPHY

Chisholm and AD, Hardin, (2005) *Epidermal morphogenesis* WormBook, ed. The C. elegans Research Community, WormBook; doi/10.1895/wormbook.1.35.1 , http://www.wormbook.org

Chow DK, Glenn CF, Johnston JL, Goldberg IG, and Wolkow C.A. (2006). *Sarcopenia in the Caenorhabditis elegans pharynx correlates with muscle contraction rate over lifespan*. Exp. Gerontol. 41, 252–260.

Collins James J, Cheng H, Hughes S and Kornfeld K. (2007) *The measurement and analysis of age-related changes in Caenorhabditis elegans*. WormBook. 1-21. https://digitalcommons.wustl.edu/open_access_pubs/3461

Corsi AK, Wightman B and Chalfie M. (2002) *A transparent window into Biology: a primer on Caenorhabditis elegans.* Genetics 200(2):387-407

Cox GN, Kusch M, DeNevi K and Edgar RS. (1981a) *Temporal regulation of cuticle synthesis during development of Caenorhabditis elegans*. Dev. Biol. 84, 277–285

Dedkova EN and Blatter LA. (2013) *Calcium signaling in cardiac mitochondria*. J. Mol. Cel. Cardiol. 58, 125–133.

De Haes W, Frooninckx L, Van Assche R, Smolders A, Depuydt G, Billen J and Temmerman L. (2014) *Metformin promotes lifespan through mitohormesis via the peroxiredoxin PRDX-2*. Proc Natl Acad Sci USA 111(24):E2501–E2509

de la Fuente S, Fonteriz RI, Montero M and Alvarez J. (2013) *Ca^{2+} homeostasis in the endoplasmic reticulum measured with a new low-Ca2+ -affinity targeted aequorin*. Cell Calcium. Jul;54(1):37-45

Dent, JA, Davis MW, and Avery L. (1997) *avr-15 encodes a chloride channel subunit that mediates inhibitory glutamatergic neurotransmission and ivermectin sensitivity in Caenorhabditis elegans.* EMBO J. 16, 5867-5879

Dorman JB, Albinder B, Shroyer T and Kenyon C. (1995). *The age-1 and d a f 2 Genes Function in a Common Pathway to Control the Lifespan of Caenorhabditis elegans.* Genetics Society of America.

Fay DS. (2013) *Classical genetic methods* WormBook, ed. The C. elegans Research Community, WormBook, doi/10.1895/wormbook.1.165.1, http://www.wormbook.org.

Feinberg EH, Vanhoven MK, Bendesky A. Wang G, Fetter RD. (2008) *GFP Reconstitution Across Synaptic Partners (GRASP) defines cell contacts and synapses in living nervous systems*. Neuron 57: 353-363.

Fleischhauer R, Davis MW, Dzhura I, Neely A, Avery L and Joho, RH. (2000) *Ultrafast inactivation causes inward rectification in a voltage-gated K(+) channel from Caenorhabditis elegans.* J. Neurosci. 20, 511-520

Fonteriz R, Matesanz-Isabel J, Arias-Del-Val J, Alvarez-Illera P, Montero M and Alvarez J. (2016) *Modulation of Calcium Entry by Mitochondria*. Adv Exp Med Biol.;898:405-21.

Franks C J, Pemberton D, Vinogradova I, Cook A, Walker RJ, and Holden-Dye, L. (2002) *Ionic basis of the resting membrane potential and action potential in the pharyngeal muscle of Caenorhabditis elegans.* J. Neurophysiol. 87, 954-961

BIBLIOGRAPHY

Garcia-Valles R, Gomez-Cabrera MC, Rodriguez-Manas L, Garcia-Garcia FJ, Diaz A, Noguera I, Olaso-Gonzalez G and Vina J (2013) *Life-long spontaneous exercise does not prolong lifespan but improves health span in mice.* Longev Healthspan 2:14

Garigan D, Hsu AL, Fraser AG, Kamath RS, Ahringer J and Kenyon, C. (2002). *Genetic analysis of tissue aging in Caenorhabditis elegans: a role for heat-shock factor and bacterial proliferation*. Genetics 161, 1101–1112.

Glenn CF, Chow, DK, David L, Cooke CA, Gami MS, Iser WB, Hanselman KB, Goldberg IG, and Wolkow CA. (2004). *Behavioral deficits during early stages of aging in Caenorhabditis elegans result from locomotory deficits possibly linked to muscle frailty.* J. Gerontol. A Biol. Sci. Med. Sci. 59, 1251–1260.

Hall DH, and Hedgecock EM. (1991) *Kinesin-related gene unc-104 is required for axonal transport of synaptic vesicles in C. elegans.* Cell. 31;65(5):837-47.

Hansen M, Taubert S, Crawford D, Libina N, Lee S-J and Kenyon C (2007) *Lifespan extension by conditions that inhibit translation in Caenorhabditis elegans*. Aging Cell 6:95–110

Herman MA. (2006) *Hermaphrodite cell-fate specification*, WormBook, ed. The C. elegans Research Community, WormBook; doi/10.1895/wormbook.1.39.1, http://www.wormbook.org.

Herndon LA, Schmeissner PJ, Dudaronek JM, Brown PA, Listner KM, Sakano, Y, Paupard MC, Hall DH and Driscoll M.(2002). *Stochastic and genetic factors influence tissue-specific decline in ageing C. elegans.* Nature 419: 808-814.

Hobert O, (2013) *The neuronal genome of Caenorhabditis elegans* WormBook ed. The C. elegans Research Community, WormBook, doi/10.1895/wormbook.1.12.2, http://www.wormbook.org.

Horvitz HR, Chalfie M, Trent C, Sulston JE and Evans PD. (1982) *Serotonin and octopamine in the nematode Caenorhabditis elegans.* Science.216:1012–1014

Hosono R, Sato Y, Aizawa SI and Mitsui Y. (1980) *Age-dependent changes in mobility and separation of the nematode Caenorhabditis elegans*. Exp Gerontol.; 15:285-289.

Huang C, Xiong C and Kornfeld K. (2004*). Measurements of age-related changes of physiological processes that predict lifespan of Caenorhabditis elegans.* Proc. Natl. Acad. Sci. U.S.A. 101, 8084–8089.

Hughes SE, Evason K, Xiong C, and Kornfeld K. (2007) *Genetic and pharmacological factors that influence reproductive aging in nematodes.* PLoS Genet. 3, e25

Kaeberlein TL, Smith ED, Tsuchiya M, Welton KL, Thomas JH, Fields S, Kennedy BK and Kaeberlein M. (2006) L*ifespan extension in Caenorhabditis elegans by complete removal of food.* Aging Cell.; 5:487-494.

Kenyon C, Chang J, Gensch E, Rudner A and Tabtlang R (1993) *A C. elegans mutant that lives twice as long as wild type.* Nature 366:461–464

Kenyon C. (2011) *The first long-lived mutants: discovery of the insulin/IGF-1 pathway for ageing*. Philos Trans R Soc Lond B Biol Sci. 12; 366(1561): 9–16.

Kenyon C. (2010) *The genetics of ageing.* Nature 464:504–512

Kenyon, C. (2005). *The plasticity of aging: insights from long-lived mutants*. Cell 120, 449–460.

Kerr R, Lev-Ram V, Baird G, Vincent P, Tsien RY and Schafer WR. (2000) *Optical imaging of calcium transients in neurons and pharyngeal muscle of C. elegans*. Neuron. 26:583- 594.

Klass M, Nguyen PN, and Dechavigny A. (1983). *Age-correlated changes in the DNA template in the nematode Caenorhabditis elegans.* Mech. Ageing Dev. 22, 253–263.

Lakowski B and Hekimi S. (1998) *The genetics of caloric restriction in Caenorhabditis elegans*. Proc Natl Acad Sci. 27;95(22):13091-6.

Lee RY, Lobel L, Hengartner M, Horvitz HR and Avery L. (1997). *Mutations in the alpha1 subunit of an L-type voltage-activated Ca2+ channel cause myotonia in Caenorhabditis elegans*. EMBO J. 16, 6066-6076.

Lee GD, Wilson MA, Zhu M, Wolkow CA, de Cabo R, Ingram DK and Zou S. (2006) *Dietary deprivation extends lifespan in Caenorhabditis elegans*. Aging Cell.; 5:515-524.

Lockery SR and Goodman MB. (2009) *The quest for action potentials in C. elegans neurons hits a plateau.* Nat. Neurosci. 12: 377-378

Luedtke S, t O'Connor V, Holden-Dye L and Walker RJ. (2010) *The regulation of feeding and metabolism in response to food deprivation in Caenorhabditis elegans* Invert Neurosci.10:63–76

Luyten W , Antal P, Braeckman BP, Bundy J, Cirulli F, Fang-Yen C, Fuellen G, Leroi A, Liu Q, . Martorell P, Metspalu A., Perola M, Ristow M, Saul N, Schoofs L, Siems K, Temmerman L, Smets T, Wolk A, and Rattan SIS. (2016) *Ageing with elegans: a research proposal to map healthspan pathways*. Biogerontology 17:771–782.

McKay JP, Raizen DM, Gottschalk A, Schafer WR,and Avery, L. (2004*) eat-2 and eat-18 are required for nicotinic neurotransmission in the Caenorhabditis elegans pharynx.* Genetics 166, 161-169.

Miyawaki A, Griesbeck O, Heim R, Tsien RY. (1999) Dynamic and quantitative Ca2+ measurements using improved cameleons. Proc Natl Acad Sci U S A.; 96:2135-2140.

Miyawaki A, Llopis J, Heim R, McCaffery JM, Adams .A, Ikura M and Tsien RY (1997) *Fluorescent indicators for Ca2+ based on Green fluorescent proteins and calmodulin*. Nature. 388:882-887.

Montero M, Alonso MT, Carnicero E, Cuchillo-Ibáñez I, Albillos A, García AG, García-Sancho J and Alvarez J. (2000) *Chromaffin-cell stimulation triggers fast millimolar mitochondrial C^{2+} transients that modulate secretion*. Nat Cell Biol.; 2:57-61.

BIBLIOGRAPHY

Morsci NS, Hall DH, Driscoll M, and Sheng ZH. (2016*) Age-Related Phasic Patterns of Mitochondrial Maintenance in Adult Caenorhabditis elegans neurons*. J. Neurosci. 36, 1373-1385.

Mozaffari MS, Liu JY, Abebe W and Baban B. (2013) *Mechanisms of load dependency of myocardial ischemia reperfusion injury.* Am J Cardiovasc Dis.; 3:180-196.

Munkácsy E, Rea SL. (2014) *The paradox of mitochondrial dysfunction and extended longevity.* Exp. Gerontol. 56, 221-233.

Nagai T, Yamada S , Tominaga T, Ichikawa M, and Miyawaki A. (2004) *Expanded dynamic range of fluorescent indicators for Ca(2+) by circularly permuted yellow fluorescent proteins.* Proc Natl Acad Sci. 20;101(29):10554-9.

Nelson FK, Albert PS and Riddle DL. (1983) *Fine structure of the Caenorhabditis elegans secretory-excretory system*. J. Ultrastruct. Res. 82: 156-171

Newell Stamper BL, Cypser JR, Kechris K, Kitzenberg DA, Tedesco PM and Johnson TE. (2018) *Movement decline across lifespan of Caenorhabditis elegans mutants in the insulin/insulin-like signaling pathway.* Aging Cell. Feb;17(1). doi: 10.1111/acel.12704. Epub Dec 7.

Olson, EN. (2006) *Gene Regulatory Networks in the Evolution and Development of the Heart.* Science.; 313:1922-1927.

Page AP and Johnstone IL. (2007). *The Cuticle*. Wormbook ed. The C. elegans Research Community, WormBook; doi/10.1895/wormbook.1.138.; http://www.wormbook.org.

Palty R, Silverman WF, Hershfinkel M, Caporale T, Sensi SL, Parnis J, Nolte C, Fishman D, Shoshan-Barmatz V, Herrmann S, Khananshvili D and Sekler I (2010) *NCLX is an essential component of mitochondrial Na+/Ca2+ exchange*. Proc. Natl. Acad. Sci. USA 107, 436-441.

Phelan P. (2005). *Innexins: members of an evolutionarily conserved family of gap-junction proteins*. Biochim. Biophys. Acta 1711: 225-245

Picard M, Ritchie D, Wright KJ, Romestaing C, Thomas MM, Rowan SL, Taivassalo T, Hepple RT (2010) *Mitochondrial functional impairment with aging is exaggerated in isolated mitochondria compared to permeabilized myofibers*. Aging Cell 9, 1032-1046.

Raizen DM and Avery L. (1994) *Electrical activity and behavior in the pharynx of Caenorhabditis elegans.* Neuron 12, 483-495.

Regmi SG, Rolland SG and Conradt B. (2014) *Age-dependent changes in mitochondrial morphology and volume are not predictors of lifespan.* Aging 6, 118-130.

Regmi SG, Rolland SG and Conradt B. *Age-dependent changes in mitochondrial morphology and volume are not predictors of lifespan.* Aging 2014 Feb;6(2):118-30.

Shimozono S, Fukano T, Kimura KD, Mori I, Kirino Y and Miyawaki A. (2004*) Slow Ca2+ dynamics in pharyngeal muscles in Caenorhabditis elegans during fast pumping*. EMBO Rep.; 5:521-526.

BIBLIOGRAPHY

Shtonda B and Avery L. (2005) *CCA-1, EGL-19 and EXP-2 currents shape action potentials in the Caenorhabditis elegans pharynx.* J. Exp. Biol. 208, 2177-2190;

Siegel MP, Kruse SE, Percival JM, Goh J, White CC, Hopkins HC, Kavanagh TJ, Szeto HH, Rabinovitch PS and Marcinek DJ (2013) *Mitochondrial-targeted peptide rapidly improves mitochondrial energetics and skeletal muscle performance in aged mice.* Aging Cell 12, 763-771

Song BM and Avery L. (2012) *Serotonin activates overall feeding by activating two separate neural pathways in Caenorhabditis elegans* J Neurosci.32(6):1920-31. doi: 10.1523/JNEUROSCI.2064-11

Steger KA, Shtonda BB, Thacker C, Snutch TP and Avery L. (2005) *The C. elegans T-type calcium channel CCA-1 boosts neuromuscular transmission.* J. Exp. Biol. 208, 2191-2203

Stiergnale T. (2006). *Maintenance of C. elegans*. Wormbook. Ed. The C. elegans Research Community, WormBook, http:/www.wormbook.org.

Sundaram MV and Buechner M. (2016) *The Caenorhabditis elegans Excretory System: A Model for Tubulogenesis, Cell Fate Specification, and Plasticity*. Genetics. 203(1):35-63

Tabara H, Grishok A and Mello CC. (1998) *RNAi in C. elegans: soaking in the genome sequence.* Science 282: 430-431.

The medical biocheistry page https://themedicalbiochemistrypage.org/es/oxidative-phosphorylation-sp.php

Timmons L and Fire A. (1998) *Specific interference by ingested dsRNA*. Nature 395: 854.

Van Raamsdonk JM, Meng Y, Camp D, Yang W, Jia X, Bénard C and Hekimi S. (2010) *Decreased energy metabolism extends life span in Caenorhabditis elegans without reducing oxidative damage*. Genetics.; 185:559-571.

Van Voorhies WA and Ward S. (1999). *Genetic and environmental conditions that increase longevity in Caenorhabditis elegans decrease metabolic rate*. Proc. Natl. Acad. Sci. U.S.A. 96, 11399–11403.

Vanfleteren JR, Braeckman BP, Roelens I and De Vreese, A. (1998). *Age-specific modulation of light production potential, and alkaline phosphatase and protein tyrosine kinase activities in various age mutants of Caenorhabditis elegans.* J. Gerontol. A Biol. Sci. Med. Sci. 53, B380–B390.

Waterson RH. (1988). *The nematode Caenorhabditis elegans.* (ed. Wood, W.B.) pp. 282-335. Cold Spring Harbor Laboratory Press, (Cold Spring Harbor Laboratory, New York)

White JG, Southgate E, Thomson JN and Brenner S. (1983) *Factors that determine connectivity in the nervous system of C. elegans*. Cold Spring Harbor Symp. Quant. Biol. 48: 633-640

Wormatlas, Handbook- Hermaphrodite. Cuticle. Base on Blaxter and Robertson. (1998) *The cuticle.* The phisiology and Biochemistry of free-living and plant-parasitic nematodes, ed. Perry RN and Wright DJ. pp25-28. http://www.wormatlas.org/hermaphrodite/cuticle/Images/cutfig3leg.htm

BIBLIOGRAPHY

Wormatlas, Handbook-Hermaphrodite. Excretory system. http://www.wormatlas.org/hermaphrodite/excretory/Images/excfig1leg.htm

Wormatlas, Handbook- Hermaphrodite. Muscle system. Somatic muscle. http://www.wormatlas.org/hermaphrodite/muscleintro/Images/MusFig3.jpg

Wormatlas, Handbook-Hermaphrodite. Sensory receptors http://www.wormatlas.org/hermaphrodite/nervous/Images/neurotable1leg.htm

Wormatlas, Handbook.Hermaphrodite. Pharynx. Base on Mango SE. (2007). *The C. elegans pharynx: a model for organogénesis*, WormBook. Ed. The C. elegans Research Community http://www.wormatlas.org/hermaphrodite/pharynx/Images/phafig1leg.htm

Wormatlas Handbook.Hermaphrodite. Pharynx. Base on Mango SE. (2007). *The C. elegans pharynx: a model for organogénesis*, WormBook. Ed. The C. elegans Research Community http://www.wormatlas.org/hermaphrodite/pharynx/Images/phafig6leg.htm

Wormatlas Handbook.Hermaphrodite. Pharynx. Base on Mango SE. (2007). *The C. elegans pharynx: a model for organogénesis*, WormBook. Ed. The C. elegans Research Community http://www.wormatlas.org/hermaphrodite/pharynx/Images/phafig7Aleg.htm

Xu S and Chisholm AD. (2014) *C. elegans epidermal wounding induces a mitochondrial ROS burst that promotes wound repair*. Dev Cell. October 13; 31(1): 48–60.

Yang W and Hekimi S. (2010b*) A Mitochondrial Superoxide Signal Triggers Increased Longevity in Caenorhabditis elegans.* PLoS Biol 8(12): e1000556. doi:10.1371/journal.pbio.1000556

Yang W and Hekimi S. (2010a*) Two modes of mitochondrial dysfunction lead independently to lifespan extension in Caenorhabditis elegans* Aging Cell. .9(3):433-47. doi: 10.1111/j.1474-9726.2010.00571.x. Epub 2010 Mar 19

Yee C, Yang W and Hekimi S. (2014) *The intrinsic apoptosis pathway mediates the prolongevity response to mitocondrial ROS in C. elegans.* Cell 8;157(4):897-909. doi: 10.1016/j.cell.2014.02.055.